Exploring the Use of RAFT-Synthesised Methacrylate-based Polymers in Formulation Science

Sara Elyasi Bakhtiari

Department of Pharmaceutics

School of Pharmacy

University College London

A thesis submitted for the degree of Doctor of Philosophy

2022

This thesis is dedicated to my parents for their endless love and support.

Declaration

I, Sara Elyasi Bakhtiari, confirm that the work presented in this thesis is my own. Where information has been derived from other sources, I confirm that this has been indicated in the thesis.

Acknowledgments

My deepest appreciation and most sincere gratitude to my supervisors, Professor Steve Brocchini and Professor Gareth Williams for accepting me into their research groups and for their guidance throughout the last three years. Our meetings have been a constant source of inspiration and motivation.

I also wish to thank Dr George Pasparakis for giving me the opportunity to join the PhD programme at UCL school of pharmacy and Dr Fanny Joubert for her help and guidance during the first year of my PhD.

I cannot begin to express my thanks to my parents. I truly owe everything to them and would not have all these amazing opportunities if it were not for them, their unending support, and love. A big thank you to my brothers, Saeid and Soroush, for putting up with me and my PhD-induced anxiety in the last few years. I am very blessed to have them in my life.

I would like to thank Fotis and Tia for their friendship, kindness, and their annual tours around Richmond. I am extremely grateful to Sahar for all the adventures, the amazing memories, and her support. I would like to acknowledge the members of the GRW and SB groups especially Nkiru, Mary, Nour, and Seb, for making my PhD experience at UCL enjoyable and a little less stressful. A special thanks to my favourite people in the school, Luis, and Carlos, for making me smile every single day and for their words of encouragement.

Thanks should also go to my dear friends Margherita, Samane, and Bahareh for their constant encouragement and moral support and to my childhood friends in Kuwait, Narmin, Marziyeh, and Salma, for their friendship. Last but not least, thanks to Emma Daniells for her help and the dearest Brigitte for her guidance and kind advice during the last few months.

Abstract

The need for speciality polymers for drug delivery applications led us to investigate the use of well-defined narrow-dispersed methacrylate-based polymers in this work, exploring their potential in pharmaceutical formulations for drug encapsulation, site-specific release, and the formation of amorphous solid dispersions (ASDs).

A library of methacrylate-based polymers including poly(poly(ethylene glycol) methyl ether methacrylate) (PPEGMA) and poly(methacrylic acid) (PMAA), as well as copolymers composed of PPEGMA and poly(2-(dimethylamino)ethyl methacrylate) (PDMAEMA), were first synthesised using reversible addition-fragmentation chain transfer (RAFT) polymerisation. The synthesis was optimised, and a high degree of control in the polymerisation process was confirmed by the reproducible synthesis of polymers and copolymers with targeted molecular weights and low polydispersity.

Nano-sized monodispersed polyelectrolyte complex (PEC) nanoparticles were next prepared via self-assembly of oppositely charged polymers, PDMAEMA and PMAA. The PECs did not entrap hydrophobic drugs (paclitaxel or dexamethasone) efficiently. Hydrophilic drugs including gemcitabine, 5-fluorouracil, and carmofur, on the other hand, were efficiently loaded into the nanoparticles. However, as anticipated, their release from the PECs was very rapid in media at physiological pH and mildly acidic pH.

Methacrylic acid polymers with DPs of 80 and 20 were able to produce ASDs of lidocaine, a poorly water-soluble drug, after ball milling. These form as a

result of the interactions between the acidic polymer and the basic drug. X-ray diffraction and differential scanning calorimetry analysis confirmed that the ASDs maintained their amorphous nature and were stable under accelerated storage conditions (40 °C and 75% RH) over 9 months. Dissolution studies revealed that the presence of the acidic polymer in the formulation and the amorphous nature of the formulation (lack of crystal lattice) removed the energy barrier to dissolution, lowered the microenvironment pH, and resulted in an increase in the dissolution rate and solubility of the drug.

Impact Statement

In this thesis, the use of narrow molecular weight distribution methacrylate-based polymers in formulations was investigated. The polymers were prepared by a controlled radical polymerisation process known as reversible addition-fragmentation chain-transfer (RAFT) polymerisation. Narrow molecular weight block copolymers were also prepared that could further be used to develop new formulations to improve the therapeutic effects of existing drugs and active agents.

This study demonstrated the ability of the well-defined polymers to self-assemble and form stable polyelectrolyte complex (PEC) nanoparticles capable of encapsulating active agents. The polyelectrolyte complex nanoparticles have the potential to be formulated with photosensitisers and used for photodynamic therapy.

This research provides new knowledge on development of amorphous solid dispersions (ASDs) where a ball milling process was found that could fabricate polymeric ASDs. Well-defined low molecular weight methacrylic acid polymers were used to form stable ASDs and enhance the dissolution rate and solubility of a model BCS class II drug. These polymers could be used toward improving the dissolution rate of other BCS class II or IV drugs. This, in turn, will increase absorption and bioavailability of these classes of drugs. Long term benefits of developing new ASD-based medicines for patients include an increase in the therapeutic effect of the drug as well as improvement in patient compliance as the oral dosage forms of these formulations can reduce the necessity to

administer such drugs by injection or the need to formulate a large amount of a drug substance in the hopes of achieving an efficacious dose.

Table of Contents

List of Figures

List of Schemes

List of Tables

List of Abbreviations

ACVA	4,4'-Azobis(4-cyanovaleric acid)
AIBN	Azobisisobutyronitrile
API	Active pharmaceutical ingredient
APS	Ammonium persulfate
ASD	Amorphous solid dispersions
ATRP	Atom transfer radical polymerization
BCS	Biopharmaceutical Classification System
BMA	Butyl methacrylate
CTA	Chain transfer agent
DEAEMA	Diethylaminoethyl methacrylate
DEX	Dexamethasone
DLS	Dynamic light scattering
$Đ_M$	Polydispersity Index
DMAEMA	2-(Dimethylamino) ethyl methacrylate
DMF	Dimethylformamide
DMSO	Deuterated dimethyl sulfoxide
DP	Degree of polymerisation
DPBS	Dulbecco’s phosphate buffered saline
DSC	Differential scanning calorimetry
DVS	Dynamic vapor sorption
EE	Encapsulation efficiency
EPR	Enhanced permeability and retention
FaSSGF	Fasted state simulated gastric fluid
FaSSIF	Fasted state simulated intestinal fluid
FDA	Food and Drug Administration
FTIR	Fourier transform infrared spectroscopy
5-FU	5-Fluorouracil
GEM	Gemcitabine

GI	Gastrointestinal
GPC	Gel permeation chromatography
HCl	Hydrochloride
HME	Hot-melt extrusion
HPLC	High performance liquid chromatography
HPMC	Hydroxypropyl methyl cellulose
HPMCAS	Hydroxypropyl methylcellulose acetate succinate
LAM	Less activated monomer
LC	Loading capacity
LCST	Lower critical solution temperature
LID	Lidocaine
MAA	Methacrylic acid
MAM	More-activated monomer
MMA	Methyl methacrylate
M_n	Number average molecular weight
M_w	Weight average molecular weight
MWCO	Molecular weight cut-off
NCS	Neocarzinostatin
NIPAAM	N-isopropylacrylamide
NMP	Nitroxide mediated polymerization
NMR	Nuclear magnetic resonance
NP	Nanoparticle
NSAID	Non-steroidal anti-inflammatory drugs
PAA	Poly(acrylic acid)
PBS	Phosphate buffered saline
PDEA	Poly(2-(diethylamino)ethyl methacrylate))
PDI	Polydispersity index
PDMEAMA	Poly(2-(dimethylamino) ethyl methacrylate)
PEC	Polyelectrolyte complex
PEG	Poly(ethylene glycol)

PEGDA	Poly(ethylene glycol) diacrylate
PEGMa	Poly(ethylene glycol) methacrylate
PEGMA	Poly(ethylene glycol) methyl ether methacrylate
PEI	Poly(ethylene imine)
PEO	Poly(ethylene oxide)
PEVP	Poly(N-ethyl-4-vinylpyridinium bromide)
PGMA	Poly(glyceryl methacrylate)
PLA	Poly(lactic acid)
PMAA	Poly(methacrylic acid)
PMANa	Poly(sodium methacrylate)
PMMA	Poly(methylmethacrylate)
PNIPAAM	Poly(N-isopropylacrylamide)
PPEGMA	Poly(poly(ethylene glycol) methyl ether methacrylate)
PPGMA	Poly(poly(propylene glycol methacrylate))
PSS	Poly(styrenesulfonic acid)
PTA	Phosphotungstic acid hydrate
PVP	Polyvinylpyrrolidone
RAFT	Reversible addition-fragmentation chain transfer
RBC	Red blood cells
RDRP	Reversible deactivation radical polymerisation
RH	Relative humidity
RMS	Root-mean-square
SI-RAFT	Surface initiated reversible addition-fragmentation chain transfer
TEM	Transmission electron microscopy
TEMED	N,N,N′,N′-Tetramethylethylenediamine
TGA	Thermogravimetric analysis
VPTT	Volume phase transition temperature
XRD	X-ray diffraction

Chapter 1 Introduction

1.1 Polymers

Polymers have been widely used as pharmaceutical excipients. They play an important role in drug delivery. This includes altering the pharmacokinetic profiles of formulations and masking the undesired physicochemical properties of drugs. Some of the applications of polymer excipients in oral drug delivery systems include acting as bulking agents, binders, and disintegrants (1). However, the use of polymers in pharmaceutical formulations has evolved in recent years. Some polymers are used to enable controlled release of drugs while others are utilised to target a specific site for the release of drugs (2). The efficacy of some drugs is hindered by their low solubility, absorption, or bioavailability. For example, oral administration of drugs that display poor dissolution in the gastrointestinal (GI) tract leads to low absorption and bioavailability of the drug (3). Natural or synthetic polymers can be used in formulations to overcome these challenges.

The demand for more advanced formulations for drug delivery applications has highlighted the need for speciality polymers. Increasingly complex pharmaceutical formulations utilise different polymers for site-specific drug release, modified drug release, or to form amorphous solid dispersions (1). Use of narrow-dispersed methacrylate-based polymers for site-specific release of drugs and formation of amorphous solid dispersions will be investigated in this thesis.

1.1.1 Reversible deactivation radical polymerisation

Polymers are macromolecules comprised of repeat units derived from the polymerisation reaction of precursor reagents known as monomers. Polymers are broadly synthesised by either step or addition polymerisation reactions. Addition polymerisation reactions include free radical processes that are used to make many well-known polymers (e.g., polyethylene, polymethacrylates). During the last 3 decades, free radical polymerisation processes have been developed giving polymers with more narrow molecular weight distribution and more defined architectures (e.g., block co-polymers). These reversible deactivation radical polymerisation (RDRP) methods include atom transfer radical polymerisation (ATRP), nitroxide mediated polymerisation (NMP), and reversible addition–fragmentation chain transfer (RAFT). RDRP is a chain-growth polymerisation where propagating polymer radicals partition between active and dormant stages (4). Reversible deactivation of propagating radicals in NMP and ATRP methods is done by radical-radical reaction and atom transfer, respectively. In RAFT polymerisation, the chain transfer process between the dormant species and growing chains is carried out using a chain transfer (or RAFT) agent. The chain transfer process in RAFT polymerisation allows the equilibration of propagating species with dormant species, providing equal opportunity for all chains to grow while minimising termination events to control the molecular weight dispersity (**Scheme 1.1**) (5).

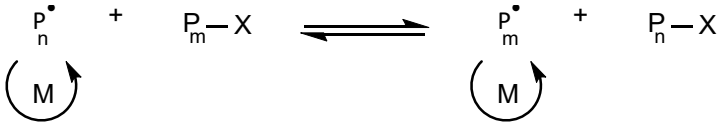

Scheme 1.1. *Reversible deactivation by degenerative chain transfer (6). Abbreviations: P, polymer; and M, monomer.*

1.1.2 Reversible addition-fragmentation chain transfer polymerisation

Among the various methods available to generate polymers, RAFT polymerisation can be applied to a wide range of functional monomers. These simply need to be capable of undergoing radical polymerisation in at least one solvent. RAFT polymerisation was first developed in 1998 (7). The RAFT process is simple and provides good control, allowing the formation of polymers with target molecular weight and narrow molecular weight distribution by equilibrating activation and deactivation and use of a chain transfer agent (CTA) (8, 9). CTA agents are thiocarbonyl compounds in the form of ZC(=S)SR (**Scheme 1.2**).

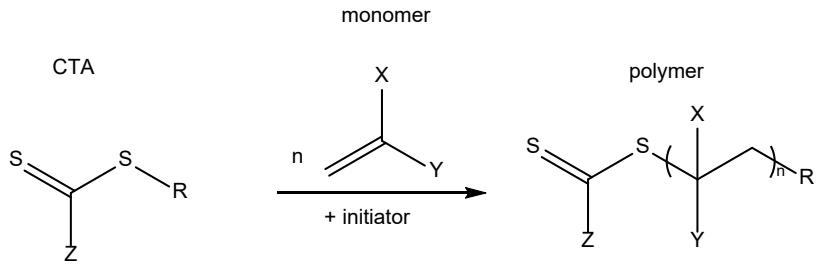

Scheme 1.2. *The overall outcome of using a RAFT agent to polymerise a monomer (8).*

As with any radical addition polymerisation process, chain propagation is initiated by the presence of a free radical initiator (I). The molar ratio of monomer to CTA controls the degree of polymerisation and molecular weight

of the polymer, while the ratio of monomer to initiator affects the rate of polymerisation. The CTA to initiator ratio affects the functionality at the polymer chain ends. In well-designed experiments, the number of CTA radical-derived chains is greater than the number of initiator derived chains. Therefore, the number of initiator-derived chains can be minimised by using a high ratio of CTA to initiator (6). The synthesis of a polymer with narrow molecular weight distribution requires a fast initiation rate compared to the propagation rate and controlled chain transfer and termination events. This allows chains to start growing at the same time, leading to the formation of polymers with the same chain length. The resultant simultaneous chain growth also creates a dynamic equilibrium where the termination step is suppressed, which leads to formation of narrow-dispersed polymers.

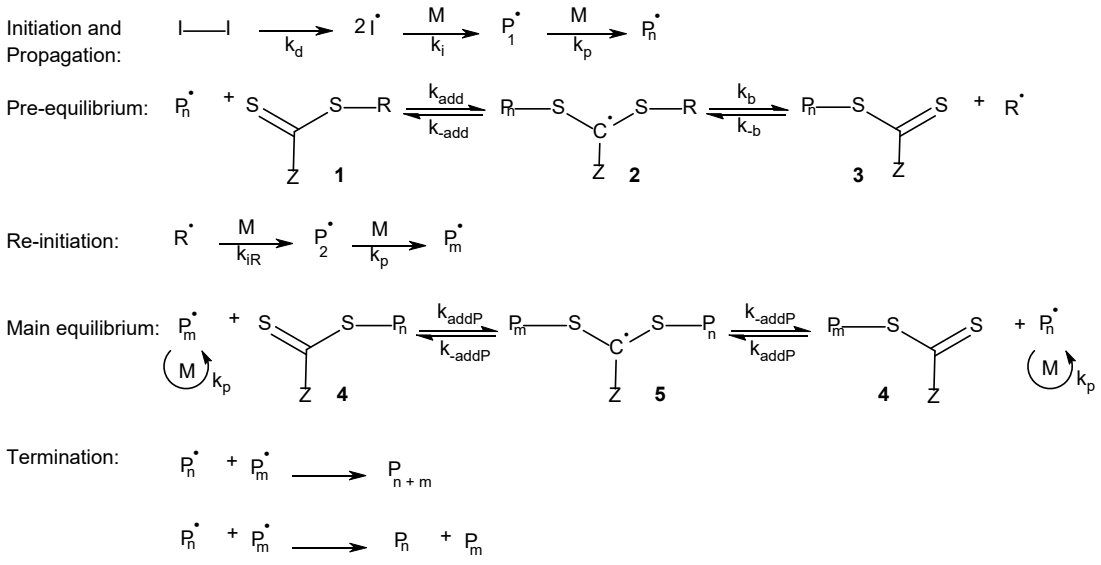

Scheme 1.3. *Stages of RAFT polymerisation. Chain transfer agent* ***2*** *reacts with propagating radicals by reversible chain transfer.*

The RAFT polymerisation process begins with the initiator decomposing into the initiating species, often by heterolytic bond cleavage (**Scheme 1.3**).

Azobisisobutyronitrile (AIBN) and 4,4'-azobis(4-cyanovaleric acid) (ACVA) are two of the most widely used initiators in RAFT polymerisation. The initiating species (I•) can then undergo reaction with an olefinic monomer that is able to generate a propagating radical (P_1•). Monomer adds to the propagating chain one monomer at a time to grow the polymer chain (P_n•). This is the essence of addition polymerisation reactions. P_n• reacts with the RAFT agent **1** forming an intermediate **2** which then fragments to give the macro-RAFT agent **3**. The RAFT agent forms a labile bond that can undergo heterolytic cleavage, leading to formation of a radical from the leaving group of the RAFT agent **3**. The pre-equilibrium stage of the polymerisation terminates when the chain transfer agent is fully consumed. The preference for the intermediate radicals (**2** or **5**) to fragment to products or to the starting materials can be described by the partition coefficient (Ø) (10). The partition coefficient can be calculated by dividing the rate constant of the fragmentation (k_b) by the sum of the rate constants of fragmentation and addition (k_{-add}). For the synthesis of narrow dispersed polymers Ø should be greater than 0.5.

After the pre-equilibrium stage, the RAFT agent-derived radical can then re-initiate polymerisation. Next, the radicals are shared between polymers reversibly in the main equilibrium stage **4**. RAFT polymerisation relies on the persistent radical effect and can provide good control of polymerisation through rapid equilibration of chains such that all chains have an equal opportunity to grow (9). Once monomer is consumed, the polymer chain will have a thiocarbonylthio end-group which can act as a macro-RAFT agent to undergo chain propagation by the addition of a second monomer, resulting in the synthesis of block copolymers (**Scheme 1.4**). RAFT agents do not

completely inhibit formation of dead chains through termination. However, the formation of dead chains is suppressed by formation of many more polymer molecules with RAFT agent-derived ends compared to conventional radical polymerisations. This is a result of RAFT providing reversible deactivation of propagating radicals and the persistent radical effect.

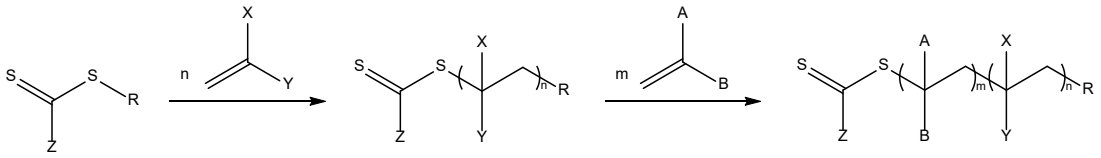

Scheme 1.4. *Synthesis of block copolymers by sequential RAFT polymerisation (8).*

The Z group of a CTA (ZC(=S)SR) controls the reactivity of the RAFT agent and affects the rate of radical addition and fragmentation. The most reactive chain transfer agents include carbon (dithioesters) or sulphur (trithiocarbonates) adjacent to the thiocarbonyl group. The R group, on the other hand, is the leaving group that must be fragmented to form a radical, and needs to be reactive enough to re-initiate polymerisation (10). **Figure 1.1** shows the general guidelines for selection of a RAFT agent with a suitable R group.

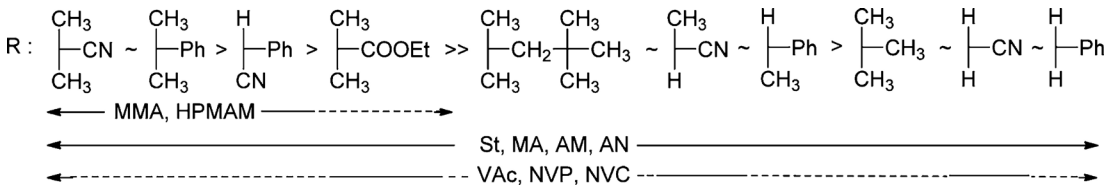

Figure 1.1. *Guidelines for choosing a RAFT agent with a suitable R group. From left to right, transfer coefficients and fragmentation rates decrease. Dashed line indicates partial control over polymerisation. Taken with permission from Keddie et al., Copyright © 2012, American Chemical Society (10). Abbreviations: MMA, methyl methacrylate; HPMAM, N-(2-hydroxypropyl) methacrylamide; St, styrene; MA, methyl acrylate; AM, acrylamide; AN, acrylonitrile; Vac, vinyl acetate; NVP, N-vinylpyrrolidone; NVC, N-vinylcarbazole.*

The activity of a CTA can be determined using the chain transfer coefficient (C_{tr}). Chain transfer coefficient is the ratio between the rate of chain transfer (K_{tr}) and rate of propagation (k_p). More active chain transfer agents have a higher C_{tr} compared to less active CTAs. The selection of a RAFT agent with suitable Z and R groups depends on the monomer structure and is an important factor for achieving control over the polymerisation and ensuring the formation of polymers with a low polydispersity index. Monomers can be divided into two groups termed “more-activated monomers” (MAMs) and “less activated monomers” (LAMs) based on their reactivity in a free radical process (8). The vinylic group of MAMs is adjacent to a carbonyl group, an aromatic ring, or a nitrile. LAMs on the other hand are monomers with an adjacent electron rich atom. For good control over polymerisation of MAMs, a more reactive RAFT agent is required as they produce less reactive macro-radicals. **Figure 1.2** shows the general guidelines for selection of the Z group in RAFT polymerisation (10).

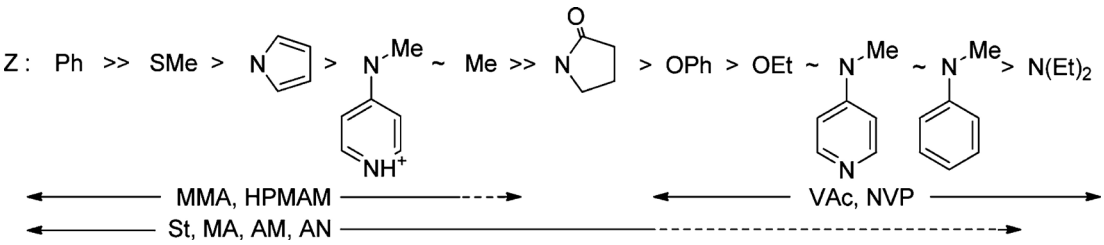

Figure 1.2. *Guidelines for choosing a RAFT agent with a suitable Z group. From left to right, addition rates decrease, and fragmentation rates increase. Dashed line indicates partial control over polymerisation. Taken with permission from Keddie et al., Copyright © 2012, American Chemical Society (10). Abbreviations: MMA, methyl methacrylate; HPMAM, N-(2-hydroxypropyl) methacrylamide; Vac, vinyl acetate, NVP, N-vinylpyrrolidone; St, styrene; MA, methyl acrylate; AM, acrylamide; AN, acrylonitrile.*

For a RAFT polymerisation of more-activated monomers to display a linear increase in molecular weight (M_n) and degree of polymerisation (DP) with an

increase in monomer conversion, a more active chain transfer agent (with C_{tr} of at least 10) should be used (8). The preparation of well-defined methacrylate-based polymers and copolymers using sequential RAFT polymerisation is the main focus of Chapter 2.

1.2 Polymers in formulation and drug delivery

Following oral administration, the stability, dissolution, and bioavailability of a drug is influenced by the pH changes along the GI tract. One approach to ensure the stability and efficacy of an acid-labile drug is to use enteric coatings, which prevent dissolution of the drug in the acidic environment of the stomach and facilitate its dissolution in the neutral environment of the small intestine (1). Polymers can also be used for enteric coating of tablets that cause GI irritations.

Non-steroidal anti-inflammatory drugs (NSAIDs) such as aspirin, naproxen and diclofenac are widely used to reduce inflammation and relieve pain. These medicines can cause gastric ulcers and bleeding which may lead to hospitalisation. Enteric coating of these tablets can reduce the adverse events associated with these medicines by restricting their dissolution in the stomach (1). Polymers have also been used to form monolithic matrix systems where the polymer swells upon hydration and forms a barrier through which the drug is slowly released into the surroundings. Cellulose derivatives such as hydroxypropyl methyl cellulose (HPMC) are commonly used for controlled drug delivery.

Anionic methacrylate-based homo- and co-polymers containing repeating carboxylic acid groups along the polymer main chain have been reported to display tunable hydrophilic/hydrophobic properties depending on the pH of the solution (2). These polymers are often used in formulations for oral delivery of drugs. The release of the drug is triggered at specific pH values depending on the polymer used in the formulation (11). At specific pH values, acidic polymers dissolve upon deprotonation of their carboxylic acid groups. This in turn can lead to an increase in the absorption and bioavailability of a drug. Anionic methacrylate-based polymers have shown potential for use in targeted drug delivery. For instance, Eudragit L100-55, a methacrylic acid and ethyl acrylate copolymer, has been found suitable for drug delivery to the duodenum, as it dissolves at pH above 5.5 (12). Eudragit S100, a methacrylic acid and methyl methacrylate copolymer, dissolves in solutions with pH greater than 7 and therefore is suitable for drug delivery to the ileum.

The use of cationic methacrylate-based polymers for colon-specific delivery of drugs has also been investigated. Eudragit E, an acid-soluble pH-responsive copolymer composed of butyl methacrylate (BMA), 2-dimethaylaminoethyl methacrylate (DMAEMA), and methyl methacrylate (MMA), is only soluble at pH below 5. This polymer can therefore be used to protect a drug in the alkaline environment of the small intestine and release the drug at the reduced pH environment of an inflamed colon. An enteric coating material can also be used to protect the acid soluble Eudragit E from dissolving in the acidic environment of the stomach. Coating dexamethasone tablets with Eudragit E and using hydroxypropyl methylcellulose acetate succinate (HPMCAS) for enteric coating of the formulation was found suitable for colon-specific delivery of the

drug for treatment of inflammatory bowel disease (13). For a more detailed discussion about the use of polymers in formulation for oral drug delivery see section 1.3.

1.2.1 Polymer nanocarriers

Methacrylate molecules contain a highly reactive double bond. RAFT polymerisation can then be used to synthesise methacrylate-based polymers and copolymers with narrow molecular weight distribution and produce stimuli responsive polymers. Site-specific drug release can be achieved using responsive mechanisms or external stimuli such as pH change, use of magnetic fields, light, or hyperthermia (14). Smart drug delivery systems release drug molecules upon stimulation; therefore, their use can increase bioavailability of the drug at the target and decrease drug release in the blood stream and thus decrease occurrence of side effects (15).

In 1975, Helmut Ringsdorf described the concept of polymer-drug conjugates to enhance the biological activity of low molecular weight drugs (14). A schematic is shown in **Figure 1.3**. In this model, different areas along the polymer chain were intended for specific effects. The biodegradable backbone of the model was used to increase the solubility of the polymer macromolecule with high molecular weights and increase its circulation time. The second area is where the drug is conjugated and includes linkage spacers that can attach the drug and facilitate its release at a target site. The third area features the transport system. The transport system incorporates a target-specific homing device and a nonspecific resorption enhancer.

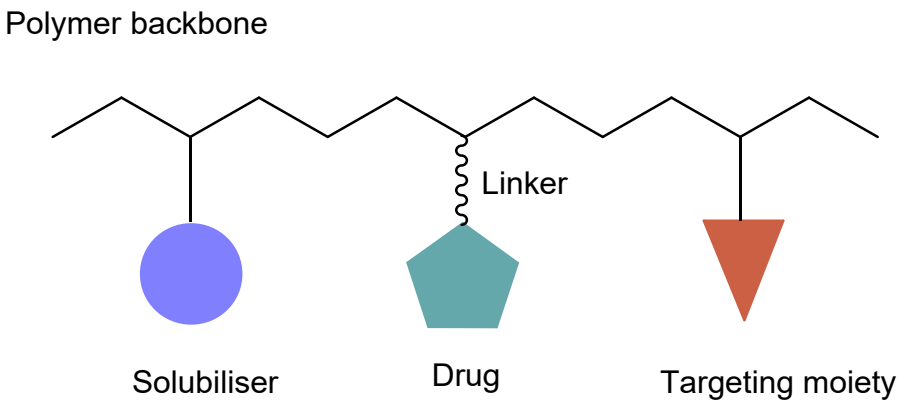

Figure 1.3. *A model designed by Helmut Ringsdorf representing pharmacologically active polymers (14).*

In cancer chemotherapy, the main limitation to an effective treatment is systemic toxicity (15). Therefore, only a maximum tolerated dose of potent anticancer drugs can be used for chemotherapy as there is a significant chance of toxicity to healthy tissues if a higher dose is used. In 1979, a study reported the synthesis of a product named SMANCS by conjugation of the anticancer protein neocarzinostatin (NCS) with a polymer (styrene maleic acid copolymer, SMA) (16). The researchers reported that the polymer-conjugated proteins tended to accumulate with much greater concentration than NCS in cancer tissues (17). Furthermore, they showed that the clearance of these macromolecules from the cancer tissues by the blood capillary or the lymphatic system decreased markedly. They concluded that this arose because of the hyper-vascular nature of the tumours, their enhanced permeability, and a lack of lymphatic drainage. SMANCS is clinically used for the treatment of hepatoma in Japan.

The enhanced permeability and retention (EPR) effect is a phenomenon which allows selective accumulation of macromolecules and lipids of higher than 40 kDa in a variety of solid tumours (17). Such macromolecules also have a

molecular size larger than the renal excretion threshold, limiting their clearance, which is another essential factor in achieving EPR effect (18). Nano-sized particles can also accumulate at tumour sites owing to the EPR effect. Nanoparticles can further achieve high plasma concentrations and therefore have long plasma half-life (19). This is due to their large size and inability to penetrate through the tight endothelial junctions of healthy blood vessels.

Successful tumour-targeted therapy requires drug accumulation and specific drug release in tumour tissue, with minimal release during circulation (20). The combination of the EPR effect (passive targeting) and delivering a drug to a specific diseased area (active targeting) using a targeting moiety (ligands, antibodies, etc) or using stimuli-responsive carriers can ensure increased antitumor and reduced systemic side effects. Using such approaches to improve the tumour selectivity of anticancer drugs is therefore a major objective for the treatment of cancer.

Cancerous tissues have slightly lower pH than normal tissues (21). This arises due to conversion of glucose to lactic acid as a means to maintain the nutritional needs of fast-growing cancer cells and allow tumour growth (Warburg effect) (22). The resulting acidic microenvironment is therefore an attractive target for cancer diagnosis and treatment. Many pH-responsive strategies have been developed during the past few years for tumour imaging and drug delivery using polymers as nanocarriers.

1.2.2 Stimuli-responsive polymers

Anticancer drugs can be conjugated to polymers to increase their stability as well as their selectivity. For instance, gemcitabine, when administered alone, is hydrolysed by the enzyme cytidine deaminase, resulting in its rapid clearance and lack of efficacy. Conjugation of gemcitabine to a methacrylate-based monomer (mono-2-methacryloyloxy ethyl succinate) and polymerising the GEM-monomer conjugate using RAFT polymerisation (shown in **Figure 1.4**) was reported to resolve this issue and result in the formation of sub-90 nm nanoparticles with pH-sensitivity following a solvent evaporation process (23).

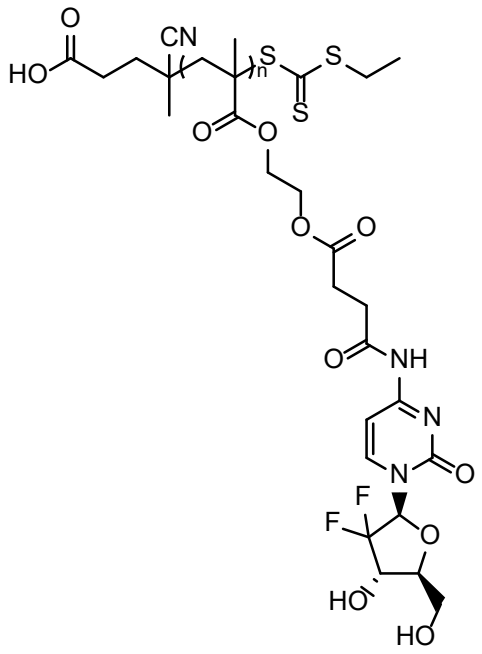

Figure 1.4. *Structure of methacrylate-based GEM-monomer conjugate polymerised using RAFT polymerisation (n = 20 or 100) (23).*

Methacrylate-based polymers with cationic charge have been used to complex with anionic macromolecules including short interfering RNA (siRNA) or DNA. For instance, polymeric micelle carriers composed of a RAFT synthesised

copolymer with a dimethylaminoethyl methacrylate (DMAEMA) block and a second block consisting of DMAEMA, propylacrylic acid (PAA), and butyl methacrylate (BMA) (shown in **Figure 1.5**) were used for siRNA delivery (24). The PDMAEMA block was used to mediate siRNA binding, whereas the second block was designed to disrupt the membrane at mildly acidic pH. The incorporation of BMA, the hydrophobic block, was found to induce formation of spherical micelles with average diameter of 40 nm. In the acidic conditions of endosomes (pH 5.8-6.6), the micelles are protonated, resulting in a net positive charge which allows interaction with endosomal membranes and enhances the delivery of siRNA into the cytoplasm.

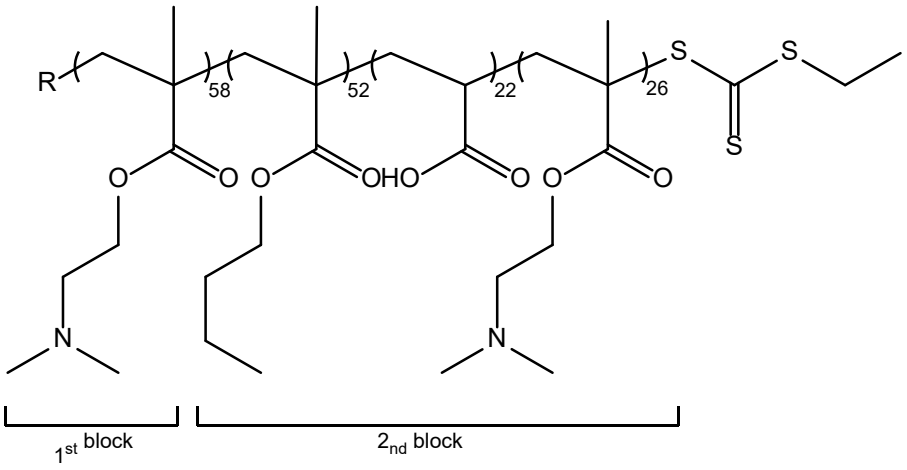

Figure 1.5. *Structure of poly[poly(DMAEMA)-b-poly(BMA-co-DMAEMA-co-PAA)] synthesised via RAFT polymerisation (24).*

Thermoresponsive methacrylate-based polymers that exhibit a lower critical solution temperature (LCST) have also been of great interest in recent years (25). These polymers are water-soluble below the critical temperature, whereas above the critical temperature they undergo a solution phase transition and become insoluble. The RAFT synthesised block copolymer

poly(2-ethylhexyl methacrylate)-b-poly(di(ethylene glycol)-oligo(ethylene glycol)methyl ether methacrylate) was used for the delivery of squalenoyl-gemcitabine and paclitaxel for the treatment of pancreatic cancer (26). The copolymers self-assembled in water into sub-50 nm micelles. Above the LCST, the corona of the micelles was disrupted leading to the release of both drugs (**Figure 1.6**). A similar copolymer, poly(diethylene glycol) methacrylate-co-poly(oligoethylene glycol)methacrylate-b-poly(2-ethylhexyl) methacrylate, has been employed as a coating on liposome nanocarriers loaded with gemcitabine and cisplatin (27). The release of the drugs was thermally triggered.

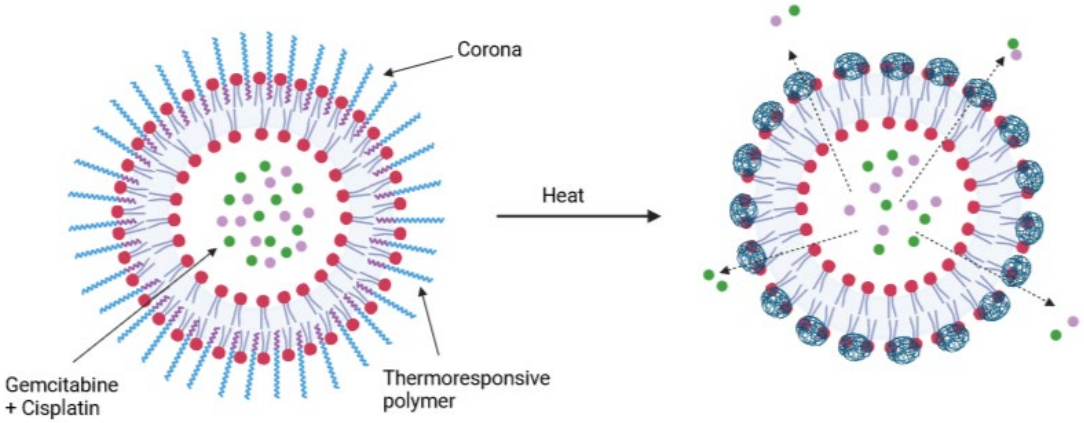

Figure 1.6. *The thermoresponsive polymer-coated liposome encapsulated with gemcitabine and cisplatin undergoes coil to globule transition leading to disruption of the lipid membrane and release of the drugs (27). Created with BioRender.com.*

In a recent study, a block copolymer of poly(methacrylic acid) and poly(N-isopropylacrylamide) (PNIPAAM) synthesised by surface initiated reversible addition-fragmentation chain transfer (SI-RAFT) polymerisation was used as the shell of a nanocarrier with silica as the core (28). SI-RAFT polymerisation is a method to graft polymers from silica surfaces with a sufficiently high density. PNIPAAM is thermoresponsive and exhibits hydrophobic-hydrophilic

phase transition at temperatures above its LCST. The formulation was used to encapsulate doxorubicin. At neutral pH, the electrostatic interaction between the positively charged doxorubicin and negatively charged poly(methacrylic acid) prevented the release of the drug, whereas at acidic pH the electrostatic interaction was weakened due to the protonation of the anionic polymer, which led to the release of doxorubicin. The release in acidic pH was enhanced further at elevated temperature due to the phase transition and collapse of PNIPAAM. Doxorubicin-loaded nanoparticles were found to be more cytotoxic against Hela cells than free doxorubicin.

1.2.3 Polyelectrolyte complex nanoparticles

Polyelectrolytes are polymers that have a net negative or positive charge. Polyelectrolyte complex (PEC) nanoparticles are usually made by mixing two solutions of oppositely charged polyelectrolytes. PEC nanoparticles usually have small sizes and a narrow size distribution due to the electrostatic interactions between the opposite charges forming a charged-neutralised core (29). The surface of the particles is composed of the polyelectrolyte in excess, and thus the NPs overall typically carry a positive or a negative charge. One of the polyelectrolytes (the cationic polymer or the anionic polymer) is often copolymerised with a neutral hydrophilic polymer which forms the corona of the PECs surrounding the core and is responsible for the stabilisation and solubilisation of the formulation (**Figure 1.7**). Chapter 3 of this thesis is mainly focused on the formation of pH-responsive polyelectrolyte complex nanoparticles using RAFT-synthesised methacrylate-based polymers and the

impact of acidic pH on the hydrodynamic diameter of the nanoparticles as well as the release of drugs from the PECs.

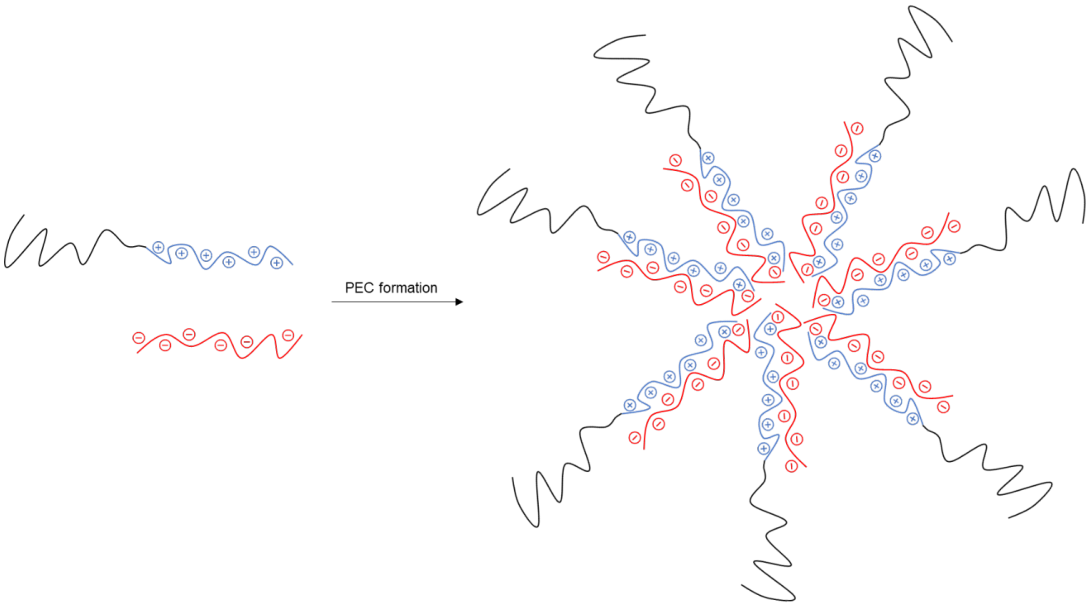

Figure 1.7. *Formation of a complex via association of the cationic block of a copolymer with an anionic homopolymer. The neutral segment of the copolymer forms the corona.*

PECs were first investigated as potential nanocarrier systems over 20 years ago. In a study performed by Harada and Kataoka in 1995, poly(L-lysine) (P(Lys)) and poly(aspartic acid) (P(Asp)) were used as the polycation and polyanion segments of the complex, respectively (30). Both polyelectrolytes were copolymerised with poly(ethylene glycol) (PEG), which was used as the hydrophilic segment. A neutral polyelectrolyte complex was formed and found to be monodispersed with spherical particle shapes. Formation of polyion complex nanoparticles has also been reported using poly(L-lysine) as polycation and DNA as the polyanion (31). The resultant water-soluble complex had a diameter of 50 nm and used PEG blocks as the stabilising segment.

Kabanov et al. reported formation of water-soluble complexes comprising poly(sodium methacrylate) (PMANa) homopolymers and block copolymers of poly(ethylene oxide) (PEO) and poly(*N*-ethyl-4-vinylpyridinium bromide) (PEVP) (32). Self-assembly was derived by the interaction between the negatively charged PMANa and the positively charged PEVP. The polyelectrolytes formed the core of the PECs while PEO formed the corona. In a similar study, anionic poly(acrylic acid) (PAA) and the cationic-neutral diblock copolymer poly(N-methyl-2-vinylpyridinium)-b-poly-(ethylene oxide) (PM2VP-b-PEO) formed spherical complexes in aqueous solution (33).

The driving force for the formation of PECs consisting of water-soluble polymers is the association of the oppositely charged polyelectrolytes. Upon mixing solutions of poly(acrylic acid) and poly((dimethylamino)ethyl methacrylate)-co-poly(glyceryl methacrylate), phase separation occurred followed by immediate rearrangement of the polymers into stable PECs with the neutral block of the copolymer forming the shell (34).

One use of polymers is to make PECs that can be used for targeted drug delivery. The potential of a pH-responsive polyelectrolyte complex system based on methacrylate-based polymers to encapsulate drugs is discussed in more detail in Chapter 3.

1.3 Amorphous solid dispersions

Methacrylates can also be used for other forms of drug delivery. Oral drug delivery is the most commonly used route of administration. It is cost-effective, non-invasive, and such medicines are easy to administer, which increases

patient compliance (35). An active pharmaceutical ingredient from an orally administered dosage form must permeate across the gut intestinal membrane to reach the blood circulation, which is followed by first pass metabolism and distribution throughout the body. In addition, drugs in solid form administered orally must first dissolve in the gastrointestinal fluids prior to their absorption into the systemic circulation. Therefore, drug bioavailability and clinical efficacy depend heavily on the solubility and dissolution rate. Solubility is the capacity of a solute to dissolve in a solvent, whereas dissolution is the process of the solute dissolving in the solvent and is measured as a rate.

In 1995, Amidon et al. introduced the Biopharmaceutical Classification System (BCS) shown in **Figure 1.8**. Active pharmaceutical ingredients were classified into four groups based on their solubility and permeability (36). Class I compounds have a high solubility and permeability. Class II compounds have a high permeability but low aqueous solubility. Class III compounds have a high solubility and low permeability. Class IV compounds have both low solubility and low permeability. The following discussion is focused on Class II compounds as many marketed drugs belong to this group and are ideal candidates for formulation development. Class II compounds also make up 50-60% of the current drugs in development (37).

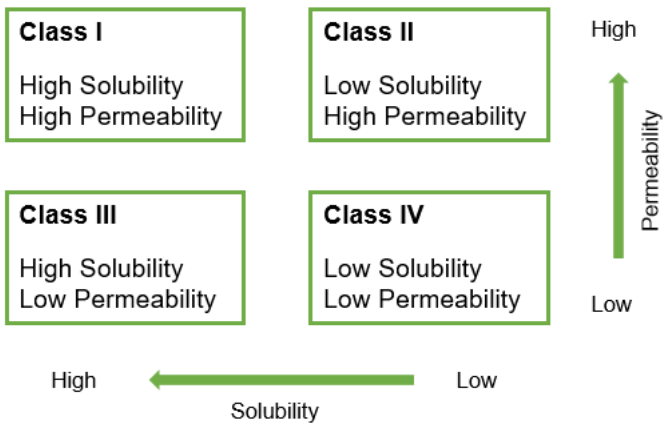

Figure 1.8. *The four classes of drug substance based on their solubility and permeability, also known as the Biopharmaceutical Classification System (BCS).*

Active pharmaceutical ingredients can also be classified using the Developability Classification System (DCS) (38). The class II category in this system is divided into class IIa and IIb. Class IIa drugs have limited dissolution rate whereas for class IIb drugs, it is the solubility of the compounds that limits their bioavailability. The gastrointestinal absorption of BCS class II drugs (poorly water-soluble drugs) can be limited by their dissolution rate. Therefore, increasing the kinetic solubility of class II drugs using cost effective and scalable methods has been of growing interest. Many formulation strategies have been developed to achieve this goal, including particle size reduction, drug salt formation, and amorphous solid dispersions (35).

Reducing the size of the particles is one way to increase their dissolution rate. According to the Noyes-Whitney equation, particles with reduced sizes have larger exposed surface area to water which should increase their dissolution rate (39). This equation (Equation 1.1) defines dissolution rate (dX/dt) as:

$$dX/dt = (A \times D/\delta) \times (C - X/V) \qquad (1.1)$$

Where *dX/dt* is the rate of drug dissolution, *X* is the mass of drug dissolved at a given point in time, *t* is time, *A* is the surface area of the drug, *D* is the diffusion coefficient, *δ* is the thickness of the effective diffusion layer, *C* is the saturation solubility of the drug and *V* is the volume of the dissolution medium (40).

Salt formation is an alternative approach to modify the solubility of ionisable drugs (41). The water-soluble salt forms of some poorly soluble drugs are used in practice as their solubility in water is higher than the original form of the drugs. For instance, tetracycline hydrochloride exhibits a higher solubility than the base form of the drug (42). However, salt formation does not necessarily enhance the solubility of a drug in gastric fluid due to the common ion effect. This effect may also lead to low absorption and bioavailability of a drug. For example, the solubilities of hydrochloride forms of the basic drugs papaverine and demeclocycline were lower than their free base form at low pH values (43).

Salt forms of drugs may also be less permeable, since ionised species cannot pass through the lipid membranes which bound the intestinal lumen. Use of ciprofloxacin hydrochloride was found to significantly reduce the permeability of the drug compared to its free base form (44). Another challenge to developing a salt form of a drug is that some salt forms have a tendency to form polymorphs. For example, 28 forms of sertraline HCl, the active ingredient in Zoloft, were identified by several companies (45). Emergence of an

unexpected new polymorph of a drug can affect the quality of the drug and hence delay its development.

Another method for improving the aqueous solubility of poorly water-soluble drugs is to intimately mix the drug with a physiologically inert water-soluble polymeric carrier to form amorphous solid dispersions (ASDs) (46). Formulating solid dispersions is often considered when salt formation is not possible, for instance when a drug is not ionisable (41). An ASD formulation can also be used when salt forms do not deliver the required improvement in properties: as noted above, the salt form of a drug may not be able to enhance bioavailability of the drug due to restricted dissolution in the GI fluid and/or reduced permeability.

Most crystalline drugs are thermodynamically stable enough to meet regulatory requirements. Crystalline solids have strong intermolecular forces (e.g., H-bonding) existing between individual molecules, which provides an energy barrier (the lattice energy) to dissolution. API solubility is also inhibited by this lattice energy. In contrast, the amorphous form of a drug lacks long range order and possess higher free energy than crystalline drug forms. The amorphous form thus has no crystal lattice energy barrier to dissolution resulting in reduced intermolecular forces between molecules which can lead to increased dissolution rate (35).

A polymeric amorphous solid dispersion system is defined as a dispersion of a drug in an amorphous form within an amorphous polymer carrier matrix. Drug molecules can be isolated in the carrier matrix (solid solution) or dispersed in

carriers (solid suspension). Polymers used in ASD systems improve the kinetic stability of the amorphous form of a drug. When formulating an ASD formulation and choosing a polymer to stabilise the drug, it is important to use a sufficiently high drug load to ensure that the medicine is effective in patients.

Flory-Huggins theory is a lattice-based theory that describes the thermodynamics of polymer solutions. This model could also be used to assess the extent of miscibility of a drug in a polymer. Highly miscible systems are preferred as they are found to be resistant to drug crystallisation (47). In the solid state, polymers can inhibit crystallisation by several mechanisms including reducing the molecular mobility of the drug in the solid dispersion, increasing the energy needed for nucleation, and interacting with the drug (48). Dispersion of the drug into the polymer matrix restricts its molecular mobility and increases the activation energy required for crystallisation (**Figure 1.9**). Within the entangled polymer chains there is little movement. If an active pharmaceutical ingredient (API) is compatible with the polymer, then an amorphous polymer can serve to mix well with an amorphous API. This has been shown to slow nucleation events thus prolonging the amorphous form.

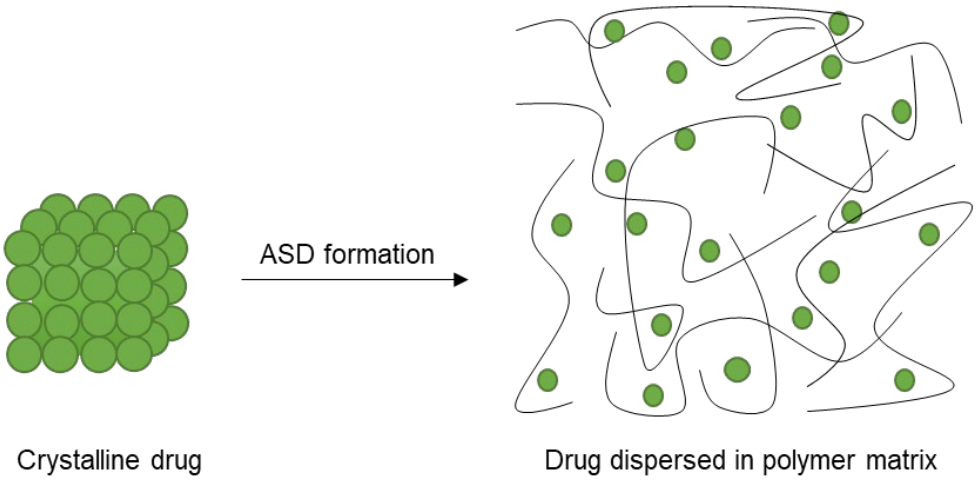

Figure 1.9. *The structure of a crystalline drug and its ASD following mixing with a polymer carrier. The mobility of the drug in ASD is restricted and hence recrystallisation is delayed.*

1.3.1 Glass transition temperature

The glass transition temperature (T_g) is the temperature at which an amorphous material transforms from a rubbery state to a glassy state upon cooling (35). The glassy state of a drug has a higher free energy, entropy, and volume compared with the crystalline drug in a rubber state. T_g is a critical property of ASDs which can significantly influence their physical stability. The glass transition temperature of a mixture can be estimated using the Gordon-Taylor equation (Equation 1.2).

$$T_g = \frac{w_1 T_{g1} + K w_2 T_{g2}}{w_1 + k w_2} \qquad (1.2)$$

where w_1 and w_2 refer to weight fractions of the two components in the ASD, T_g is the glass transition temperature of the mixture, and T_{g1} and T_{g2} correspond to the glass transition temperature of each component. K is a constant. The K value can be determined experimentally or calculated using Equation 1.3.

$$K = \frac{T_{g1}\rho_1}{T_{g2}\rho_2} \qquad (1.3)$$

ρ_1 and ρ_2 refer to the densities of the components.

An inert, thermally stable, and water-soluble polymer with a high glass transition temperature is considered to be a desirable polymer for solid dispersion formulations. When a drug with a low T_g is mixed with a high-T_g polymer, the T_g of the ASD will be between the T_g values of the components. The increased T_g and the glassy environment of the formulation reduce the mobility of the drug. Also, it will result in an increase in the energy necessary for the drug to convert into its crystalline form (35, 49). Therefore, use of an amorphous polymer with a high T_g is essential for producing and maintaining the amorphous form of drugs in an ASD (50). Choosing the right polymer is very important as it impacts the physical stability of the drug during storage as well as its dissolution rate and consequently the permeation and bioavailability of the drug (49). Formation of polymeric amorphous solid dispersion of a BCS class II drug is the main focus of Chapter 4.

1.3.2 Preparation of amorphous solid dispersions

ASDs can be made by processes that result in the drug substance forming an amorphous solid, for instance by heating and melting a mixture of the drug and carrier polymer followed by resolidification via cooling (**Figure 1.10a**) (35). This hot-melt extrusion (HME) method is often used to achieve efficient mixing of a drug substance with a polymer (51). The challenge with this method is that the polymer(s) and the drugs must be thermally stable at the extrusion temperatures used. There are a number of HME-fabricated medicines on the

market: for instance, Kaletra (lopinavir/ritonavir) is an FDA-approved solid dispersion antiretroviral product used for treatment of HIV (35). The formulation contains a copolymer of vinyl pyrrolidone and vinyl acetate.

Alternatively, solid dispersions can be formed upon evaporation of a solution containing a drug and polymer (**Figure 1.10b**). The advantage of this method is that, typically, only low temperatures are needed to evaporate volatile organic solvents (52). The challenges are dissolving the drug and polymer in the same solvent, the cost of production, and the phase separation that may occur during solvent evaporation. Spray drying is a popular processing method for development of solid dispersions of poorly water-soluble drugs. Following a rapid one-step evaporation of the solvent from a solution of drug, the drug molecules get entrapped in a polymer matrix. An example of a spray-dried medicine is Intelence (etravirine) developed by Janssen, which is used for the treatment of HIV (3). This ASD contains HPMC as the carrier polymer. A few examples of the marketed products based on ASDs formed by HME and spray drying are listed in **Table 1.1**.

Table 1.1. *ASD based medicines approved by FDA. Adapted from Lin et al. (47).*

Product name	Drug	Polymer	Preparation method	Year of approval
Sporanox®	Itraconazole	HPMC	Spray drying	1992
Prograf™	Tacrolimus	HPMC	Spray drying	1994
Gris-PEG™	Griseofulvin	PEG	HME	2000
Crestor®	Rosuvastatin	HPMC	Spray drying	2002
Kaletra®	Lopinavir/ritonavir	PVP-VA	HME	2005
Eucreas®	Vildagliptin/metformin HCl	HPC	HME	2007
Intelence®	Etravirine	HPMC	Spray drying	2008
Onmel™	Itraconazole	HPMC	HME	2010
Novir®	Ritonavir	PVP-VA	HME	2010
Incivo®	Telaprevir	HPMCAS	Spray drying	2011
Noxafil®	Posaconazole	HPMCAS	HME	2013
Orkambi®	Lumacaftor/ivacaftor	HPMCAS/SLS	HME	2015

Mechanical milling has been used to produce small particles by grinding and mixing them together. Samples are placed in sealed milling jars with millimetre-sized milling balls which grind the samples (**Figure 1.10c**). Ball milling does not require use of solvents and it is a suitable technique for formulating thermally unstable drugs. The shear force in this technique breaks the lattice of a drug and disperses the drug in the polymer (53). Ball milling has been used to produce ciprofloxacin amorphous solid dispersions with various polymers (44). This technique has also been used in combination with hot-melt

extrusion in a study to form ASDs of resveratrol, a drug with antioxidant and anti-inflammatory properties (53).

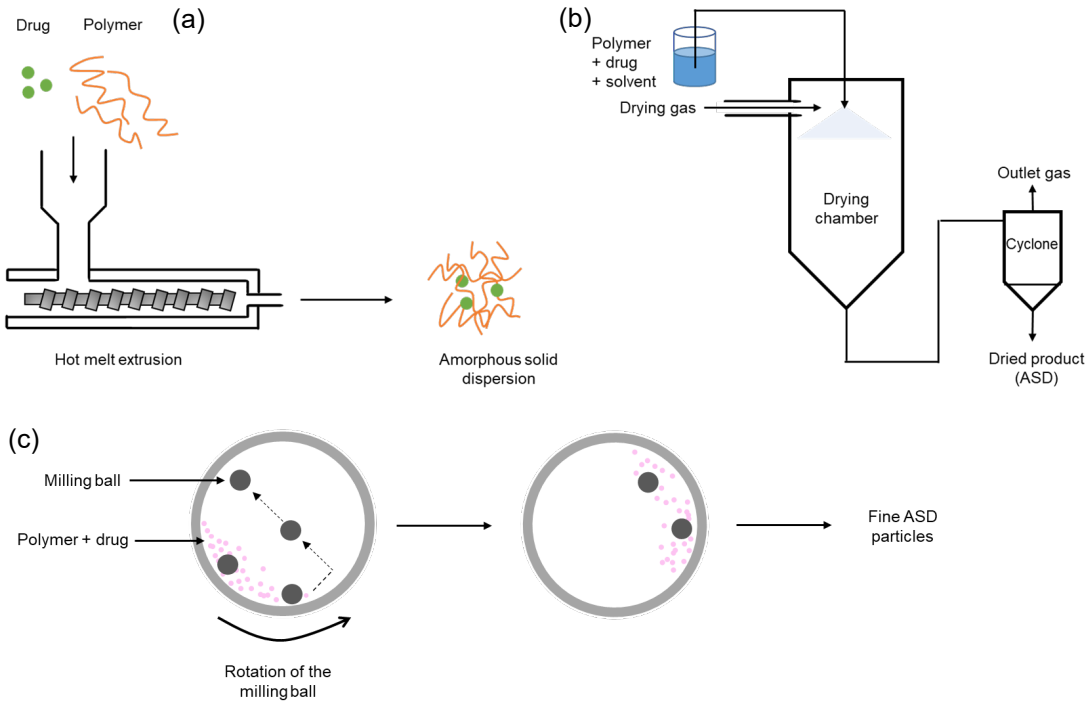

Figure 1.10. *Diagrams of (a) hot melt extrusion, (b) spray drying, and (c) ball milling.*

While milling has been less developed as a commercial formulation route than HME or spray drying, its utility has been demonstrated industrially. Olaparib, a poly(ADP-ribose) polymerase inhibitor, was developed by AstraZeneca and showed promising results for treatment of ovarian cancer (54). However, olaparib has low solubility (0.1 mg/ml) and only moderate permeability and is classified by the BCS as a class IV drug. The drug was first formulated as a solid dispersion using HME with the water-soluble surfactant lauroyl polyoxylglyceride. However, since a dose of 400 mg twice daily was recommended (16 capsules per day), a second-generation oral formulation was developed. In the new formulation, olaparib was formulated as a solid dispersion with copovidone using hot-melt extrusion. The cooled extrudate is

then milled to form flowable particles. In 2017, Olaparib tablets (150 mg) were approved by the FDA for treatment of relapsed ovarian cancer.

In order to prevent crystallisation of a drug, polymers with functional groups that are either donors or acceptors of hydrogen bonds can be used, because specific interactions between the polymer and the drug can enhance the stability of the formulation (55). In addition to H-bonding, there may be other non-covalent interactions between drug molecules and polymer molecules such as van der Waals forces, ionic, and electrostatic interactions. Amorphous solid dispersions of ciprofloxacin, a weakly basic drug, were prepared by ball milling with various polymers in an attempt to improve the solubility and bioavailability of this poorly water-soluble drug (44). Amorphisation of ciprofloxacin was possible only when acidic polymers such as Eudragit L100, Eudragit L100-55, Carbopol, and HPMCAS were used, since the carboxylate groups of the polymers interacted with the secondary amine of ciprofloxacin. **Figure 1.11** shows an illustration of the interaction between the positively charged amine group of a poorly-water soluble drug with the negatively charged carboxylate group of a polymer.

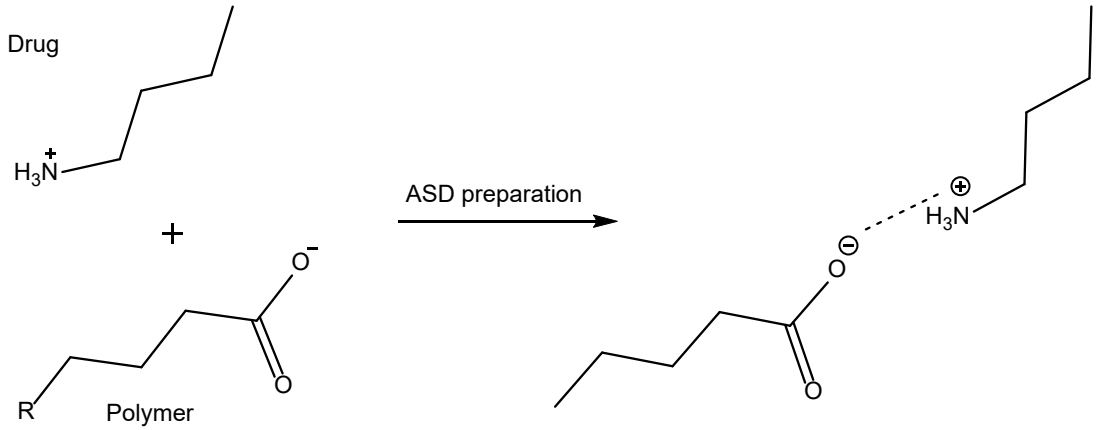

Figure 1.11. *An illustration of the interaction between a positively charged amine group of a poorly water-soluble drug with a negatively charged carboxylate group of a polymer following ASD preparation.*

1.3.3 Dissolution of polymeric amorphous solid dispersions

Dissolution characteristics of amorphous solid dispersions and the stability of the supersaturated state of a drug (when the amount of drug in solution is greater than the equilibrium solubility of the drug) can significantly enhance the bioavailability of the drug (52). Although *in vitro* dissolution tests may not accurately mimic the *in vivo* performance of a formulation, dissolution testing can be used to correlate dissolution differences between candidate formulations. During dissolution of an ASD, a supersaturated solution is often generated, and some polymers can inhibit drug crystallisation by prolonging the supersaturation state. The dissolution and solubilisation of an amorphous solid dispersion often follows a “spring and parachute” model (**Figure 1.12**) (56).

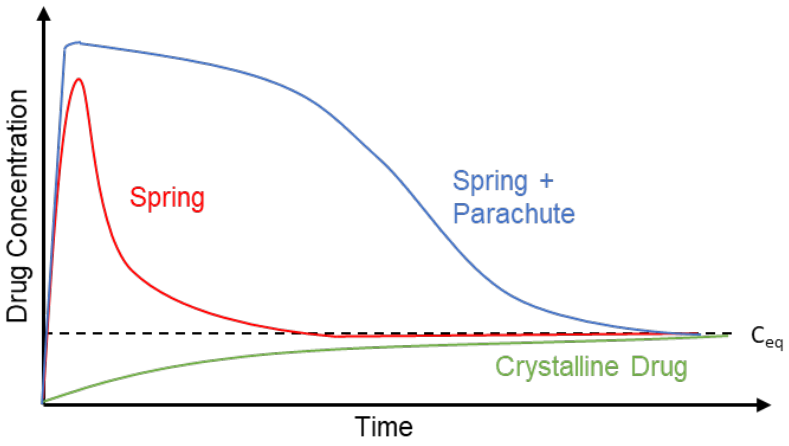

Figure 1.12. *The "spring and parachute" model. The drug and the hydrophilic polymer are dissolved to generate a supersaturated solution (spring). This is followed by a decrease in the drug concentration in solution due to absorption (parachute).*

Upon adding an amorphous solid dispersion to media, dissolution occurs rapidly, and a supersaturated solution is generated followed by a drop in the concentration of the drug in the media as crystallisation occurs. This ultimately reduces the concentration in solution to the equilibrium solubility of the crystalline drug (spring trace in **Figure 1.12**) (57). Polymers present in amorphous solid dispersions, however, can inhibit crystallisation of the drug. Polymer-drug interactions play an important role in stabilising the drug in solution and inhibiting crystal growth. Hydrophilic polymer carriers solubilise the drug and help maintain the supersaturated state by acting as parachutes over a period of time sufficient for the drug to get absorbed (58). The crystallisation of celecoxib from aqueous solutions of the pure drug and an ASD containing polyvinylpyrrolidone (PVP) was examined by Gupta et al. (59). The presence of higher amounts of PVP in the solid dispersion was found to delay crystallisation of the supersaturated drug solution. In addition, after 75 days of storage at 0% relative humidity (RH), the solid amorphous form of the pure drug showed 80% recrystallisation whereas storage of the 10% (w/w)

polymer/drug dispersion at 25 °C and 80% relative humidity (RH) condition for 75 days resulted in a 10% crystalline material.

1.4 Aims and objectives

The main objective of this thesis is to investigate the use of methacrylate-based polymers including poly(poly(ethylene glycol) methyl ether methacrylate), poly(2-(dimethylamino) ethyl methacrylate), and poly(methacrylic acid) with narrow molecular weight distribution in different formulation designs, including the fabrication of polyelectrolyte complex nanoparticles as well as amorphous solid dispersions.

Chapter 2 focuses on RAFT polymerisation of methacrylate-based monomers and details the synthesis of well-defined polymers and copolymers with narrow polydispersities. The broad aim of this project was to synthesise a library of cationic copolymers and anionic homopolymers with different lengths of the charged segments that could be used to form polyelectrolyte complex nanoparticles or amorphous solid dispersions .

Chapter 3 explores the ability of the synthesised polymers and copolymers of opposite charges to form stable monodispersed polyelectrolyte complex nanoparticles. We hypothesised that the narrow-dispersed polyelectrolytes may self-assemble by electrostatic interactions between the oppositely charged polymers, PDMAEMA and PMAA, with the non-ionised hydrophilic section, PPEGMA, acting as the stabilising agent. Their ability to encapsulate a number of anticancer drugs and facilitate the release of the drugs at mildly acidic pH is also covered in this chapter. It was hypothesised that the

destabilisation of the PECs at acidic pH would increase the rate of drug release compared to pH 7.4.

Chapter 4 focuses on development of amorphous solid dispersion formulations and the ability of RAFT-synthesised methacrylic acid polymers to produce ASDs with a model BCS class II drug, lidocaine, and overcome its problem of poorly water-solubility. We hypothesised that these acidic polymers will be able to produce lidocaine ASDs via formation of stabilising ionic interactions with the basic drug.

Chapter 2 Synthesis of methacrylate-based polymers and copolymers using RAFT polymerisation

2.1 Introduction

2.1.1 Methacrylate-based polymers

Poly(ethylene glycol) (PEG) has been widely studied as it is a non-ionic water-soluble polymer. The covalent conjugation of PEG to particles or molecules such as therapeutic drugs or proteins is known as PEGylation. PEGylation has proven to be beneficial for drug delivery as it decreases early degradation of drugs by enzymes and prevents adsorption of plasma proteins. The latter can trigger an immune response, and thus PEGylation can prolong circulation times to increase therapeutic efficacy (30, 60, 61).

Constructing PEG-based drug delivery systems has been explored extensively. Covalent conjugation of poly(ethylene glycol) onto the solvent-accessible side chains of proteins or nanoparticles is believed to offer advantages over EPR-based targeting of drugs to tumours as it increases their solubility, serum stability, and size (62, 63). The EPR effect allows the transport of macromolecules into tumour tissues (64). For instance, Doxil is an FDA-approved PEGylated liposomal formulation of doxorubicin. The PEG coating prolongs the circulation half-time of doxorubicin and aids passive accumulation of the drug at tumour sites, hence inhibiting early clearance and increasing the bioavailability (65). Oncaspar (pegaspargase), a PEGylated form of L-asparaginase, is another example of a PEGylated drug and is used as a first-line treatment of acute lymphoblastic leukaemia (66).

Another approach for taking advantage of the benefits of PEG for drug delivery is to use polymerisable functionalised PEG molecules such as poly(ethylene glycol) methyl ether methacrylate (PEGMA) (67). PEGMA has a methacrylate backbone with PEG chains. PEGMA monomers with different repeat units of PEG and varied molecular weights are available in the market. RAFT polymerisation allows for controlled polymerisation to yield well-defined high molecular weight PEG-based polymers (**Figure 2.1**).

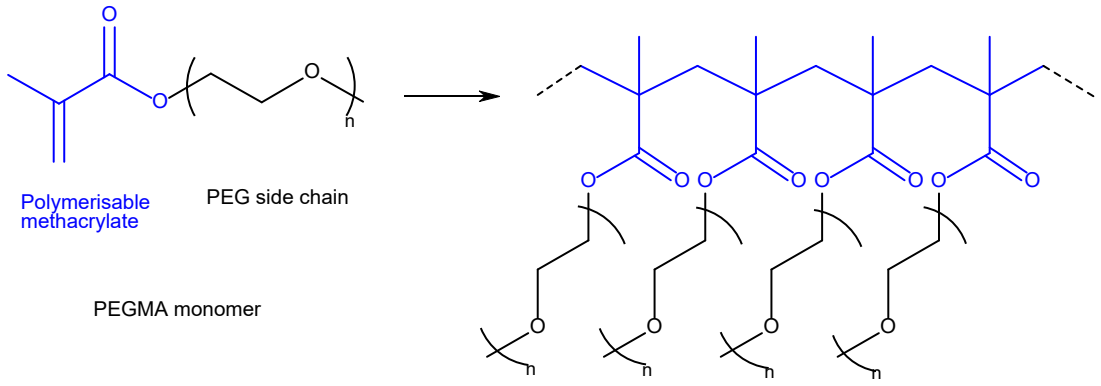

Figure 2.1. *Molecular structure of a PEGMA monomer and poly(PEGMA) containing a linear methacrylate backbone with a side chain of PEG (68).*

The number of repeat units and length of PEG can be altered by using PEGMA monomers of different molecular weights. Also, the length of the methacrylate backbone in PEGMA polymers could be altered by using different concentration ratios of monomer per RAFT agent. PEG-based polymers can be insoluble in water, readily soluble, or thermoresponsive, depending on the length of the PEG, the end group of PEG, and the nature of the polymerisable moiety. Poly(PEGMA)s with short PEG length (i.e., 4/5 PEG units) are hydrophilic polymers which exhibit a lower critical solution temperature in water and are believed to be thermoresponsive biocompatible materials (68). The

carbon-carbon backbone of the PEGMA polymer create a hydrophobic effect while the ether oxygens of PEG form stabilising H-bonds with water (**Figure 2.1**). Below the LCST, polymer-water interactions and the hydrophobic interactions between the polymer molecules are balanced, allowing the polymer to be soluble in water, whereas above the LCST polymer-polymer interactions are favoured, causing the polymers to precipitate at high temperatures.

Poly(2-(dimethylamino) ethyl methacrylate) (PDMAEMA) is responsive to changes in both pH and temperature (69). PDMAEMA is a weak polybase and is positively charged and soluble in water at neutral and acidic pH owing to protonation of the pendent tertiary amine groups (70). The chemical structure of DMAEMA monomer is shown in **Figure 2.2**.

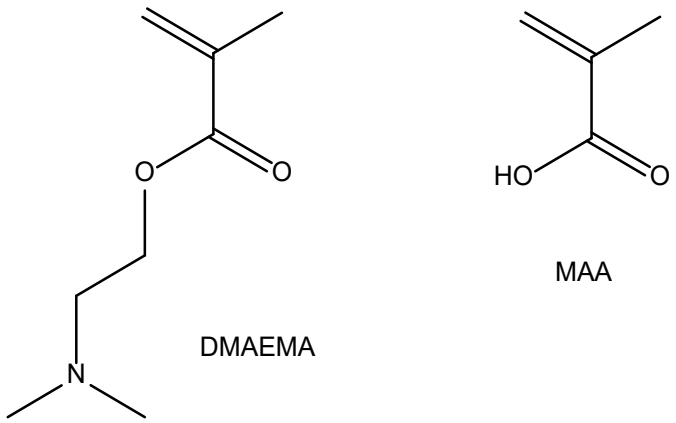

Figure 2.2. *Chemical structures of 2-(dimethylamino) ethyl methacrylate (DMAEMA) and methacrylic acid (MAA).*

Doubly responsive copolymers of poly(DMAEMA) and poly(poly(propylene glycol methacrylate)), poly(PPGMA), form reversible micelles in aqueous solutions (71). At elevated temperature and low pH, the hydrophobic

poly(PPGMA) forms the core of the micelles, and the protonated hydrophilic poly(DMAEMA) forms the corona. The reverse occurs at lower temperature and raised pH: micelles are formed with a hydrophilic poly(PPGMA) corona and the hydrophobic poly(DMAEMA) in the core.

Poly(methacrylic acid) (PMAA) is an anionic polyelectrolyte. The chemical structure of the MAA monomer is given in **Figure 2.2**. PMAA is soluble in water at all temperatures at neutral pH since it is deprotonated and negatively charged. The presence of PMAA has been observed to increase the hydrophilicity of polymeric micelles at neutral pH by forming hydrogen bonds with water (72). The solubility of PMAA decreases at lower pH due to protonation of the polymer.

These polymers could be used to design new drug delivery systems that are responsive to changes in pH and temperature in a physiological environment. Formation of responsive nano-sized polyelectrolyte complex nanoparticles using well-defined oppositely charged polyelectrolytes will be covered in detail in Chapter 3.

2.1.2 Characterisation

The chemical characteristics of polymers can be determined using nuclear magnetic resonance (NMR) spectroscopy. The two most common nuclei used in NMR spectroscopy, ^{1}H and ^{13}C, provide information about the environments of hydrogen and carbon atoms in the polymer structure (73). The intensity of the proton signals in a ^{1}H NMR spectra is proportional to the molar concentration of the species in the sample solution. Therefore, critical

information such as monomer conversion, degree of polymerisation (DP), and molecular weight of polymers (M_n) can be obtained from NMR spectra of the polymer reaction mixtures and end-group analysis. However, due to the reduced resolution of NMR spectroscopy for polymers with molecular weights greater than 25 kDa, use of NMR for measuring M_n of polymers is limited to polymers with lower molecular weights (74).

Gel permeation chromatography (GPC) is a type of liquid chromatography used to separate dissolved polymer molecules by their size in solution. A polymer solution dissolved in a liquid mobile phase flows through a stationary phase of tightly packed porous beads. The mode of separation is based on the size of the polymer molecules in solution (74). Polymer size in solution is a function of their molecular weight, structure, solubility, and non-covalent interactions with the stationary phase. Polymers elute from the column at different times, with larger polymers eluting first since molecules with smaller size are retained for longer times in the porous structures of the stationary phase (75). As a result, molecules with smaller solution sizes have an increased retention time.

In GPC, polymers are broadly fractionated by their molecular weight and are identified by the detectors usually using refractive index detectors. An elutogram is then generated displaying the molecular weight distribution of polymer species in the sample. In order to estimate the molecular weight of the polymer sample, the retention data are compared to a calibration based on a set of well-characterised monodispersed polymer standards, making GPC a relative method for estimation of molecular weight. The standards are usually

different to the polymers being analysed. The following important data for the polymer sample can then be estimated; number average molecular weight (M_n), weight average molecular weight (M_w), and molecular weight distribution (Đ).

2.2 Objectives

The motivation of our work was first to prepare PEGMA polymers using RAFT polymerisation. PEGMA homopolymers were then used as precursors to synthesise copolymers with DMAEMA. Poly(DMAEMA) possesses tertiary amine pendant groups resulting in cationic charge at physiological pH. Homopolymers of methacrylic acid were also synthesised to later prepare nanoparticle solutions containing oppositely charged polyelectrolytes. We aimed to synthesise well-defined polymers with narrow molecular weight distribution, and thus RAFT polymerisation was the selected polymerisation method.

2.3 Experimental

2.3.1 Materials

Poly(ethylene glycol) methyl ether methacrylate (PEGMA), methacrylic acid (MAA), 2-(dimethylamino) ethyl methacrylate (DMAEMA), 4-cyano-(phenyl-carbonothioylthio) pentanoic acid (CTA), and azobisisobutyronitrile (AIBN) were purchased from Sigma-Aldrich. 1,4-Dioxane and diethyl ether were supplied by Honeywell Specialty Chemicals. Hexane was purchased from Fisher Chemicals. Methanol (MeOH, 100%) was purchased from VWR

Chemicals. Deuterated dimethyl sulfoxide (d6-DMSO) was supplied by Cambridge Isotope Laboratories.

2.3.2 Synthesis of poly(PEGMA)

PEGMA **1** (1.00 g, 3.30 mmol, 20 eq.), CTA **2** (46.60 mg, 0.16 mmol, 1 eq.) and AIBN (2.74 mg, 0.016 mmol, 0.1 eq.) were dissolved in dioxane (7 ml) in a 25 ml single neck round bottom flask. The reaction mixture was sealed with a rubber septum and purged using argon for 30 minutes; the flask was then heated at 70 °C for 17 h under magnetic stirring as shown in **Figure 2.3**. The reaction was stopped by exposing the solution to open air via a needle and the polymer was precipitated twice in a 250 ml conical flask under mild stirring using 70 ml of cooled hexane (10× the volume of dioxane). The precipitated sample was washed with acetone (6 ml) and solvent was removed under vacuum using a Buchi Rotavapor R300. The poly(PEGMA) **3b** was obtained as a pink viscous liquid (owing to the colour of the CTA) in a 70% yield (735 mg) and was characterised using NMR spectroscopy and GPC. The same procedure was repeated with 10 (**3a**), 30 (**3c**), 50 (**3d**), and 70 (**3e**) equivalents of PEGMA.

2.3.3 Synthesis of poly(PEGMA)-co-poly(DMAEMA)s

Poly(PEGMA) **3b** (0.20 g, 0.028 mmol, 1 eq.), 2-(dimethylamino) ethyl methacrylate (DMAEMA) **4** (0.34 g, 2.10 mmol, 77 eq.) and AIBN (0.46 mg, 0.0028 mmol, 0.1 eq.) were dissolved in dioxane (3.78 ml) in a 10 ml single neck round bottom flask. The reaction mixture was sealed with a rubber septum and purged using argon for 30 minutes; the flask was then heated at

70 °C for 17 h under magnetic stirring. The reaction was stopped by exposing the solution to open air via a needle and the polymer was precipitated in a 100 ml conical flask using 38 ml of cooled hexane (10× the volume of dioxane) under mild stirring. The precipitated sample was washed with acetone (4 ml) and solvent was removed under vacuum using a rotary evaporator. The poly(PEGMA-co-PDMAEMA) **5b** was obtained as a viscous pink viscous liquid in a 75% yield (405 mg) and was characterised using NMR spectroscopy and GPC. The same procedure was repeated with 87 (**5a**), 48 (**5c**), and 30 (**5d**) equivalents of DMAEMA to prepare copolymers with a total DP of 100 using poly(PEGMA) **3a**, **3c**, and **3d** respectively. In addition, two copolymers with a total DP of 50 were synthesised with 27 (**5e**) and 15 (**5f**) targeted repeat units of DMAEMA using poly(PEGMA) **3a** and **3b** respectively.

2.3.4 Synthesis of poly(MAA)

Methacrylic acid **6** (1.00 g, 11.60 mmol, 85 eq.), CTA **2** (38.00 mg, 0.14 mmol, 1 eq.) and AIBN (2.24 mg, 0.014 mmol, 0.1 eq.) were dissolved in methanol (7 ml) in a 25 ml single neck round bottom flask. The reaction mixture was sealed with a rubber septum and purged using argon for 30 minutes; the flask was then heated at 70 °C for 17 h under magnetic stirring. The reaction was stopped by exposing the solution to open air via a needle and the polymer was precipitated twice in a 250 ml conical flask using 70 ml of cooled diethyl ether (10× the volume of methanol) with mild stirring. The obtained polymer was then washed with methanol (6 ml) and solvent was removed using vacuum using a rotary evaporator. PMAA **7b** was obtained as a pink powder in a 84% yield (667 mg) and was characterised using NMR spectroscopy and GPC. The

same procedure was repeated with 76 (**7a**), 58 (**7c**), 41 (**7d**), 28 (**7e**), and 18 (**7f**) equivalents of MAA.

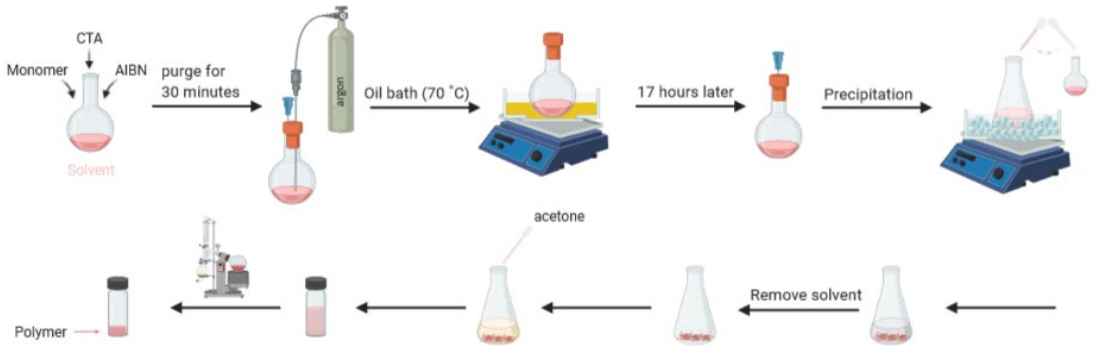

Figure 2.3. *Polymer synthesis process. Created with BioRender.com.*

2.3.5 Polymer characterisation

Solution state ^{1}H NMR spectra were recorded in d_6-DMSO using a Bruker Avance 400 MHz NMR spectrometer and were analysed using the Topspin software. The average length of the polymer molecules and the average molecular weight of the polymers and copolymers were measured by end-group analysis. This was done by comparing the proton signals from the repeat units of a polymer to those of the CTA agent.

Gel permeation chromatography (GPC) was conducted with DMF containing 5 mM NH_4BF_4 as the mobile phase, at 70 °C and with a flow rate of 1.00 mL/min. Polymer aliquots (100 µl, 5 mg ml^{-1} in DMF) were filtered through a nylon membrane with 0.22 µm pore size and were injected in a Malvern Viscotek system equipped with a refractive index (RI) detector. Poly(methylmethacrylate) (PMMA) standards were used for calibration and the OMNISEC software was used to determine the average molecular weight (M_n)

and polydispersity index ($Đ_M$). Four PMAA standards each containing two PMMA homopolymers with different molecular weights were used to calibrate the instrument. The molecular weights of the PMMA calibrants were as follows: sample 1 (26550 Da and 569000 Da), sample 2 (4770 Da and 98550 Da), sample 3 (10280 Da and 223900 Da) and sample 4 (960 Da and 72000 Da).

2.4 Results and discussion

2.4.1 Preparation of poly(poly(ethylene glycol) methyl ether methacrylate)

Poly(PEGMA)s (**3**) were synthesised using azobisisobutyronitrile (AIBN) and 4-cyano-(phenyl-carbonothioylthio) pentanoic acid **2**, which act as initiator and CTA respectively (**Scheme 2.1**). The target degrees of polymerisation were 10 (**3a**), 20 (**3b**), 30 (**3c**), 50 (**3d**) and 70 (**3e**).

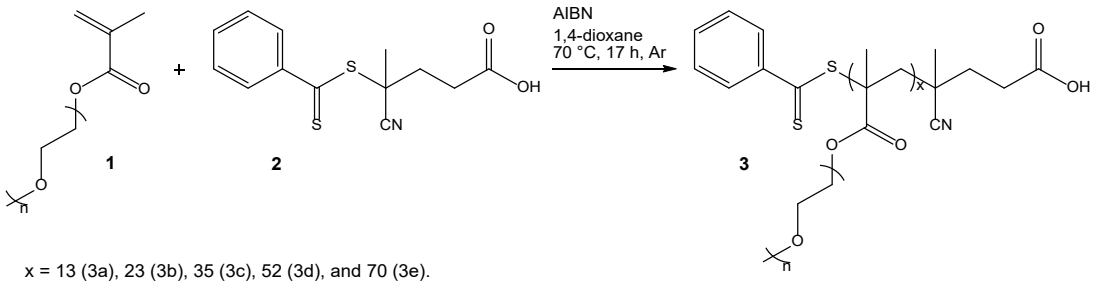

Scheme 2.1. *RAFT polymerisation of PEGMA **1** using 4-cyano-(phenyl-carbonothioylthio) pentanoic acid **2** as CTA, AIBN as initiator, and 1,4- dioxane as solvent.*

Monomer conversion was determined from the ^{1}H NMR spectrum of the crude non-purified material. The NMR peaks at $\delta_H \sim 4.03$ and 4.21 ppm were assigned to the methylene protons -C(=O)-OC**H$_2$**- of the polymer and monomer respectively, and the ratio of their integrals corresponds to the

monomer conversion. For instance, from the ^{1}H NMR spectrum of the crude sample of poly(PEGMA)$_{23}$ **3b**, a monomer conversion of 83% was calculated by dividing the integral at 4.03 ppm by the sum of the integrals at 4.03 and 4.21 ppm and multiplying by 100 (**Figure 2.4**). The monomer conversions of PEGMA polymers were found to range from 78% to 86%.

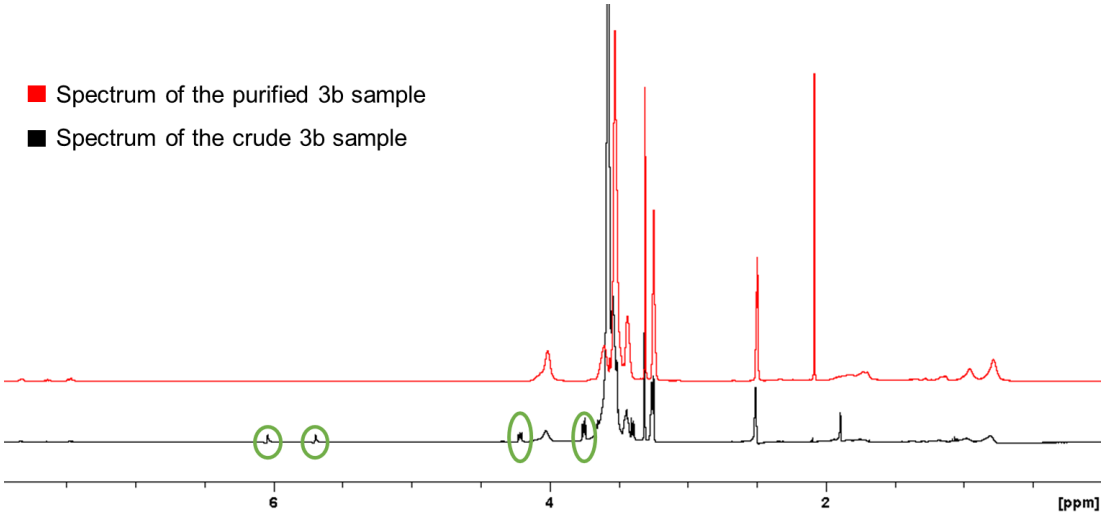

Figure 2.4. *^{1}H NMR spectra of the crude (black) and purified (red) poly(PEGMA)$_{23}$ **3b** samples. The circled proton signals of the unreacted monomers in the spectrum of the crude sample were cleared after purification.*

The absence of the peaks at $\delta_H \sim 5.70$ and 6.04 ppm (assigned to the –C=C**H**$_2$ group of the PEGMA monomers) indicates the complete removal of unreacted monomers after purification (**Figure 2.4**). The peaks at $\delta_H \sim 0.80$ and 1.74 ppm were assigned to –C**H**$_3$ and –C**H**$_2$ in the main chain repeat units of poly(PEGMA), respectively. The peaks at 2.1 and 2.5 ppm were assigned to acetone and d_6-DMSO, respectively. The ^{1}H NMR spectrum of the purified polymer **3b** is shown in **Figure 2.5**.

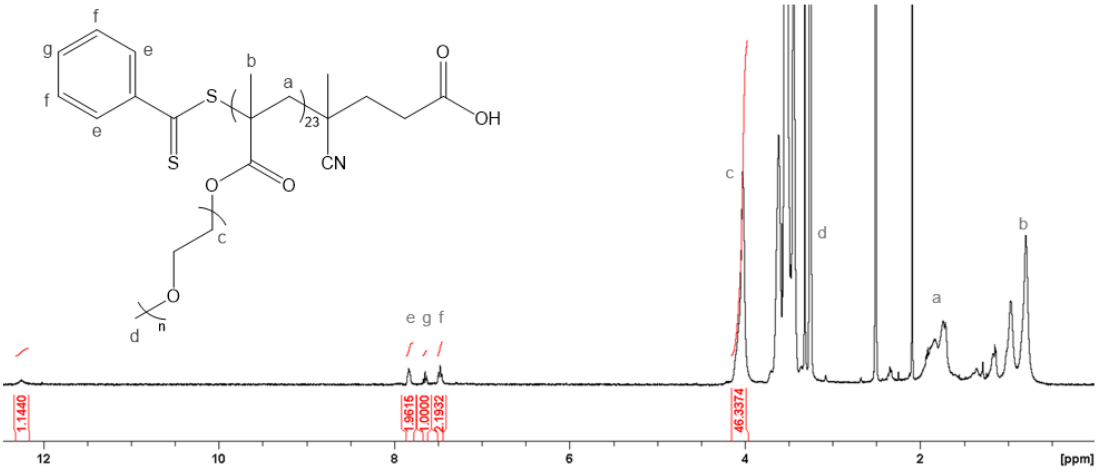

Figure 2.5. *^{1}H NMR (400 MHz, DMSO-d_6) spectrum of polymer **3b** (DP 23) and its proton labels. The integration of the aromatic proton (g) was calibrated to 1. The DP of the polymer was estimated by integrating the methylene -C(=O)-OC**H**$_2$- group of PEGMA divided by 2.*

The single peak at δ_H ~ 3.26 ppm was assigned to the methyl group –OC**H**$_3$ of poly(PEGMA). The single peak at δ_H ~ 12.26 ppm corresponds to the –O**H** group of the CTA. Finally, the peaks at δ_H ~ 7.48, 7.65, 7.83 ppm were triplet and were assigned to the aromatic protons of the CTA. The chain length (i.e., the degree of polymerisation) can be estimated using NMR spectroscopy by considering the number of protons and comparing the integral of the peaks assigned to the aromatic C**H** proton of the CTA and the methylene -C(=O)-OC**H**$_2$- group of the PEGMA. Details are reported in **Table 2.1** for each polymer that was prepared. According to the NMR spectrum, the synthesised poly(PEGMA) had a DP of 23 and M_n of 7200 Da (**Equation 2.1**).

$$M_{n^{poly(PEGMA)}} = \left[\left(I^{CH_2OCO}/_{I^{CH}}\right)/2\right] \times {M_W}^{PEGMA} + {M_W}^{CTA}$$

Equation 2.1. *Calculation of M_n based on end group NMR analysis where ${M_W}^{PEGMA}$, ${M_W}^{CTA}$, I^{CH2OCO}, and I^{CH} correspond to the molar mass of PEGMA, molar mass of the CTA, signal integration at 4.03 ppm of CH_2OCO of the polymer, and signal integration at 7.65 ppm of the aromatic proton of the CTA, respectively.*

The DP of the PEGMA polymers estimated by ^{1}H NMR are similar to the targeted DPs shown as [PEGMA]:[CTA] in **Table 2.1**. This confirms the good control of the RAFT process over the polymerisation of PEGMA. At the end of the polymerisation process, the polymers possess the R group of the RAFT agent at one end and the (Z─C(=S)S─) group at the other, which enables onward synthesis of block copolymers via the sequential polymerisation of the second monomer, DMAEMA.

The GPC traces of each PEGMA polymer that was prepared are shown in **Figure 2.6** and the M_n and polydispersity index ($Đ_M$) values are listed in **Table 2.1**. Peak tailing was observed in the GPC traces of poly(PEGMA)s with lower DP. Because peak tailing can influence the quality of a separation, asymmetry factor (A_s) of each of the polymers' traces were calculated by dividing the front half width at 10% of the peak height by the back half width. The A_s values ranged from 1.16 to 2.0 which are considered acceptable. $Đ_M$ values were lower than 1.2, ranging from 1.09 to 1.2, indicating a narrow molecular weight distribution and confirming that there was good control of the polymerisation. A $Đ_M$ value between 1.2 and 1.5 would suggest some control over the polymerisation, while a $Đ_M$ value above 1.5 indicates a lack of control over the process. According to the GPC results, the PEGMA polymers with smaller chain lengths had higher polydispersity indices. This is because small changes in their repeat units are more detectable.

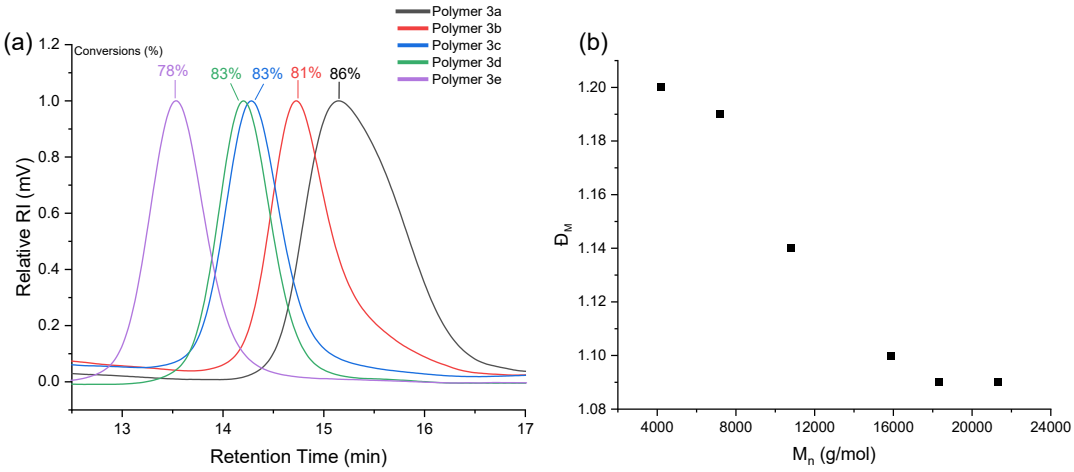

Figure 2.6. *(a) GPC traces of PEGMA polymers synthesised via RAFT polymerisation with degrees of polymerisation of 13, 23, 35, 52, and 70 (details are listed in* ***Table 2.1****); (b) index of polydispersity ($Đ_M$) versus number average molecular weight (M_n).*

Synthesis of PEGMA polymers using ATRP and group transfer polymerisation (GTP) methods has been reported previously. However, reports on synthesis of PEGMA homopolymers via RAFT polymerisation have been limited. In a study by Mertoglu et al., a series of water-soluble monomers were polymerised in water via RAFT (77). Controlled polymerisation in water was possible with styrene-based, acrylamide, and methacrylic monomers. Poly(PEGMA)s with molecular weight of 56000 Da and polydispersity index of 1.1 were synthesised using $PEGMA_{475}$ as the monomers and 4-thiobenzoylthio-4-cyanopentanoic acid as the RAFT agent. Even though different solvent (water) and reaction temperature (55 ˚C) were used for the RAFT polymerisation of $PEGMA_{475}$ than in this project, synthesis of PEGMA polymers with low polydispersity using RAFT polymerisation was possible in different reaction conditions.

Table 2.1. *^{1}H NMR and GPC results for the synthesised poly(PEGMA)s.*

P(PEGMA)	[PEGMA]:[CTA]	Monomer Conversion (%)	M_n [a] (Da)	M_n [b] (Da)	$Đ_M$	DP [a]
3a	10	86	4200	3600	1.2	13
3b	20	83	7200	5600	1.19	23
3c	30	83	10800	6700	1.14	35
3d	50	83	15900	16300	1.1	52
3e	70	78	21300	18100	1.09	70

[a] estimated using ^{1}H NMR spectroscopy.
[b] estimated using GPC.

2.4.2 Preparation of poly(PEGMA)-co-poly(DMAEMA) block copolymers

For the successful synthesis of well-defined block copolymers using RAFT polymerisation, the macro-R group (the synthesised first block of the copolymer) must be a good homolytic leaving group. PEGMA polymers, as macro-RAFT agents, produce stabilised propagating radicals necessary for reinitiating polymerisation of the second monomer. The concentration of the initiator also plays an important role in the formation of polymers with similar chain lengths and a narrow molecular weight dispersity. Generation of initiator-derived chains and formation of dead chains can be minimised by using a low concentration of the initiator compared to the concentration of the macro-RAFT agent (8).

Each poly(PEGMA) was used as a macro-CTA for the RAFT polymerisation of DMAEMA to form hydrophilic pH-responsive block copolymers containing a total of 100 or 50 repeat units per chain (**Scheme 2.2**). For instance, for the

copolymerisation of poly(PEGMA)$_{23}$ **3b** to a total DP of 100, a [poly(PEGMA)$_{23}$]: [CTA] ratio of 77 to 1 was used. The ratio of the integrals of the peaks assigned to the methylene protons -C(=O)-OC**H$_2$**- of the polymer and monomer observed in the NMR spectrum of the crude sample corresponds to the monomer conversion, which was found to range from 66 to 97% (**Table 2.2**).

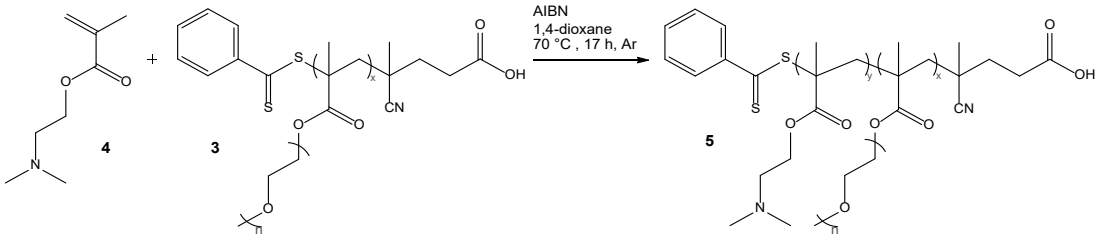

Scheme 2.2. *RAFT polymerisation of poly(PEGMA)* ***3*** *with DMAEMA* ***4*** *using AIBN as initiator, and 1, 4-dioxane as solvent.*

^{1}H NMR spectroscopy of the purified copolymers was carried out to verify the composition. The structure of copolymer **5b** and its ^{1}H NMR spectrum are displayed in **Figure 2.7**. The ^{1}H NMR spectrum of copolymer **5b** after purification shows no trace of unreacted monomers. The peak at $\delta_H \sim 3.99$ ppm was assigned to the –C**H$_2$**O- group of both poly(PEGMA) and poly(DMAEMA). The peaks at 2.1 and 2.5 ppm were assigned to acetone and d$_6$-DMSO, respectively.

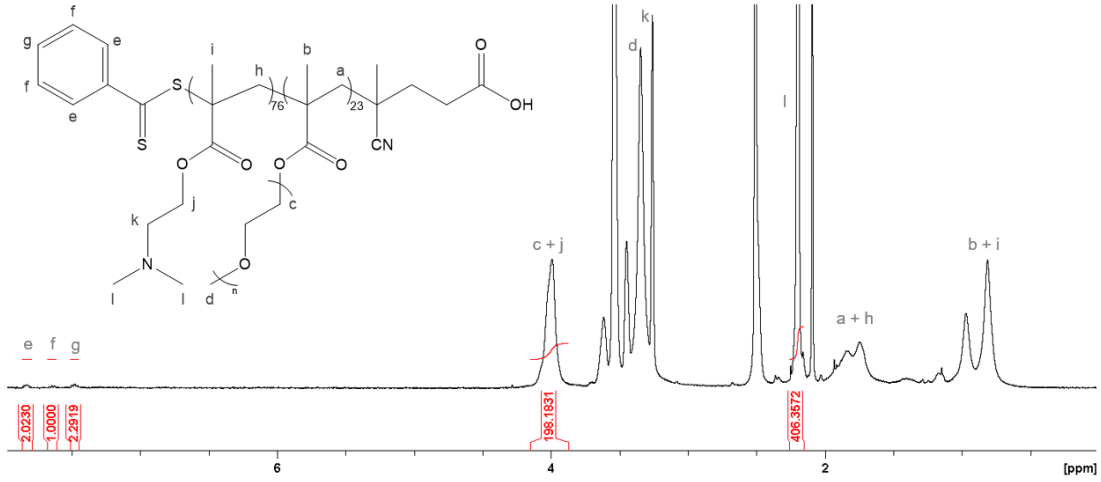

Figure 2.7. *^{1}H NMR (400 MHz, DMSO-d_6) spectrum of copolymer **5b** (DP 99) and its proton labels. The integration of the aromatic proton (g) was set to 1. The DP of the copolymer was estimated by integrating the methylene -C(=O)-OC**H**$_2$- group of PEGMA and DMAEMA and dividing by 2. The DP of DMAEMA was calculated by subtracting the DP of poly(PEGMA) from the total DP of the copolymer.*

The integration of the peak at 3.99 ppm was compared with the signal integration of the aromatic protons of the CTA to estimate the degree of polymerisation. The degree of polymerisation of the PEGMA-DMAEMA copolymer **5b** (99) was calculated by dividing the integration of this peak by two, since the integral corresponds to two protons. The degree of polymerisation of DMAEMA (76) was calculated by subtracting the DP of PEGMA (23) from the total DP (99). The DP of DMAEMA could also be estimated by integrating the peak assigned to the methyl groups of the tertiary amine. The molecular weights of the copolymers were calculated using **Equation 2.2**. The molecular weight of copolymer **5b** was found to be 18800 Da. The NMR results of the copolymers including their estimated molecular weight and DP are summarised in **Table 2.2**.

$$M_{n^{copolymer}} = \left[\left(\left(I^{CH_2OCO}/_{I^{CH}}\right)/2\right) - DP_{PPEGMA}\right] \times M_W{}^{DMAEMA} + M_n{}^{PPEGMA} + M_w{}^{CTA}$$

Equation 2.2. *Calculation of M_n of the copolymer based on end group NMR analysis where DP_{PEGMA}, $M_w{}^{DMAEMA}$, $M_n{}^{PPEGMA}$, and $M_w{}^{CTA}$ correspond to the degree of polymerisation of poly(PEGMA), molar mass of DMAEMA, number average molecular weight of the poly(PEGMA) used as macro-RAFT agent, and molar mass of CTA, respectively. I^{CH2OCO} and I^{CH} correspond to signal integration at 3.99 ppm of CH_2OCO from both polymers and signal integration at 7.65 ppm of the aromatic proton of the CTA, respectively.*

As with the previous ^{1}H NMR spectra, the aromatic protons of the CTA were found at $\delta_H \sim$ 7.48, 7.65, 7.83 ppm. The presence of a broad singlet peak at $\delta_H \sim$ 2.19 ppm indicates the presence of DMAEMA in the copolymer. The peaks detected at $\delta_H \sim$ 0.81 and 1.75 ppm were assigned to the –C**H**$_3$ and –C**H**$_2$ groups of the repeat units in the main chain of poly(PEGMA) and poly(DMAEMA). The peaks at $\delta_H \sim$ 3.26 and 3.34 ppm were assigned to the two protons of the -C**H**$_2$N- group of poly(DMAEMA) and the three protons in the C**H**$_3$-O- group of poly(PEGMA), respectively.

The DP of the DMAEMA block of the copolymers estimated by ^{1}H NMR are similar to the targeted DPs shown as [DMAEMA]:[macro-CTA] which confirms the suitability of the RAFT polymerisation for synthesis of block copolymer via sequential polymerisation. This also confirms the ability of the previously synthesised PEGMA polymers to act as macro-RAFT agents and reinitiate polymerisation of DMAEMA.

The GPC results of the copolymers including the M_n and $Đ_M$ of each copolymer are summarised in **Table 2.2**. The narrow molecular weight dispersities of the block copolymers indicate the ability of the R group of the macro-RAFT agent to fragment and reinitiate polymerisation and facilitate efficient chain transfer. Thus, the poly(PEGMA)s acted as an effective macro-RAFT agent to give

block copolymers. The block copolymers had narrow molecular weight distributions ranging from 1.1 to 1.2. Copolymerisation of poly(PEGMA)s with DMAEMA was associated with a shift of the peaks to shorter elution times on GPC. Copolymer **5b** was eluted 1.19 minutes sooner than its poly(PEGMA) precursor **3b** which indicates an increase in the size of the polymers in solution after copolymerisation (**Figure 2.8**).

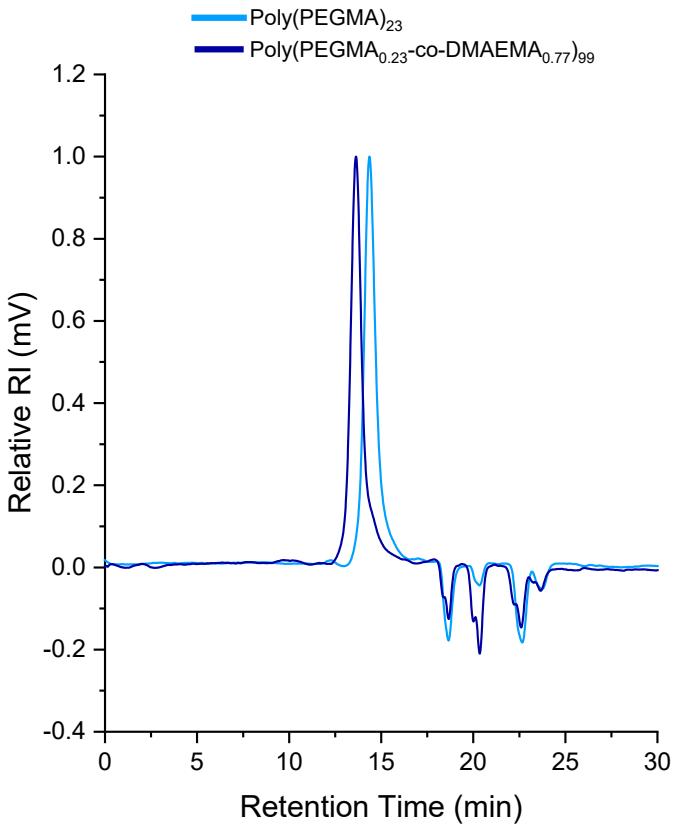

Figure 2.8. *GPC traces of the PEGMA homopolymer* ***3b*** *(DP=23, M_n=5600, M_w/M_n=1.19) and the resultant copolymer* ***5b*** *(DP_{PEGMA}=23, DP_{DMAEMA}=76, M_n=20800, M_w/M_n=1.19) measured in DMF over 30 minutes. The GPC traces also show solvent inverse peaks between 17 and 25 min.*

Copolymerisation of PEGMA and DMAEMA has previously been reported. Formation of a similar copolymer, poly(DEAEMA-co-PEGMa), was reported by Shahalom et al. (76). The copolymers were prepared using conventional free-radical copolymerisation of diethylaminoethyl methacrylate (DEAEMA) and

poly(ethylene glycol) methacrylate (PEGMa) and had a polydispersity of 2.0. The RAFT process used here is clearly advantageous in producing more monodispersed materials.

RAFT polymerisation has also been used to synthesise similar copolymers. Fournier et al. synthesised random copolymers of $PEGMA_{300}$ and DMAEMA via RAFT polymerisation using azobisisobutyronitrile as initiator, 2-cyano-2-butyldithiobenzoate (CBDB) as the RAFT agent, and toluene as solvent (78). The polydispersity index of these random copolymers was in the range of 1.11 to 1.30. An increase in the PEGMA content of the copolymers was reported to result in an increase in the PDI value which is in contrast with the results obtained here (see **Table 2.2**). This could be due to the synthesis of different type of polymers: the literature report concerns random copolymers, whereas in this chapter we synthesised block copolymers synthesised using sequential polymerisation.

Synthesis of well-defined block copolymers composed of $PEGMA_{475}$ and DMAEMA by sequential RAFT polymerisation was reported by Venkataraman et al. (79). $PEGMA_7$-block-$DMAEMA_{53}$ polymers with PDI of 1.25 were synthesised under similar conditions as reported here and were used to complex with DNA. DMAEMA has also been copolymerised with poly(2-hydroxyethyl methacrylate (PHEMA), an uncharged non-toxic hydrophilic polymer via sequential RAFT polymerisation (80). Water soluble block copolymers with narrow polydispersities were reportedly formed and used to complex with plasmid DNA. The linear block copolymers in the mentioned studies were constructed to provide better accessibility for charge-to-charge

interaction with DNA compared to random copolymers and provide gene transfection efficiency as well as biocompatibility. Similarly, in this project, block copolymers were synthesised with the aim to interact and complex with an oppositely charged polyelectrolyte. However, here we aim to use the complexes for drug delivery.

Table 2.2. *^{1}H NMR and GPC data for the copolymers.*

Copolymer	Macro-CTA	[DMAEMA]:[Macro-CTA]	Monomer Conversion (%)	M_n [a] (Da)	M_n [b] (Da)	$Đ_M$	DP [a]
5a	3a	87	69	17300	20700	1.2	98
5b	3b	77	66	18800	20800	1.19	99
5c	3d	48	95	24700	27800	1.15	110
5d	3e	30	97	27400	30400	1.14	111
5e	3b	27	75	11300	13000	1.13	51
5f	3c	15	86	13300	16100	1.11	53

[a] estimated using ^{1}H NMR spectroscopy.
[b] estimated using GPC.

2.4.3 Preparation of poly(methacrylic acid)

Poly(methacrylic acid) (PMAA) **7** was also synthesised using RAFT polymerisation (**Scheme 2.3**). To reduce the formation of initiator-derived dead chains a high ratio of CTA to AIBN ([CTA]/AIBN]=10) was chosen. High monomer conversions (84-95%) were achieved while maintaining low polydispersity (<1.2). Degrees of polymerisation similar to those of the poly(DMAEMA) blocks of the copolymers were targeted; 85, 76, 58, 41, 28, and 18.

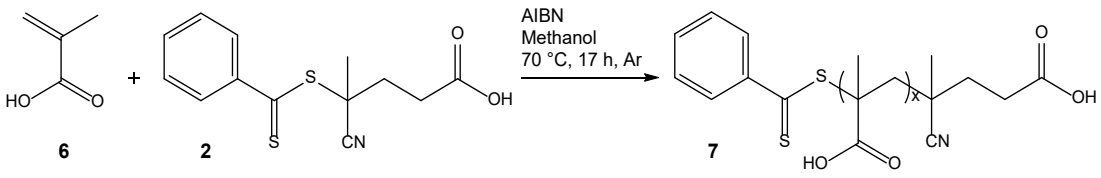

x = 88 (7a), 75 (7b), 52 (7c), 46 (7d), 31 (7e), and 23 (7f).

Scheme 2.3. *RAFT polymerisation of MAA* ***6*** *using 4-cyano-(phenyl-carbonothioylthio) pentanoic acid* ***2*** *as CTA, AIBN as initiator, and methanol as solvent.*

Methanol was the solvent of choice as it has been reported to be a suitable solvent for polymerisation of MAA and to provide good control over polymerisation, whereas using water/dioxane as the solvent led to CTA degradation and poor polymerisation control (81). The monomer conversion was determined using NMR spectroscopy of the crude samples (non-purified samples), and the findings are listed in **Table 2.3**. Peaks in the NMR spectrum at $\delta_H \sim 5.59$ and 5.98 ppm are assigned to the protons of the –C=C**H**$_2$ group of the monomers (**Figure 2.9**). These peaks decrease in intensity as polymerisation proceeds.

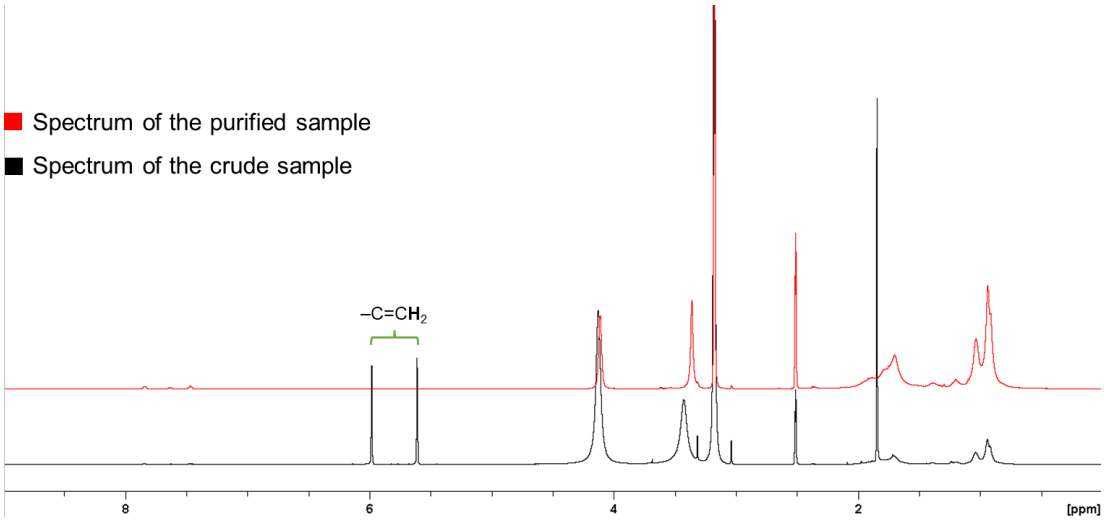

Figure 2.9. *^{1}H NMR spectra of the crude (black) and purified (red) poly(MAA)$_{75}$* ***7b*** *samples. The assigned proton signals of the unreacted monomers at δ_H ~ 5.59 and 5.98 ppm in the spectrum of the crude sample were cleared after purification.*

The peaks at δ_H ~ 0.94 and 1.70 ppm were assigned to -C**H**$_3$ and -C**H**$_2$ groups of the polymer repeat unit. As the polymerisation proceeds, signals of the methacrylate backbone increase. A monomer conversion of 84% was found by calculating the ratio of the integrals of these monomeric and polymeric signals. The peak at 2.5 ppm was assigned to d_6-DMSO. The structure of PMAA and the ^{1}H NMR spectrum of polymer **7b** (after purification) are displayed in **Figure 2.10.**

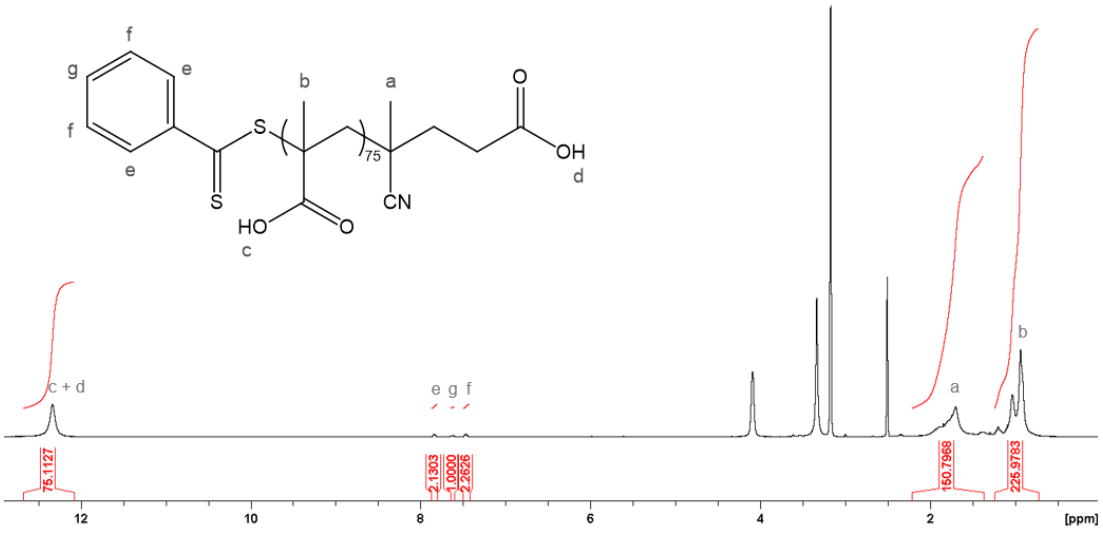

Figure 2.10. *^{1}H NMR (400 MHz, DMSO-d_6) spectrum of polymer **7b** (DP 75) and its proton labels. The integration of the aromatic proton (g) was set to 1. The DP was estimated by integrating the hydroxyl group of methacrylic acid.*

The absence of the peaks at δ_H ~ 5.59 and 5.98 ppm in the spectra of the purified samples indicates the complete removal of the unreacted MAA monomers. In addition, after polymerisation, a broadened peak at δ_H ~ 12.34 ppm was observed in the spectrum. This peak was assigned to the –O**H** group of both the CTA and PMAA. Additionally, peaks at δ_H ~ 7.46, 7.63 and 7.84 ppm were detected and attributed to the protons of the CTA benzyl group. Hence, we can estimate the chain length of the polymer by comparing the integrals of the peak of CTA to that of the -C**H**$_3$ group of the polymers. For polymer **7b**, a degree of polymerisation of 76 was chosen to match the DP of the DMAEMA block of copolymer **5b**. According to the NMR spectrum, the synthesised poly(methacrylic acid) had a DP of 75 and M_n of 6700 Da.

According to the ^{1}H NMR results, MAA polymers with DPs similar to the targeted DPs (shown as [MAA]:[CTA] in **Table 2.3**) were synthesised. The average molecular weight (M_n) and dispersity ($Đ_M$) were estimated by GPC

(**Figure 2.11**). The monomer conversion, $Đ_M$ and M_n are summarised in **Table 2.3**. The amount of tailing of the GPC traces of MAA polymers was calculated. The A_s values ranged from 1.1 to 2.0 with MAA polymers with lower DPs (23 and 31) showing the most tailing. The $Đ_M$ values of the polymers range from 1.05 to 1.15 indicating a narrow molecular weight distribution. The polydispersity of polymers usually decreases with increasing degrees of polymerisation, which is also seen in this work. In theory, using RAFT polymerisation allows chains to start growing at the same time. However, in practice, all chains do not start growing at the same time, leading to retardation. The retardation effect does not influence the polydispersity significantly; however, it is more detectable in polymers with low DPs. Therefore, the synthesised polymers with lower degrees of polymerisation (and lower molecular weights) have higher polydispersity values as small variations in their repeat units are more noticeable.

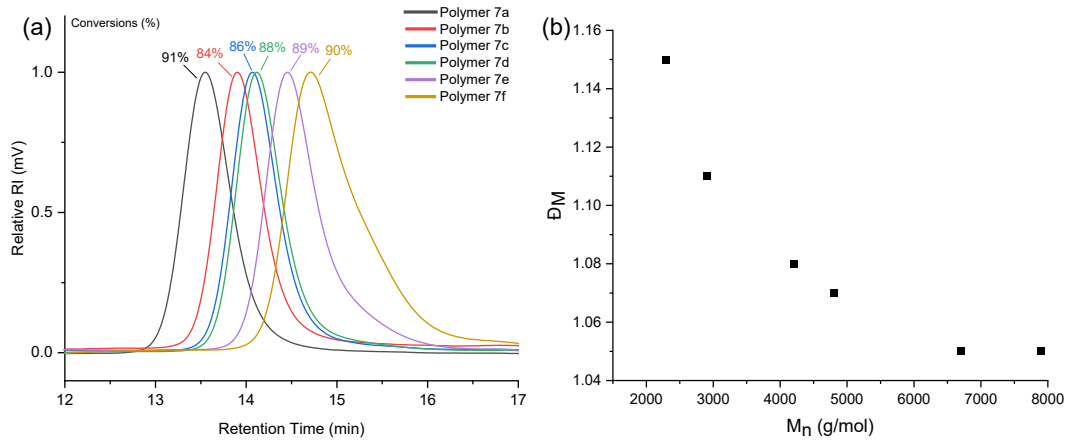

Figure 2.11. *(a) GPC traces of methacrylic acid homopolymers synthesised via RAFT polymerisation with degrees of polymerisation of 23, 31, 46, 52, 75, and 88 (details are listed in* ***Table 2.3****); (b) index of polydispersity ($Đ_M$) versus number average molecular weight (M_n).*

RAFT polymerisation of MAA has been previously investigated in detail. Chaduc et al. reported synthesis of well-defined MAA polymers using RAFT polymerisation in different solvents including methanol, dioxane, and water (82). A linear increase in the molar mass of the polymers was observed with increasing conversion in all the solvents. The PDI of the polymers synthesised in water were found to be lower than that in methanol or dioxane. Control over polymerisation of MAA in water however was lost at pH above the pK_a of MAA. RAFT homopolymerisation of MAA in water/dioxane and methanol has also been reported by Pelet et al. (81). PMAAs with different molecular wights up to 113900 Da with narrow PDI were successfully synthesised in methanol. The polymers had high conversions and the PDI of the MAA homopolymers decreased as the DP of the polymers increased. This was in agreement with the results described in this chapter.

Table 2.3. *^{1}H NMR and GPC results for poly(MAA) samples.*

P(MAA)	[MAA]:[CTA]	Monomer Conversion (%)	M_n [a] (Da)	M_n [b] (Da)	$Đ_M$	DP [a]
7a	85	84	7900	15500	1.05	88
7b	76	84	6700	12800	1.05	75
7c	58	86	4800	10700	1.07	52
7d	41	88	4200	10200	1.08	46
7e	28	89	2900	7200	1.11	31
7f	18	90	2300	5300	1.15	23

[a] estimated using ^{1}H NMR spectroscopy.
[b] estimated using GPC.

2.5 Discussion

The thiocarbonylthio CTA used in this project has previously been reported to be suitable for RAFT polymerisation of methacrylic monomers, providing good control over their polymerisation by providing a high rate of reversible chain transfer and rapid equilibration of growing polymer chains (8, 83, 84). As shown in Tables 2.1-2.3, RAFT polymerisation allowed for synthesis of polymers and copolymers with close-to target DPs and narrow PDI values. This was made possible by choosing the right RAFT agent for the polymerisation reaction as well as using the correct amount of initiator and RAFT agent for each reaction.

Radically polymerisable monomers can be divided into two groups based on their reactivity: “more activated monomers” (MAMs) and “less activated monomers” (LAMs). The vinyl group of MAMs is conjugated to an aromatic group, a nitrile, or a carbonyl group; whereas the vinyl group of LAMs is adjacent to oxygen, nitrogen, or sulphur (4). All the monomers used in this work are considered to be MAMs as their vinyl group is conjugated to a carbonyl group. Therefore, a chain transfer agent with high reactivity toward radical addition was used to ensure successful RAFT polymerisation (10). This was particularly important for the synthesis of block copolymers where monomers were sequentially added. The molecular weights of the polymers increased with an increase in their degree of polymerisation. The synthesized PEGMA homopolymers were able to efficiently re-initiate polymerisation of the second monomer and facilitated the synthesis of block copolymers with increased degrees of polymerisation and molecular weights as evidenced from

the ^{1}H NMR results and the existence of a single peak in the GPC traces of the copolymers.

According to the GPC results, the synthesized polymers and copolymers have a narrow distribution of molecular weights with polydispersity values ranging from 1.05 to 1.2. A slight tailing was detected in some of the GPC traces of polymers with lower molecular weights (**Figure 2.6a**, **Figure 2.11a**). The presence of shouldering peaks can be due to presence of dead chains and/or injecting unfiltered samples. Peak tailing can influence the quality of a separation; however, the degrees of tailing in all the GPC traces were acceptable as the asymmetry factors (A_s) were no more than 2. Additionally, the prevalence of dead chains formed through termination during RAFT polymerisation is negligible; therefore, the quality of the final product is not affected.

The principle of polymer separation in GPC columns is based on the size of the polymer coils formed in solution rather than the molecular weights of the polymers. In addition, the results obtained from GPC require conversion into molecular weight scale using a calibration method using PMMA standards which makes GPC a relative method of analysis and susceptible to significant errors. The dissimilarities between the synthesised methacrylic acid polymers and the PMMA standards used for calibration as well as their conformation differences in solution could also result in inaccurate estimation of the molecular weight of the samples. Due to the strong dependence of the data on the calibrant, GPC was used in conjunction with ^{1}H NMR spectroscopy to corroborate data for estimating the molecular weight characteristics of the co-

polymers. In addition, GPC is unable to provide molecular weight measurements of different blocks of block copolymers. ^{1}H NMR, on the other hand, is a more accurate quantitative method of analysis that does not require calibration. However, reduction of the resolution is expected for polymers samples with molecular weights greater than 25 kDa (74). Nevertheless, the results obtained from ^{1}H NMR and GPC are consistent as regards to the increase in the molecular weights of the homopolymers with increasing degrees of polymerisation.

2.6 Conclusions

A library of methacrylate-based polymers (PPEGMA and PMAA) and copolymers (poly(PEGMA-co-DMAEMA)) were synthesised via RAFT polymerisation. The degree of polymerisation and molecular weights of the polymers and copolymers were controlled by varying the monomer to CTA ratios. Copolymers of PPEGMA and PDMAEMA were obtained by sequential RAFT polymerisation with purification processes undertaken before and after the addition of the second monomer. Optimal control in RAFT polymerisation was achieved by choosing an appropriate RAFT agent for the monomers and was confirmed by the synthesis of polymers with targeted DPs and the low PDI of the polymers determined by ^{1}H NMR analysis and GPC, respectively. The reproducibility and the control over synthesis of polymers with narrow molecular weight distribution offered by RAFT polymerisation have a major effect on the performance of these polymers. This includes the size and size distribution of the complexes formed by these polymers as well as the drug loading and release profile. Variations in drug loading capacity and release

profile of complexes formed using polymers with wide molecular weight distribution would ultimately affect the *in vivo* performance of drugs.

The copolymers were synthesised with a biocompatible block of PEGMA and a cationic block of DMAEMA with the aim to complex with the synthesised anionic homopolymer (PMAA) to form polyelectrolyte complex nanoparticles.

Chapter 3 Preparation of PEC nanoparticles and encapsulation and release of model drugs

3.1 Introduction

It is well-established that the driving force of formation of polyion complex micelles formed from oppositely charged block copolymers is the electrostatic interaction between the charged segments (85). Similarly, formation of polyelectrolyte complex nanoparticles in solution is derived by spontaneous polyelectrolyte coacervation as a result of electrostatic interactions between a cationic and anionic polymer. In addition, their stability is determined by the net charge of the PECs and the repulsion between nanoparticles with similar charges (86). Therefore, strong overall positive or negative net charges are needed for the formation of stable PECs. Other key parameters affecting the properties of PECs are the molecular weights of the polymers, polymer concentration in solution, and the molar mixing ratio of the polycation to polyanion.

Methacrylic acid has a pK_a value of 4.65; therefore, at pH values higher than 4.65, it is deprotonated and becomes ionised and negatively charged. 2-(Dimethylamino) ethyl methacrylate, on the other hand, has a basic character with pK_a of 8.44, below which it is positively charged. Similar polymers have previously been used to form polyelectrolyte complexes. A mixture of poly(ethylene oxide-block-2-(diethylamino)ethyl methacrylate) (PEO_{113}-b-$PDEA_{50}$) copolymer and poly(methacrylic acid) (PMAA) was found to form three types of complexes in solutions with different pH values (87). At pH

above 8, PMAA did not interact with the copolymer and did not participate in the formation of complexes, but micelles with mean diameter of 25 nm were formed with PEO as the corona and hydrophobic PDEA in the core. At pH 6-8.5, PDEA was partially protonated and micelles with mean diameter of 32-35 nm were formed with charge compensated PDEA/PMAA cores and PEO as the corona. Further lowering of the pH of the solution was found to cause dissociation of the particles.

Polyelectrolyte complexes can be used as drug delivery systems. An example of PECs for drug delivery are complexes formed from a random copolymer of diallyldimethylammonium (DADMA) and acrylic acid (AA) as the polycation and poly(styrenesulfonate) as polyanion (88). These were reported to have pH-tunable solubility and were suggested to be suitable as enteric coating materials for gastrointestinal drug delivery, as the coating would be ionised and soluble in intestinal fluid at high pH.

pH-Responsive nanoparticles sense changes in the pH of their environment and respond to them by altering their structure, e.g., swelling, dissociation, or changing surface characteristics (e.g., charge). These changes can then facilitate drug release at the acidic target site rather than releasing the drug in the blood stream. For instance, a paclitaxel-loaded micellar system consisting of poly(ethylene glycol)-block-polylactide exhibited pH-triggered release of the drug in acidic environments (89). In this chapter, we mainly focus on the formation of polyelectrolyte complex nanoparticles using the RAFT-synthesised cationic copolymers and anionic homopolymers. A schematic representation of a PEC formed using the block copolymer consisting of a

cationic and a neutral hydrophilic block, poly(PEGMA-co-DMAEMA), and the anionic homopolymer, PMAA, with similar polyelectrolyte chain length can be seen in **Figure 3.1**.

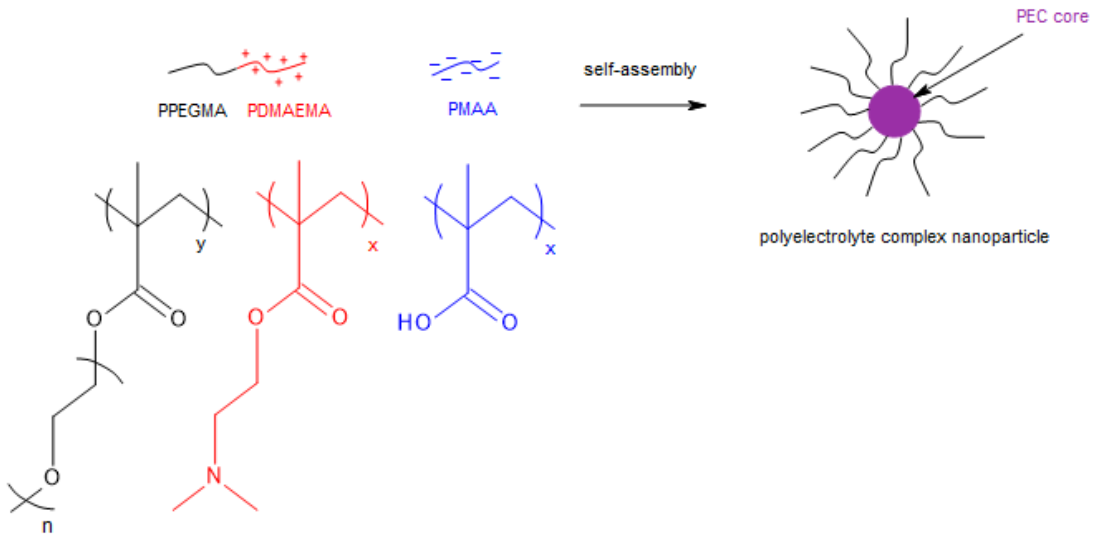

Figure 3.1. *Self-assembly of the cationic copolymer and the anionic homopolymer into a PEC nanoparticle. A core-shell structure is formed through electrostatic interaction between the polyelectrolytes.*

3.2 Objectives

The first objective of this chapter was to prepare pH-responsive polyelectrolyte complex nanoparticles using the polymers synthesised in Chapter 2. Under physiological conditions, poly(2-(dimethylamino) ethyl methacrylate) (PDMAEMA) block of the copolymer and poly(methacrylic acid) (PMAA) are expected to bind electrostatically to form the charge neutralised core of the PECs. The hydrophilic non-ionic block of the copolymer, poly(poly(ethylene glycol) methyl ether methacrylate) (PPEGMA), is expected to form the shell of the PECs. The hydrophilic corona stabilises the complex and prevents aggregation of the particles. The impacts of polymer concentration, polymer

addition order, molar mixing ratio, and solution pH and temperature on the formation of nanoparticles were explored. The PECs with optimal properties were identified and explored for drug loading and release.

Hydrophobic and hydrophilic anticancer drugs including paclitaxel, gemcitabine, 5-fluorouracil (5-FU), and carmofur were encapsulated in the PECs. Preliminary results were obtained for the encapsulation efficiency of these drugs. The release profiles at neutral pH and in a slightly acidic media were studied. At mildly acidic pH, the cationic block of the copolymer is expected to remain positively charged whereas the polyanion is protonated, leading to a reduced electrostatic interaction between the polyelectrolytes which could theoretically result in drug release. A schematic representation of the behaviour of the polymers at mildly acidic pH and the resultant drug release from the PECs is shown in **Figure 3.2**. Dexamethasone-loaded PECs were also prepared and incorporated into a hydrogel for consideration as a potential ocular formulation.

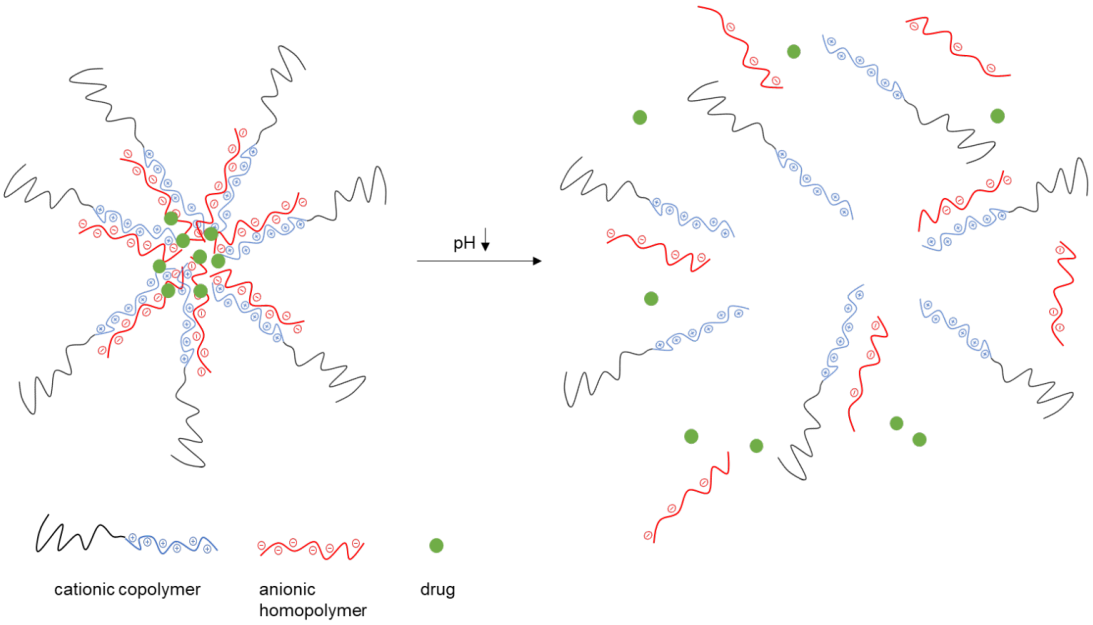

Figure 3.2. *Schematic representation of stimuli-responsive drug release from PEC nanoparticles.*

3.3 Experimental

3.3.1 Materials

Phthalocyanine was purchased from Frontier Scientific. Paclitaxel was supplied by Fluorochem. Gemcitabine was purchased from Carbosynth limited. Carmofur and 5-fluorouracil were obtained from ChemCruz (Santa Cruz Biotechnology). Dexamethasone (DEX), N-isopropylacrylamide (NIPAAM), ammonium persulfate (APS), poly(ethylene glycol) diacrylate (PEGDA), N,N,N′,N′-Tetramethylethylenediamine (TEMED), and Dulbecco's phosphate buffered saline (PBS) were purchased from Sigma-Aldrich. Acetonitrile and HPLC water were sourced from Fisher Scientific.

3.3.2 Preparation of nanoparticles

Solutions of 1 mg/ml of poly(PEGMA-co-DMAEMA) **5** and PMAA **7** of different chain lengths were prepared in deionised water in separate vials. Details of the RAFT-synthesised polymers are presented in Chapter 2. Nanoparticles of 1:1 polycation to polyanion mass ratio as well as nanoparticles with different molar ratios of polycation to polyanion (0.25, 0.5, 1, 2, and 4) were prepared by mixing the solutions. The samples were then filtered using 0.45 μm filters. By way of example, nanoparticles with a 1:1 mass ratio of polyanion to polycation were prepared as follows: 0.5 ml poly(PEGMA-co-DMAEMA)/water (1 mg/ml) was mixed with 0.5 ml PMAA/water (1 mg/ml). The mixture was sonicated for 10 seconds and filtered using 0.45 μm filters. Nanoparticles with a total polymer concentration of 1 mg/ml were prepared.

Solutions of 1 mg/ml of poly(PEGMA-co-DMAEMA) **5** and PMAA **7** with similar chain lengths of the charged segments were prepared in water. Nanoparticles of 1:1 polycation to polyanion molar ratio were prepared by mixing solutions of cationic copolymers and anionic homopolymers. For instance, 1 ml of a polycation solution (poly($PEGMA_{0.23}$-co-$DMAEMA_{0.77}$)$_{99}$) **5b** and 364 μl of a polyanion solution (poly$(MAA)_{75}$) **7b** were mixed together to prepare the optimal PEC nanoparticles formulation (**NP2**). The mixture was then sonicated for 10 seconds and filtered using 0.45 μm filters.

The impact of different molar ratio of the cationic copolymers to the anionic homopolymers (C/A) with similar chain lengths on formation of PECs was investigated. C/A ratios of 0.25, 0.5, 1, 2, and 4 were used to prepare each of the polyelectrolyte complex nanoparticles. Hydrodynamic size and zeta

potentials of the filtered nanoparticles were measured using dynamic light scattering (DLS).

One nanoparticle formulation was chosen for further investigation, based on the size, PDI and zeta potential. The formulation with one-to-one molar ratio of poly(PEGMA$_{0.23}$-co-DMAEMA$_{0.77}$)$_{99}$ and poly(MAA)$_{75}$ was chosen as the optimum formulation as it led to formations of PECs with small sizes and low PDI. The impact of polymer concentration on the hydrodynamic diameter was investigated. While the molar ratio of polycation to polyanion was maintained, nanoparticles with five different total polymer concentrations (4 mg/ml, 2 mg/ml, 1 mg/ml, 0.5 mg/ml, and 0.25 mg/ml) were synthesised.

Effects of polymer addition order on these nanoparticles were also tested at a total polymer concentration of 1 mg/ml. A one-to-one molar ratio of the cationic copolymer and anionic homopolymer was maintained.

3.3.3 Impact of pH changes of the size distribution of PECs

The pH responsiveness of the PEC nanoparticles was investigated by observing changes in their hydrodynamic size at different pH environments (7.4, 6.5, and 5.5) using DLS. The nanoparticle samples were placed in an incubator with a temperature of 37 ˚C under stirring. At different time intervals, their size was determined using DLS.

The effects of combination of pH and temperature on the mean diameter and zeta potential of the polymers and nanoparticles were also tested. Samples of poly(PEGMA$_{0.23}$-co-DMAEMA$_{0.77}$)$_{99}$ and poly(MAA)$_{75}$ with a total polymer

concentration of 1 mg/ml in PBS at three different pH values (5.5, 6.5, and 7.4) were mixed together to prepare 1:1 molar ratio nanoparticles. The unfiltered samples were taken for DLS size and zeta potential measurements at four different temperatures (25, 37, 45, and 60˚C).

3.3.4 Characterisation

DLS size measurements and zeta-potentials were obtained using a Nano-ZS instrument (Malvern). Samples were filtered using 0.45 μm filters before analysis by DLS. Transmission electron microscopy (TEM) images were recorded by Dr Fanny Joubert and Dr Andrew Weston using a Philips/FEI CM120 Bio Twin TEM. PEC nanoparticle samples in water (1 mg/ml) were directly dispensed onto TEM grids and left to dry with staining using an aqueous 3% phosphotungstic acid hydrate (PTA) solution.

3.3.5 Stability studies

Nanoparticles synthesised by mixing a 1:1 molar ratio of poly$(MAA)_{75}$ and poly$(PEGMA_{0.23}$-co-$DMAEMA_{0.77})_{99}$ with five different total polymer concentrations (0.25, 0.5, 1, 2, and 4 mg/ml) were stored at room temperature over 28 days. Samples were taken for size and zeta potential measurements every 7 days.

3.3.6 Haemolysis assay

The haemolytic activity of the polymers and nanoparticles was assessed using freshly obtained blood from adult female Wistar rats. All animal handling was performed by licensed researchers. Red blood cells (RBC) were separated

from the plasma by centrifugation and washed with Dulbecco's phosphate buffered saline (DPBS, Sigma Aldrich) three times. The RBC suspension was diluted with DPBS to a total volume of 50 ml.

The RBC suspension (180 µl) was then added to the wells of a clear 96-well plate (Corning). Polymer solutions and nanoparticle suspensions (20 µl) in DPBS at four different concentrations (1 mg/ml, 500 µg/ml, 100 µg/ml, and 20 µg/ml) were added to the wells to give a final polymer or nanoparticle concentration of 100 µg/ml, 50 µg/ml, 10 µg/ml, and 2 µg/ml. For negative and positive control measurements, DPBS and a solution of Triton-X in DPBS (10% v/v) were added to the wells, respectively. The plates were incubated at 37 °C for 1 hour. Next, the plates were centrifuged and 100 µl of the supernatant from each well was removed and deposited into a clean microplate. The procedure was carried out three times, and in each independent plate three wells were used for each concentration. Absorbance was read at 540 nm using a SpectraMax M2e microplate reader. The extent of haemolysis was calculated using Equation 3.1:

$$Haemolysis\ (\%) = \frac{Sample\ absorbance}{Positive\ control\ absorbance} \times 100 \qquad (3.1)$$

3.3.7 Dye encapsulation

Phthalocyanine solutions of 0.1 mg/ml, 0.2 mg/ml, and 0.4 mg/ml (10%, 20%, and 40% w/v) were prepared using methanol and used in the fabrication of NP2 suspensions. Methanol was evaporated under controlled conditions (100 rpm, 100 mBar, 40 °C) using a Buchi Rotavapor R300. The samples were filtered using 0.45 µm pore size filters. The filtered samples contained particles

with phthalocyanine encapsulated and the absorbance at 615 nm (A_{615nm}) of the NPs suspension was measured using a Cary 100 UV-vis spectrophotometer (Agilent Technologies). Encapsulation efficiency (EE) and loading capacity (LC) were determined using Equations 3.2 and 3.3, based on a predetermined calibration curve.

$$Encapsulation\ Efficiency\ (\%) = \frac{mass\ of\ encapsulated\ dye/drug}{mass\ of\ dye/drug\ used} \times 100 \qquad (3.2)$$

$$Loading\ Capacity\ (\%) = \frac{mass\ of\ dye/drug\ loaded}{mass\ of\ polymers\ and\ dye/drug} \times 100 \qquad (3.3)$$

3.3.8 Drug encapsulation

A 0.2 mg/ml solution of a range of model drugs (paclitaxel, gemcitabine, 5-fluorouracil, and carmofur) in methanol was prepared and used to prepare 1 mg/ml solutions of the cationic copolymer and the anionic homopolymer in separate vials by adding the drug/MeOH solutions to vials containing appropriate amount of the polymers. 364 µl of PMAA/drug solution was added to the 1 ml of the poly(PEGMA-co-DMAEMA) solution. The total polymer concentration in the sample was 1 mg/ml. Methanol was evaporated under controlled conditions (100 rpm, 100 mBar, 40 °C) using a Buchi Rotavapor R300 until a thin film was formed in the vial. This was followed by the addition of 1.364 µl water. The samples were then sonicated for 2 minutes and passed through a 0.45 µm filter. The filtered samples were centrifuged in Vivaspin 6 centrifugal concentrators with molecular weight cut-off (MWCO) of 3000 at 10000 rpm for 15-20 minutes at 25 °C. Following centrifugation, the supernatant was collected and the entrapment efficiency (EE%) and loading

capacity (LC%) were determined by High performance liquid chromatography (HPLC) or UV spectroscopy.

HPLC experiments were conducted using an Agilent 1100 series. An Eclipse Plus C18 column (Agilent) and a Phenomenex Synergi™ 4 µm Hydro-RP column were used for paclitaxel and gemcitabine, respectively. Equations 3.2 and 3.3 were used to calculate EE and LC. The mobile phase for paclitaxel was acetonitrile/water (55:45 v/v). The wavelength and the run time were set to 227 nm and 15 minutes, respectively. A calibration curve for paclitaxel was made with 0.0002-0.4 mg/ml of the drug in acetonitrile. A retention time of around 2.4 min was observed. For gemcitabine, the mobile phase was acetonitrile/water (10:90 v/v). The wavelength was set to 270 nm with a run time of 7 minutes. A calibration curve for gemcitabine was generated with 0.0004-0.4 mg/ml of the drug in HPLC water. A retention time of around 2.6 min was observed. For both experiments, the injection volume was 20 µl with a flow rate of 1.0 ml/min.

The entrapment efficiency and drug loading capacity of 5-fluorouracil and carmofur were determined using an Agilent Cary 60 UV-Vis spectrophotometer at 265 and 246 nm, respectively.

3.3.9 Drug release

In vitro release profiles of gemcitabine, 5-fluorouracil, and carmofur from the PEC nanoparticles were explored. 1 ml of each sample was poured into Dalton's Visking dialysis tubes 3500/4 (35mm diameter, 55mm width, 5m length). Each sample contained 1 mg/ml of NP in water. The tubes were then

placed into vials containing 20 ml of PBS with different pH values (5.5, 6.5, and 7.2). The vials were incubated at 37°C under stirring at 100 rpm for 72 hours. Periodically, 1 ml aliquots were withdrawn from the vials and replaced with 1 ml of fresh prewarmed PBS. The collected samples were analysed using HPLC or UV/Vis spectroscopy. The drug release percentage was calculated based on the Equation 3.4.

$$Drug\ release = \frac{weight\ of\ drug\ released}{Total\ weight\ of\ drug\ encapsulated\ within\ nanoparticles} \times 100 \qquad (3.4)$$

3.3.10 Preparation and characterisation of dexamethasone loaded NIPAAM gels

40 mg of NIPAAM was dissolved in 1 ml of deionised water at room temperature, followed by the addition of 4 mg of APS. The solution was mixed for 15 minutes. 20 or 10 µl of PEGDA and 50 µl of TEMED were next added and the mixture vortexed for 15-20 seconds.

The volume phase transition temperature (VPTT) of the gels was measured using differential scanning calorimetry (DSC) on a Q2000 calorimeter (TA instruments, Waters LLC). Nitrogen was used as the purge gas with a flow rate of 50 ml/min. Samples were heated from 20 to 50 °C at a rate of 2 °C/min.

For the preparation of dexamethasone (DEX) loaded NIPAAM gels, dexamethasone (0.2 mg/ml) was first encapsulated into NP2 polyelectrolyte complex nanoparticles with total polymer concertation of 1mg/ml using the same protocol as above. NP/DEX suspensions were mixed with NIPAAM (40 mg) and APS (4 mg) using magnetic stirring for 15 minutes. PEGDA (20 or 10

µl) and TEMED (50 µl) were next added, and the solution was vortexed for 15-20 seconds. The entrapment efficiency and drug loading capacity of dexamethasone loaded nanoparticles were determined by HPLC using an Eclipse Plus C18 column (Agilent). The wavelength was set to 240 nm with a running time of 15 minutes. The mobile phase was HPLC water and acetonitrile 80:20 v/v for 8.5 minutes and 50:50 v/v for 6.5 minutes. The injection volume was 20 µl with a flow rate of 1.0 ml/min. A retention time of around 13.5 min was observed.

In vitro release studies were carried out using the PK-Eye model (90). The inlet port of the model was connected to a pump (ISMATEC 4 channel pump) and supplied with a constant flow of 37 °C deionised water at 2 µl/min. Dexamethasone loaded gels (200 µl) were injected using a 1 ml syringe. The following formulations were explored in the PK-Eye model: dexamethasone loaded nanoparticles, dexamethasone loaded nanoparticles in NIPAAM (20 µl PEGDA) gels, dexamethasone loaded nanoparticles in NIPAAM (10 µl PEGDA) gels. Samples were collected from the anterior cavity at each time point and analysed by HPLC (240 nm).

3.4 Results and discussion

3.4.1 Impact of molar ratio of polycation to polyanion on PEC formation

The first few samples of PEC nanoparticles were prepared using the preliminary method as illustrated in **Figure 3.3**. Solutions of poly(PEGMA-co-DMAEMA) and poly(MAA) in methanol were mixed followed by evaporation of

methanol using a rotary evaporator. The self-assembly of the copolymer and MAA polymer into PEC nanoparticles was induced by addition of water to the resultant thin film left at the bottom of the vial. However, since the copolymers and the homopolymers were soluble in water, the preparation method was subsequently simplified into mixing solutions of the cationic copolymer and the anionic homopolymer in water, followed by filtering using 0.45 μm filters.

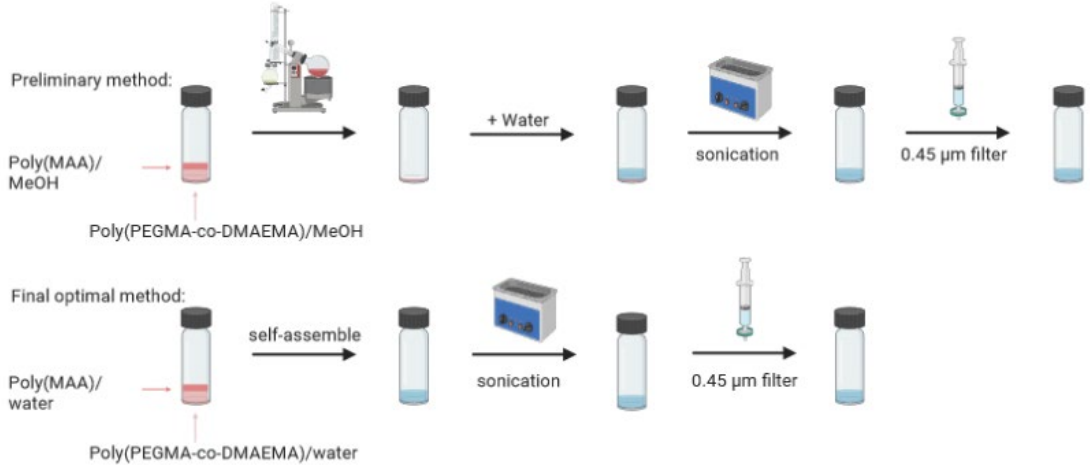

Figure 3.3. *Preparation of polyelectrolyte complex nanoparticles using the preliminary method and the final method. Created with BioRender.com.*

The first nanoparticles were prepared by mixing solutions of copolymer **5b**, poly(PEGMA$_{0.23}$-co-DMAEMA$_{0.77}$)$_{99}$, and polymer **7e**, poly(MAA)$_{31}$, at a 1:1 mass ratio. The polymers were synthesised by RAFT polymerisation and are described in detail in Chapter 2. The total concentration of polymers in solution was 1 mg/ml. DLS results (**Figure 3.4a**) confirmed the formation of nanoparticles with mean hydrodynamic diameters of 533 ± 299 nm, PDI of 0.39, and a zeta potential of -24.6 ± 2.7 mV. The same method of preparation was repeated with a copolymer with a smaller DMAEMA section. Mixing solutions of **5d**, poly(PEGMA$_{0.63}$-co-DMAEMA$_{0.37}$)$_{111,}$ and 7e, poly(MAA)$_{31}$,

resulted in the formation of nanoparticles with mean hydrodynamic diameter of 188 ± 35 nm, PDI of 0.21, and zeta potential of -22.7 ± 1.8 mV (**Figure 3.4b**).

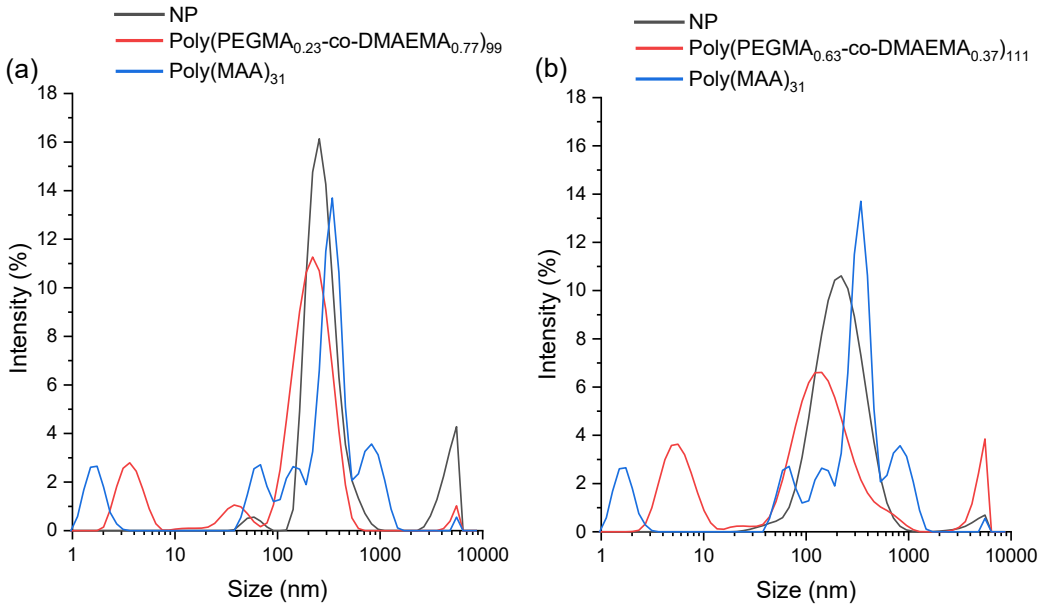

Figure 3.4. *DLS measurements of (a) copolymer* ***5b*** *(poly(PEGMA$_{0.23}$-co-DMAEMA$_{0.77}$)$_{99}$), polymer* ***7e*** *(poly(MAA)$_{31}$), and the particles formed upon mixing; and (b) copolymer 5d (poly(PEGMA$_{0.63}$-co-DMAEMA$_{0.37}$)$_{111}$), polymer 7e (poly(MAA)$_{31}$), and the particles formed by mixing. Mixing performed at 25 °C. The mass ratio of polycation to polyanion in the nanoparticle samples was 1:1.*

Both sets of initial nanoparticles were found to have rather large diameters, and the existence of multiple populations of particles can be seen in the DLS measurements (**Figure 3.4**). This is due to the presence of an excess amount of the polyanion in the formulation when using a 1:1 mass ratio, as is clear from the negative zeta potential values (86). Therefore, nanoparticles with one-to-one molar ratio of polycation and polyanion were prepared using the same copolymers and homopolymer.

The mean hydrodynamic diameter of PECs formed by mixing solutions of copolymer **5b,** poly(PEGMA$_{0.23}$-co-DMAEMA$_{0.77}$)$_{99}$, and homopolymer **7e**, poly(MAA)$_{31}$, at a 1:1 molar ratio was 91 ± 19 nm (**Figure 3.5a**), with PDI of 0.38 and zeta potential of -5.4 ± 1.2 mV. Mixing solutions of copolymer **5d**, poly(PEGMA$_{0.63}$-co-DMAEMA$_{0.37}$)$_{111}$, and polymer **7e** resulted in the formation of PECs with 150 ± 7 nm mean size (**Figure 3.5b**), PDI of 0.25, and zeta potential of -9.5 ± 1.7 mV. The mean hydrodynamic size and PDI of the 1:1 polycation/polyanion molar ratio PECs were notably lower than those prepared with a 1:1 mass ratio. The zeta potential of the 1:1 molar ratio PECs is close to zero, confirming the hypothesis that the anionic polymer **7e** was in excess when using a 1:1 mass ratio, causing the surface of the previously prepared nanoparticles to have a high negative charge.

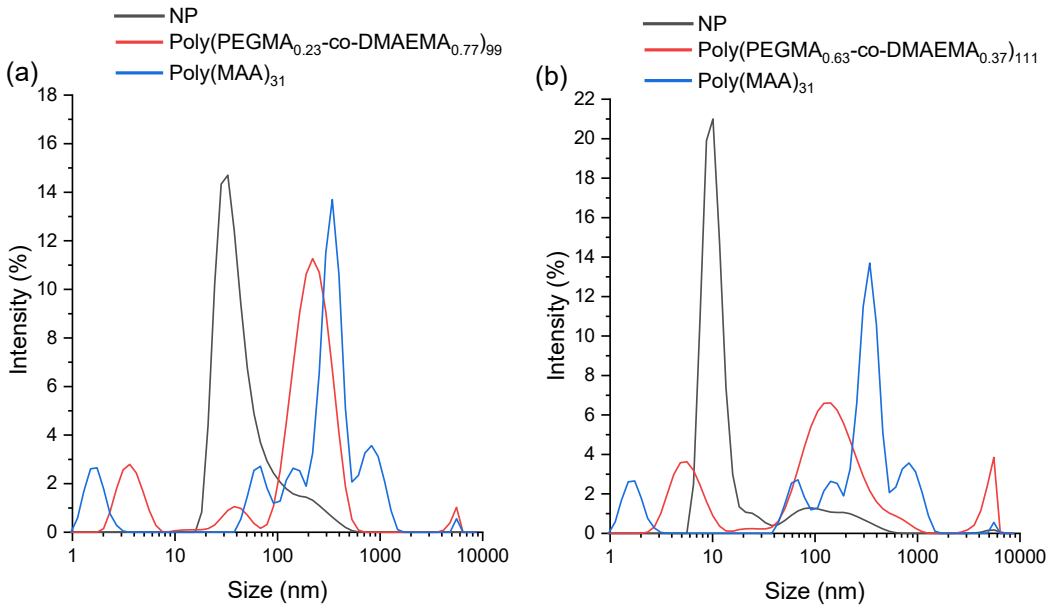

Figure 3.5. *DLS measurements of (a) copolymer* ***5b*** *(poly(PEGMA$_{0.23}$-co-DMAEMA$_{0.77}$)$_{99}$), polymer* ***7e*** *(poly(MAA)$_{31}$), and the particles formed upon mixing; and (b) copolymer* ***5d*** *(poly(PEGMA$_{0.63}$-co-DMAEMA$_{0.37}$)$_{111}$), polymer* ***7e*** *(poly(MAA)$_{31}$), and the particles formed by mixing. Mixing performed at 25 °C. The molar ratio of polycation to polyanion in the nanoparticle samples was 1:1.*

Similar trends were observed in a literature study where PEC nanoparticles were formed by mixing PDADMA-co-PAA with poly(styrenesulfonic acid) (PSS) (88). In this study, formulations with a higher ratio of PSS to the copolymer were found to be more stable, as the excess negative charges prevented the aggregation of the nanoparticles. However, 1:1 polycation/polyanion molar ratio nanoparticles had smaller hydrodynamic sizes and the zeta potentials were closer to zero.

Even though preparation of the nanoparticles with more diluted solutions of the anionic homopolymer led to formation of nanoparticles with smaller hydrodynamic diameter and PDI compared to the formulations prepared using equal amounts of polycation and polyanion, the existence of multiple size populations in the DLS measurements of these nanoparticles, indicates the presence of free polymer molecules in solution (**Figure 3.5**). Therefore, six sets of nanoparticles with 1:1 cation: anion molar ratios were prepared using cationic copolymers and anionic homopolymers of similar chain lengths to assess the impact of the chain lengths of the polyelectrolytes on the size and size distribution of PECs. The 1:1 molar ratio polycation to polyanion was maintained to provide a charge-to-charge interaction within the PECs. The aim was to form stable nano-sized PECs with low PDI.

The association of poly(PEGMA-co-DMAEMA) block copolymers (5a-5f) with the poly(MAA) homopolymers (7a-7f) into PEC nanoparticles was examined. In the formulation of these nanoparticles, the DP of PMAA was selected to match the DP of the DMAEMA block as closely as possible. Block copolymers composing of oppositely charged segments with the same chain length are

known to balance the opposite charges in a stoichiometric manner and reduce phase mixing of the inner and outer layer of polyion complexes, forming stable particles (91). The PEC formulations and their DLS size, PDI, and zeta potential measurements are listed in **Table 3.1**. DLS data are given in **Figure 3.6**.

Table 3.1. *Formulation details and size, PDI, and zeta potential of different sets of filtered PECs prepared with a 1:1 molar ratio of the cationic copolymers and anionic homopolymers with similar polyelectrolyte chain lengths prepared in water.*

Nanoparticle	Cationic copolymer / DP of PEGMA	Cationic Copolymer / DP of DMAEMA	Anionic Homopolymer / DP of MAA	Hydrodynamic Diameter (nm)	PDI	Zeta Potential (mV)
NP1	3a / 13	5a / 85	7a / 88	104 ± 13	0.25 ± 0.09	-16.9 ± 11
NP2	3b / 23	5b / 76	7b / 75	25 ± 3	0.08 ± 0.01	-23.2 ± 1.4
NP3	3d / 52	5c / 58	7c / 52	51 ± 4	0.32 ± 0.05	-8.5 ± 4.2
NP4	3e / 70	5d / 41	7d / 46	57 ± 5	0.49 ± 0.01	-15.3 ± 0.7
NP5	3b / 23	5e / 28	7e / 31	352 ± 254	0.46 ± 0.06	-8.2 ± 2.1
NP6	3c / 35	5f / 18	7f / 23	95 ± 4	0.39 ± 0.09	-11.5 ± 1.4

NP1, formulated using the lowest fraction of PEGMA, had a mean diameter of 104 nm. This is notably larger than the mean diameter of the other three nanoparticles (NP2, NP3, and NP4) formed using copolymers with total DP (DP_{PEGMA} + DP_{DMAEMA}) of around 100. Mixing solutions of the cationic copolymer **5b**, poly($PEGMA_{0.23}$-co-$DMAEMA_{0.77}$)$_{99}$, and the anionic homopolymer **7b**, poly(MAA)$_{75}$, resulted in formation of monodispersed nanoparticles with mean diameter of 25 ± 3 nm, PDI of 0.08, and zeta potential

of -23.2 ± 1.4 mV. NP3 and NP4 were prepared using copolymers with longer PEGMA sections and shorter polyelectrolyte sections. DLS size measurements of these samples showed multiple size populations indicating both the presence of complexes and free polymer in solution (**Figure 3.6**). NP5 and NP6 were formed using copolymers with total DP of 51 and 53, respectively. The repeat units of the PEGMA sections in the copolymers in these formulations are 23 and 35, respectively. The formulation with lower PEGMA fraction, NP5, had the largest mean diameter. The zeta potential values of the nanoparticles (NP1-6) did not show a clear trend.

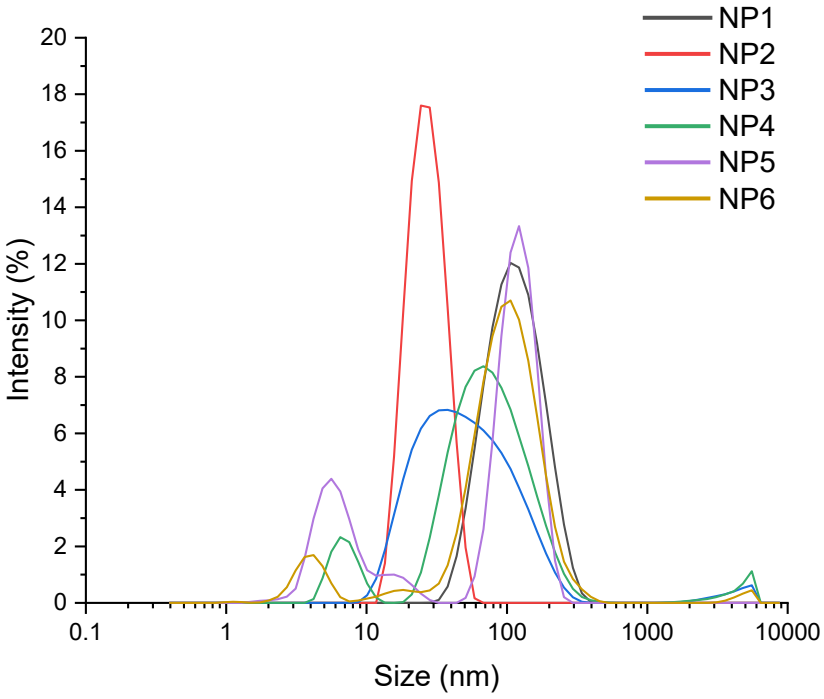

Figure 3.6. *DLS size measurements of NP1, NP2, NP3, NP4, NP5, and NP6 prepared by mixing solutions of anionic homopolymers and cationic copolymers with similar polyelectrolyte chain lengths. 1:1 molar ratios of polycation to polyanion were used for the preparation of the PECs.*

According to a study performed by Harada and Kataoka, the assembly of charged polymers with matched chain length formed particles with narrow size

distribution (92). This was reported to be due to strict phase separation between the core and the shell segments of the PECs. In this study, mixing pairs of oppositely charged block copolymers, poly(ethylene glycol)-b-poly(α,β-aspartic acid) and poly(ethylene glycol)-b-poly(L-lysine), with matched chain lengths of the charged segments of the copolymers led to formation of polyelectrolyte complexes. PECs were only formed when matched block lengths were used. The phase separation between the charge-neutralised core and the shell of these PECs was reported to require alignment of the molecular junctions of the PEG sections and the charged sections of the block copolymers. Similarly, formation of monodispersed NP2 nanoparticles was only possible when poly($PEGMA_{0.23}$-co-$DMAEMA_{0.77}$)$_{99}$ and poly$(MAA)_{75}$ of similar chain lengths were used.

Use of PEG in low weight fraction in a polymer mixture was reported to avoid steric hindrance between PEG strands, allowing formation of stable nanoparticles (93). Therefore, the fact that the smallest nanoparticles from **Table 3.1** formed with NP2 could be due to the long chain length of the ionic segments of the PEC nanoparticles and the lower weight fraction of PEGMA in the mixture. Overall, the use of a 1:1 molar ratio of copolymer **5b** and polymer **7b** gave the smallest PEC hydrodynamic size and polydispersity. This was hence selected as the optimal system, and further characterisations were carried out on this formulation (**Figure 3.7**).

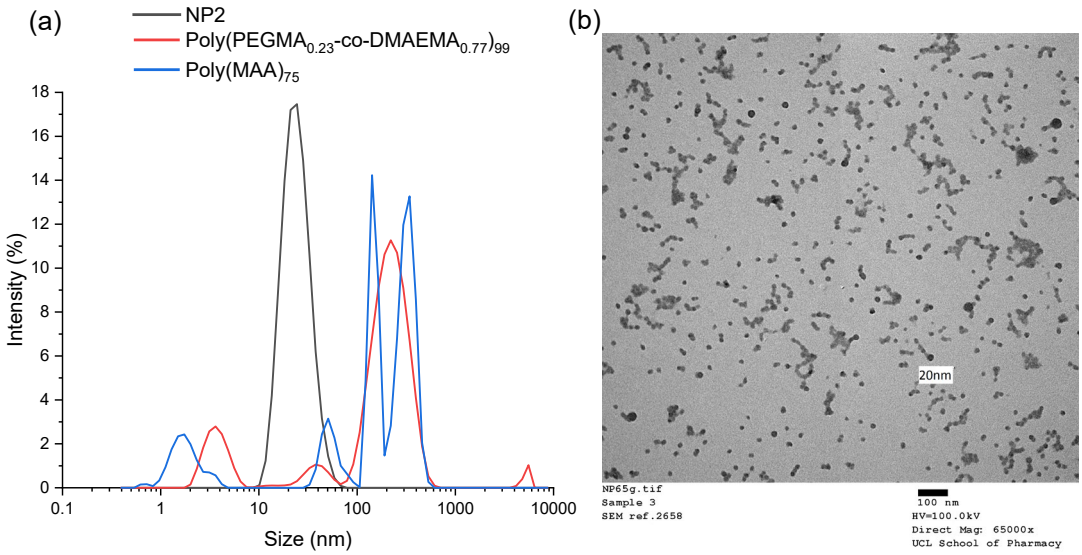

Figure 3.7. *Characterising data on the NP2 PECs. (a) DLS measurements of NP2 PECs (D_h = 25 ± 3 nm; PDI = 0.08) and its components at 25 °C; and (b) TEM image showing the PECs to have a mean size of 20 ± 3 nm.*

Images of NP2 PECs obtained from TEM were in agreement with the DLS data. According to DLS measurements, a filtered sample of 1 mg/ml copolymer **5b** in water had a mean diameter of 117 ± 18 nm and PDI of 0.86. The mean hydrodynamic diameter of 1 mg/ml anionic polymer **7b** was 550 ± 165 nm and the PDI was 0.62. Mixing solutions of the cationic copolymer **5b**, poly(PEGMA$_{0.23}$-co-DMAEMA$_{0.77}$)$_{99}$ and the anionic homopolymer **7b**, poly(MAA)$_{75}$, resulted in formation of NP2 nanoparticles with 25 ± 3 nm and 20 ± 3 nm size according to DLS and TEM images, respectively (**Figure 3.7**). The sizes obtained from DLS measurements are larger than those observed by TEM. This is expected to be because DLS provides the hydrodynamic diameter of nanoparticles in solution while TEM provides images of nanoparticles and their size in their dried state. Drying can induce shrinkage of the particles; hence the smaller nanoparticle sizes measured by TEM imaging.

The molar ratio of polycation to polyanion can impact the size and zeta potential of PECs. **Figure 3.8** displays the effect of five different polycation to polyanion (C/A) molar ratios (1:4, 1:2, 1:1, 2:1, and 4:1) on the hydrodynamic diameter and zeta potential of nanoparticles (NP1-6). The zeta potentials of the particles correlate with the molar ratio of polycation to polyanion in the formulations (**Figure 3.8**). PECs with higher polycation to polyanion molar ratios had positive or neutral zeta potentials, whereas those with a higher polyanion to polycation molar ratio had negative zeta potentials.

The size of NP1 particles formed by mixing cationic copolymer **5a**, poly(PEGMA$_{0.13}$-co-DMAEMA$_{0.85}$)$_{98}$, and anionic homopolymer **7a**, poly(MAA)$_{88}$ exhibited large standard deviations when C/A ratios of 0.5, 1, 2, and 4 were used to prepare the samples (**Figure 3.8a**). DLS measurement of these particles showed multiple size populations and the PDI ranged from 0.25 to 0.55. At a C/A ratio of 0.25, when the lowest concentration of the cationic copolymer was used, a single population of NPs with mean diameter of 143 nm, PDI of 0.19, and zeta potential of -26.5 mV was formed.

In the case of NP2, at C/A ratio of 0.25, the formulation lacked sufficient copolymer to complex with the anionic polymer (**Figure 3.8b**). As the C/A ratio increased to 0.5 and 1, the concentration of free polymer in solution decreased, which resulted in increased complexation between the polycation and polyanion and the formation of nanoparticles with sub-100 nm hydrodynamic diameter and narrow size distribution (PDI < 0.2). A further increase in the concentration of the cationic copolymer increased the polydispersity of the formulation. The positive zeta potential of these formulations is expected to be

due to increased concentration of DMAMEA and the presence of free polymer in solution.

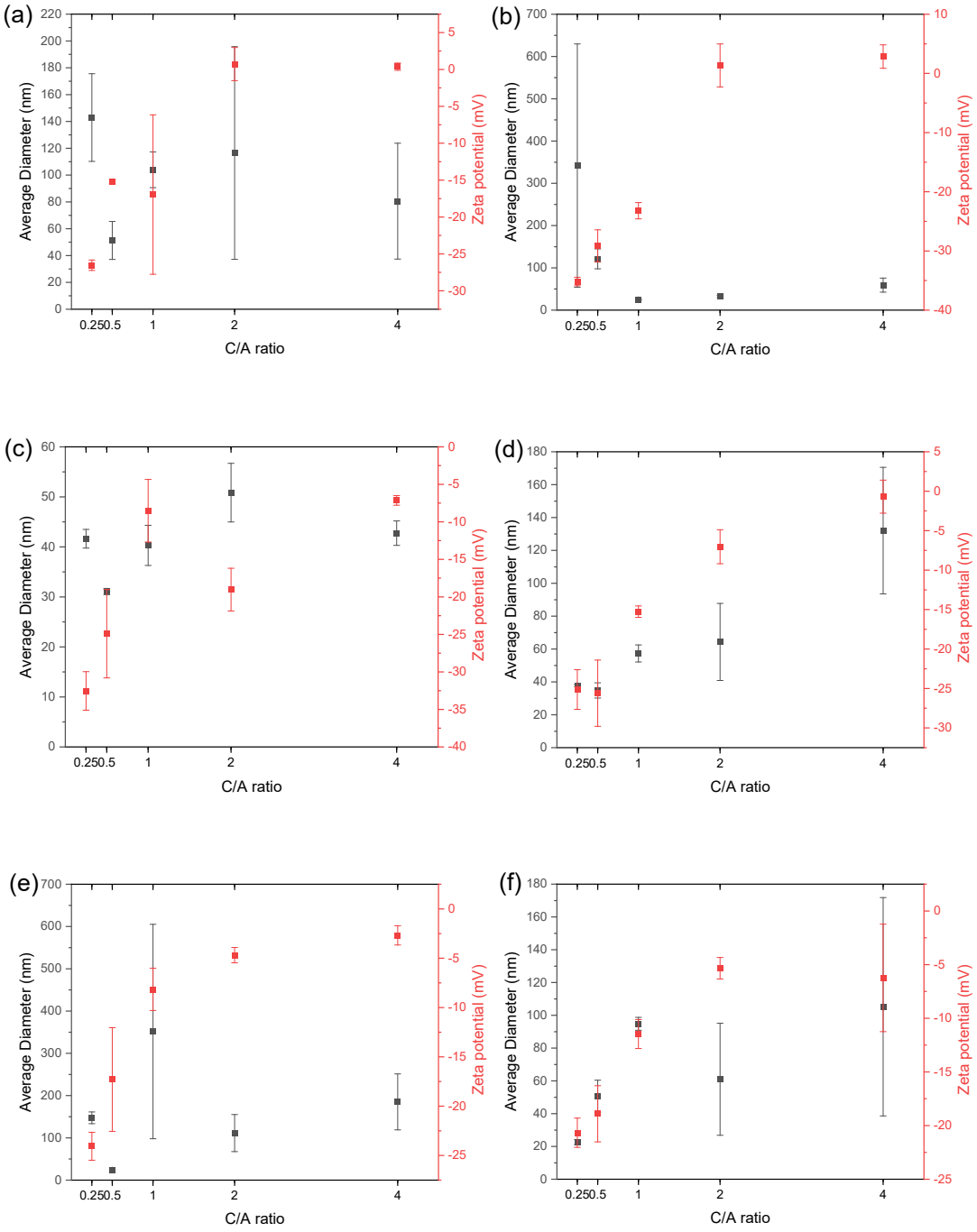

Figure 3.8. *DLS measurements (size and zeta potential) of filtered samples of (a) NP1, (b) NP2, (c) NP3, (d) NP4, (e) NP5, and (f) NP6 prepared with 5 different molar ratios of the cationic copolymer to the anionic homopolymer (C/A molar ratios of 0.25, 0.5, 1, 2, and 4), prepared in water at 25 °C. The error bars represent standard deviation.*

NP3 comprised copolymer **5c**, poly($PEGMA_{0.47}$-co-$DMAEMA_{0.53}$)$_{110}$, and polymer **7c**, poly(MAA)$_{52}$. The copolymer and polymer in this formulation failed to complex and form monodispersed nanoparticles. Their DLS measurements (**Figure 3.8c**) showed multiple size populations at all C/A ratios. The same was true for NP4 PECs formed by mixing solutions of copolymer **5d**, poly($PEGMA_{0.63}$-co-$DMAEMA_{0.37}$)$_{111}$, and polymer **7d**, poly(MAA)$_{46}$. The polydispersity of these nanoparticles decreased to around 0.28 with decreasing the concentration of the copolymer to a C/A ratio of 0.25 (**Figure 3.8d**).

The size distribution and zeta potential measurements of the NP5 (**Figure 3.8e**) and NP6 (**Figure 3.8f**) nanoparticles formed using copolymers with total DP of around 50 showed that again the components failed to complex and form monodispersed PECs. NP5 was formed using copolymer **5e**, poly($PEGMA_{0.45}$-co-$DMAEMA_{0.55}$)$_{51}$, and polymer **7e**, poly(MAA)$_{31}$. NP6 comprised of copolymer **5f**, poly($PEGMA_{0.66}$-co-$DMAEMA_{0.34}$)$_{53}$, and polymer **7f**, poly(MAA)$_{23}$. The polydispersity index of the nanoparticles with different C/A molar ratios are listed in **Table 3.2**

Table 3.2. *Polydispersity index of nanoparticles with 5 different molar ratios of the cationic copolymer to the anionic homopolymer (C/A molar ratios of 0.25, 0.5, 1, 2, and 4).*

Nanoparticles	PDI				
	C/A 0.25	C/A 0.5	C/A 1	C/A 2	C/A 4
NP1	0.19 ± 0.03	0.53 ± 0.12	0.25 ± 0.02	0.55 ± 0.18	0.54 ± 0.26
NP2	0.37 ± 0.33	0.22 ± 0.04	0.08 ± 0.01	0.40 ± 0.07	0.59 ± 0.07
NP3	0.29 ± 0.04	0.43 ± 0.01	0.32 ± 0.05	0.95 ± 0.05	1.00
NP4	0.28 ± 0.02	0.46 ± 0.06	0.49 ± 0.01	0.64 ± 0.11	0.46 ± 0.12
NP5	0.24 ± 0.03	0.45 ± 0.04	0.46 ± 0.06	0.61 ± 0.14	0.45 ± 0.07
NP6	0.49 ± 0.07	0.71 ± 0.13	0.39 ± 0.09	0.79 ± 0.27	0.73 ± 0.15

Small colloidal particles were previously reported to form by mixing solutions of poly(acrylic acid) (PAA) with molecular weight of 11300 g/mol with poly((dimethyl amino) ethyl methacrylate)-co-poly(glyceryl methacrylate) (34). Three samples of PDMAEMA-co-PGMA diblock copolymers with different ratios of DMAEMA and PGMA monomers (1:1, 1:3, and 1:9) were used. Polyelectrolyte complexes were formed when PAA was added to a solution of the block copolymer with PDMAEMA to PGMA ratio of 1:3. Association of oppositely charged PDMEAMA and PAA was reported to result in phase separation and formation of the core of the PECs, with the PGMA block of the copolymer forming the outer layer of the PECs and stabilising the particles. The combination of PAA and the copolymer with a 1:9 block ratio did not result in the formation of PECs. This was hypothesised to be due to the polycation not being able to derive phase separation. On the other hand, mixing the polyanion with a 1:1 block ratio copolymer resulted in macroscopic phase separation and formation of sediments in the sample tube. Similarly, in this

project, upon addition of poly(MAA)$_{75}$ to poly(PEGMA$_{0.23}$-co-DMAEMA$_{0.77}$)$_{99}$, phase separation occurred, and the solution became cloudy. This was followed by immediate rearrangement of the polymers into polyelectrolyte complex nanoparticles (NP2) and the nanoparticle solution became clear after a few seconds.

3.4.2 Impact of polymer concentration on PEC formation

To explore the effect of polymer concentration on PEC formation, a one-to-one molar ratio of poly(MAA)$_{75}$ and poly(PEGMA$_{23}$-co-DMAEMA$_{77}$)$_{99}$ was maintained (as for NP2). PECs were assembled from solutions at five different total polymer concentrations and their hydrodynamic size and zeta potential at 25 and 37 °C obtained. The hydrodynamic diameter and zeta potential of the polymers alone were also recorded for comparison.

As shown in **Figure 3.9**, the mean diameters of the polymers are significantly higher than those of the PECs at all concentrations, possibly due to the formation of aggregates by the former. Once the cationic copolymer and the anionic homopolymer are added together, the mean diameter reduces substantially, with sub-100 nm particles seen. The mean diameter of the PECs at 25 °C remained the same (≈ 26 nm) regardless of the total polymer concentration (**Figure 3.9a**). No clear trend was observed in the zeta potential values of the polymers and the PECs at 25 °C (**Figure 3.9b**). Increasing the temperature to 37 °C resulted in an increase in the mean diameter of the polymers but not the PECs (**Figure 3.9c**). This is because the PECs are tightly bound owing to the interaction between the oppositely charged polyelectrolytes. No clear trend was observed in terms of the zeta potentials at

37 °C (**Figure 3.9d**). The zeta potential value of the PECs with the total polymer concentration of 1 mg/ml was strongly negative (> -20 mV). The zeta potentials of the nanoparticles were similar to those of the anionic homopolymer. This could be due the complete deprotonation of the anionic homopolymer at physiological pH and the presence of the excess charge on the surface of the PECs. The nanoparticles maintained their size and charge at lower and higher polymer concentrations. NP2 PECs with a total polymer concentration of 1 mg/ml was chosen as the optimal formulation.

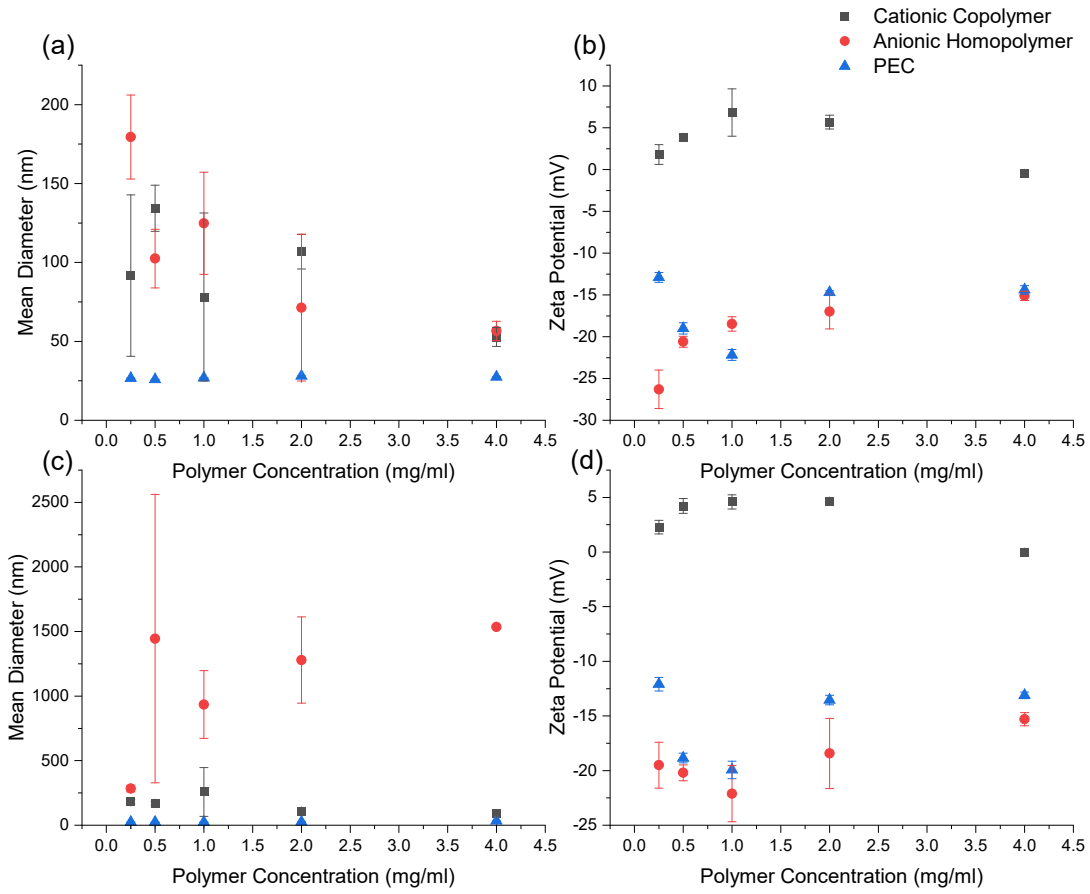

Figure 3.9. *The impact of total polymer concentration on (a) the mean hydrodynamic diameter of the cationic copolymer, poly(PEGMA$_{0.23}$-co-DMAEMA$_{0.77}$)$_{99}$, the anionic homopolymer, poly(MAA)$_{75}$, and NP2 PECs (with 1:1 polycation to polyanion molar ratio); and (b) their zeta potential at 25 °C. Panels (c) and (d) represent the mean hydrodynamic diameter and zeta potential of the polymers and PECs at 37 °C, respectively. The total polymer concentrations in solutions were 0.25, 0.5, 1, 2, and 4 mg/ml. The error bars represent standard deviation.*

3.4.3 Impact of polymer addition order on PEC formation

PECs consist of a neutral core and a hydrophilic outer shell bearing the excess charge of the polyelectrolytes (94). Changing the addition order of polyelectrolytes could result in formation of nanoparticles with different size and zeta potential, as the added polyelectrolyte needs to align its charged region with that of the oppositely charged polyelectrolyte in solution (95). Previously, all the PEC nanoparticles were prepared by adding the polyanion solution to the solution containing the cationic copolymers. The impact of polymer addition order on the PECs prepared with five different total polymer concentrations was assessed. A one-to-one molar ratio of the cationic copolymer and anionic homopolymer was maintained. C:A indicates that the anionic polymer, poly(MAA)$_{75}$, was added to the cationic copolymer, poly(PEGMA$_{0.23}$-co-DMAEMA$_{0.77}$)$_{99}$, whereas A:C indicates that the anionic polymer was first added followed by the cationic copolymer.

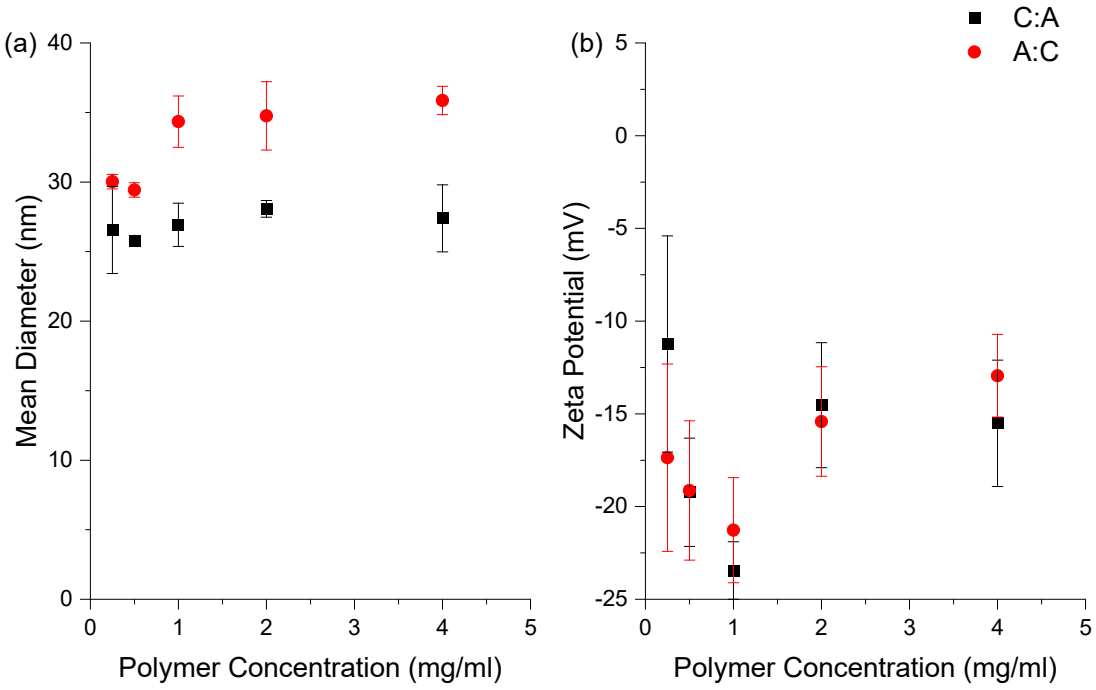

Figure 3.10. *The impact of total polymer concentration and polymer addition order on (a) the mean hydrodynamic diameter of NP2 PECs and (b) the zeta potential. C:A indicates that the anionic polymer was added to the cationic copolymer, and A:C indicates that the cationic copolymer was added to the anionic polymer. A one-to-one molar ratio of the cationic copolymer and anionic homopolymer was maintained. The error bars represent standard deviation.*

The DLS size measurements shown in **Figure 3.10a** indicate that the process of self-assembly of the oppositely charged polyelectrolytes was sensitive to the order of mixing. The mean hydrodynamic diameter of the PECs formed by adding the solution of the cationic copolymer to the solution of the anionic homopolymer were slightly larger. The addition order of the polymers also had an effect on the zeta potential of the PECs (**Figure 3.10b)**. The rest of the samples in this project were prepared by adding the solution of the anionic homopolymer to the solution of the cationic copolymer.

3.4.4 Impact of pH and temperature on PEC stability

The changes in size and size distribution of NP2 PECs (1 mg/ml) in response to pH were explored (**Figure 3.11**). The size of the PECs remained unchanged

for 48 h in PBS at pH 7.4. At pH 6.5, their size remained unchanged after 24 h but there was an increase in size and PDI at the 48-h time point. The size and size distribution of the nanoparticles increased in PBS at pH 5.5 at all timepoints, which showed that the PECs became unstable. This is likely due to the dissociation of the PECs and formation of aggregates of polymers. At a decreased pH, the negative charge of the anionic homopolymer is reduced while the cationic copolymer is positively charged which leads to reduced interaction between the polyelectrolytes within the core of the PECs. The percentage ionisation of the cationic copolymer and the anionic homopolymer at pH 7.4, 6.5, and 5.5, calculated using the Henderson-Hasselbalch equation, are listed in **Table 3.3**. Similar behaviour was observed in PEG-based micellar drug delivery system by Xiao et al. (89). The instability of the micelles at low pH was attributed to partial PEG chain shedding and formation of aggregates.

Table 3.3. *Percentage ionisation of the polymers at three different pH values calculated using Henderson-Hasselbalch equation.*

pH	% Ionised	
	PDMAEMA	**PMAA**
7.4	91.6	99.8
6.5	98.8	98.6
5.5	99.9	87.6

The increase in size and size distribution of the PECs in PBS pH 5.5 is due to the destabilisation of the particles and the reduced electrostatic interaction between positively charged PDMAEMA block of the copolymer and the less ionised PMAA at acidic pH. Similarly, in a study by Lim et al., an increase in

the size of complexes containing poly(ethylene glycol)-poly(lactic acid)-poly(ethylene imine) (PEG-PLA-PEI) triblock copolymer and poly(aspartic acid) (P(Asp)) homopolymer triggered by a decrease in pH was hypothesised to be due to the reduced electrostatic interactions between the positively charged PEI block of the triblock copolymer and the neutral P(Asp) (96). These results suggest that this formulation (NP2) could be useful for systemic drug delivery as it is stable in physiological conditions, whereas the PECs become unstable in slightly acidic environments (e.g., acidic pH of tumour microenvironment).

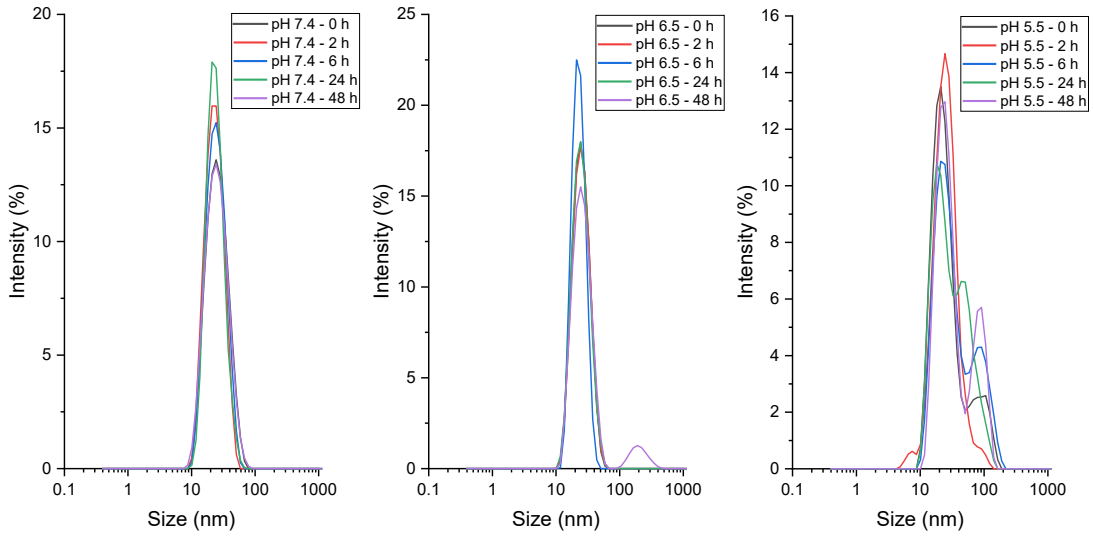

Figure 3.11. *Impact of pH on the mean diameter of NP2 PECs prepared with a 1:1 molar ratio of poly(PEGMA$_{0.23}$-co-DMAEMA$_{0.77}$)$_{99}$ and poly(MAA)$_{75}$ and 1 mg/ml polymer concentration over 48 hours.*

The changes in hydrodynamic diameter of the polymers and PECs were also investigated at different temperatures (25, 37, 45, and 60 ˚C). As expected, increasing the temperature resulted in an increase in the hydrodynamic diameter of the cationic copolymer (**Figure 3.12a**). At 25 °C, the mean hydrodynamic diameter of the copolymer was higher at pH 7.4 than in the more

acidic pH environments due to the difference in protonation of the copolymer. The zeta potential of the copolymer in PBS pH 5.5 was slightly higher than at PBS pH 7.4, because DMAEMA is protonated in acidic media. A reduction in pH of the solution at higher temperatures did not yield significant differences in the size of the copolymer. The mean diameter of the anionic polymer increased as the temperature was raised, with the change being more evident in acidic media with pH of 5.5 (**Figure 3.12b**). At this pH, the polymer solution at temperatures higher than 25 °C became cloudy as the polymer aggregated, forming particles with mean diameter above 3 μm.

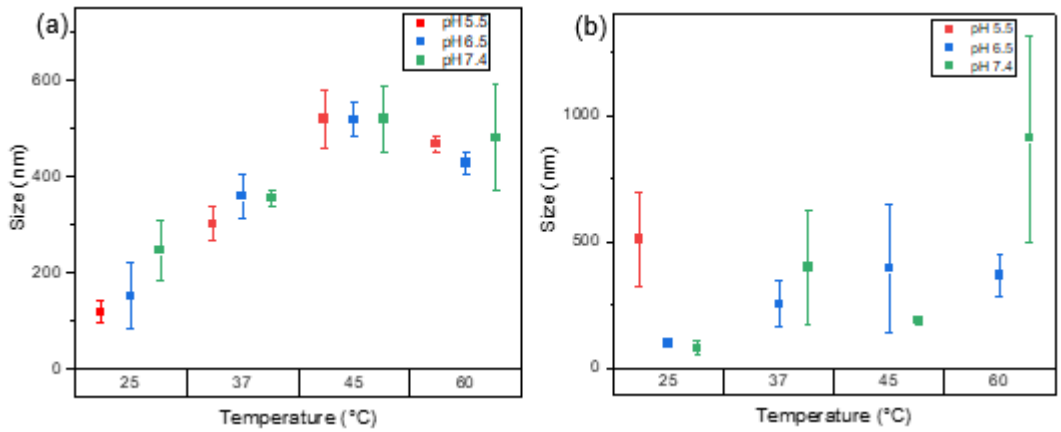

Figure 3.12. *Impact of pH and temperature on the mean diameter of unfiltered 1 mg/ml samples of (a) poly(PEGMA$_{0.23}$-co-DMAEMA$_{0.77}$)$_{99}$ and (b) poly(MAA)$_{75}$ in PBS. At pH 5.5, the size of poly(MAA)$_{75}$ at 37, 45 and 60 °C is off-scale (>1400 nm).*

The size and PDI of the PECs both increased with the temperature (**Figure 3.13**). The effect of temperature on the size was more evident in slightly acidic solutions. At 45 °C, the PDI of the PECs increased and an additional size population was observed at all three pH values, confirming the thermoresponsiveness of the nanoparticles. The PEC suspensions became cloudy at 60 °C and multiple size populations were detected. In contrast, the

zeta potential values remained unchanged with increasing temperature. The zeta potentials of the PECs in the two acidic media were less negative than those at pH 7.4. This is due to the presence of free positively charged copolymer in solution and the protonation of the anionic homopolymer in acidic solutions. The effect is most evident at pH 5.5 where existence of multiple size populations at all temperatures indicated the existence of free polymer in solution.

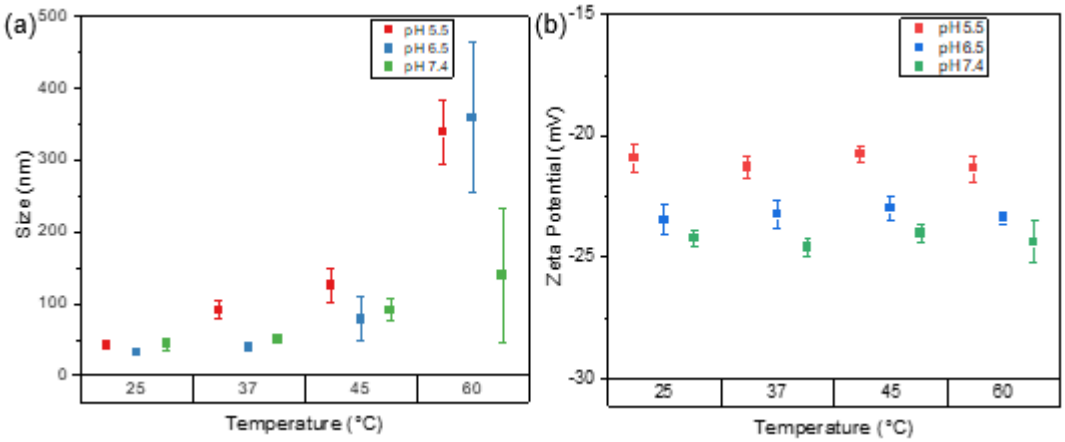

Figure 3.13. *Impact of pH and temperature on the (a) mean diameter and the (b) zeta potential of unfiltered NP2 PECs generated with a 1:1 molar ratio of poly(PEGMA$_{0.23}$-co-DMAEMA$_{0.77}$)$_{99}$ and poly(MAA)$_{75}$ and 1 mg/ml polymer concentration in PBS.*

These results suggest that the PECs are stable at physiological pH and temperature but are unstable at raised temperatures and mildly acidic pH. These characteristics of the PECs make them promising candidates for use as pH-responsive drug delivery systems.

3.4.5 Stability of PECs at room temperature

Zeta potential measurement provides information about the repulsive forces between particles. It can thus provide some information on stability, though

care must be taken when considering the data: for instance, PEGylation was shown to increase the stability of nanoparticles while neutralising the zeta potential (97). Nevertheless, nanoparticle suspensions with highly negative or positive zeta potential values are known to have higher colloidal stability than those with zeta potential values close to zero. NP2 nanoparticles at a total polymer concentration of 1 mg/ml and 1:1 polycation to polyanion molar ratio have a zeta potential of -23.2 mV. The nanoparticles are believed to be stabilised by the electrostatic repulsion between the particles preventing them from coagulating.

The change in size and size distribution of the NP2 PECs was monitored over 28 days at neutral pH (**Figure 3.14**). Fresh samples were synthesised and stored at room temperature. These samples were then taken for size and zeta potential measurements every 7 days. The results show that the mean diameter and zeta potential of the nanoparticles did not change over 28 days. There were small variations among triplicate measurements, but a unimodal size distribution was recorded at all total polymer concentrations, indicating an absence of free polymer and lack of aggregation in solution. The PECs at all concentrations therefore have a similar stability and are stable over 28 days. This is due to the strong negative charge of the PECs, as well as the use of PEGMA in the copolymer; the latter which acts as a stabiliser and solubilises the formulation.

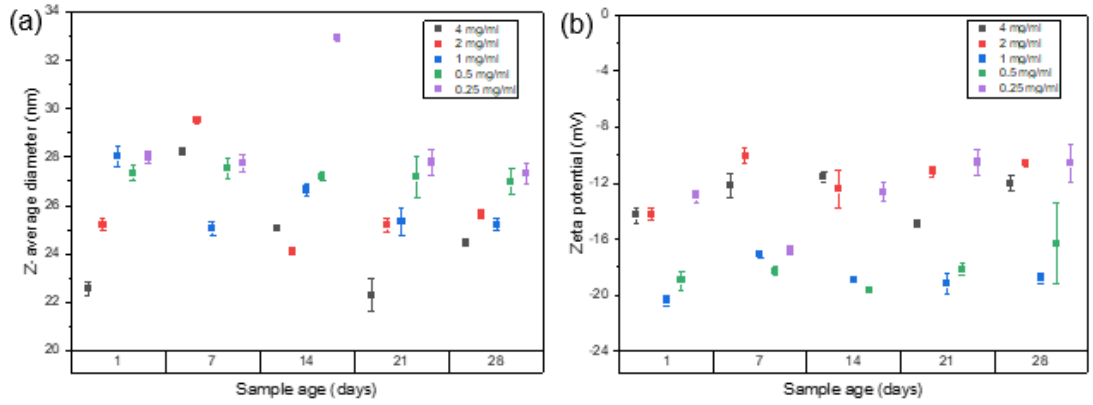

Figure 3.14. *The stability of the NP2 nanoparticles at five different total polymer concentrations over 28 days at neutral pH, showing (a) mean diameter and (b) zeta potential. The molar ratio of poly(MAA)$_{75}$ to poly(PEGMA$_{0.23}$-co-DMAEMA$_{0.77}$)$_{99}$ was 1:1. The error bars represent the standard deviation of the mean. Experiments were performed in triplicate.*

3.4.6 Haemolytic activity

Haemolysis can lead to life threatening conditions such as anaemia and renal failure (98). Blood compatibility of drug delivery systems that are developed for intravenous administration is thus essential. Therefore, a haemolysis assay was performed to assess the cytocompatibility of the polymers and PECs. RBCs were also incubated with PBS and Triton X as a negative control and a positive control, respectively. As shown in **Figure 3.15**, exposure of red blood cells to the polymers and the PECs did not cause haemolysis even at high concentrations. On the other hand, incubation of RBC with Triton X resulted in 100% haemolysis. These results confirm the blood compatibility of the PECs and indicate that they are safe to be used for systemic delivery of drugs.

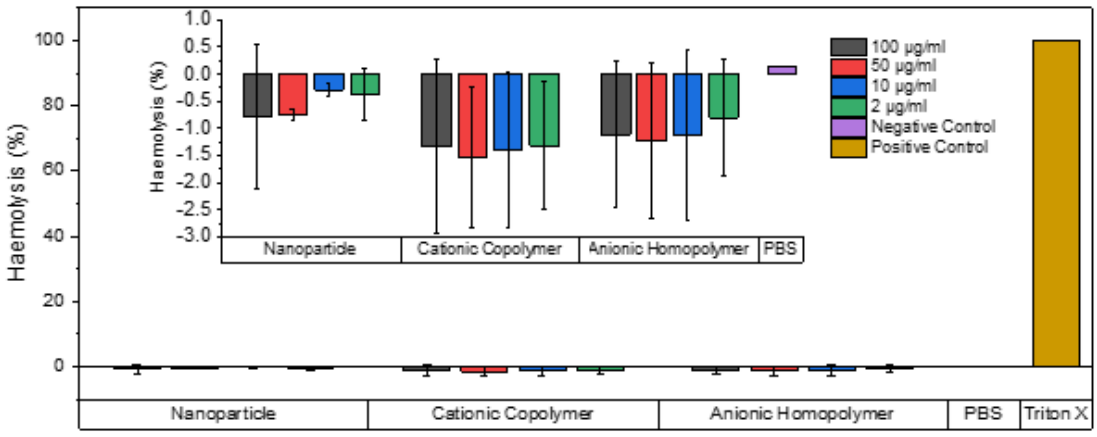

Figure 3.15. *Percent haemolysis of RBCs incubated with the cationic copolymer, anionic homopolymer, and NP2 PECs (2-100 µg/ml) for 1 hour at 37 °C. RBC was incubated with Triton X as a positive control and PBS as a negative control.*

3.4.7 Dye encapsulation

Phthalocyanine (514.5 g/mol) is an organic dye molecule. It has a strong absorption in the far-red region (670 nm) and is used as a photosensitiser in photodynamic therapy (99). The PECs were found to be capable of encapsulating this hydrophobic dye in their core during self-assembly. Photographs of phthalocyanine loaded samples of the polyanion, polycation, and PEC nanoparticles in water can be seen in **Figure 3.16**.

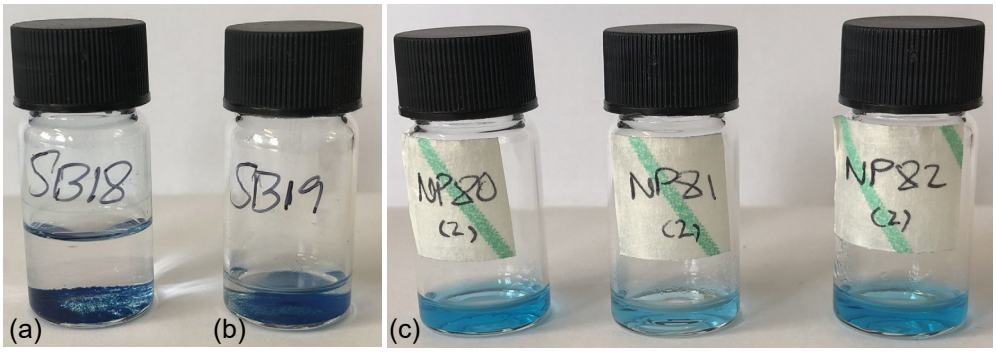

Figure 3.16. *Photographs of (a) poly(MAA) (SB18), (b) poly(PEGMA-co-DMAMEA) (SB19), and (c) three NP2 PEC nanoparticles combined with phthalocyanine (0.2 mg/ml) in water.*

The hydrophobic dye precipitated in vials containing the polymers, whereas phthalocyanine loaded nanoparticles were dispersed in water. The PECs loaded with the dye were stable at room temperature and there was no visible unencapsulated phthalocyanine compound or precipitation in these vials.

The encapsulation efficiency and loading capacity of NP2 nanoparticles with dye concentration of 0.1 mg/ml were found to be 48 ± 8 % and 4 ± 1 %, respectively. The encapsulation efficiency of the dye reached a maximum when 0.2 mg/ml dye solution was used for encapsulation, with EE% reaching 71 ± 2 % and LC of 11 ± 2 %. The encapsulation efficiency decreased to 37 ± 7 % when a higher concentration of dye (0.4 mg/ml) was used for encapsulation. The loading capacity was 9 ± 2 % for this sample. This is due to the lack of PEC nanoparticles available to encapsulate the dye.

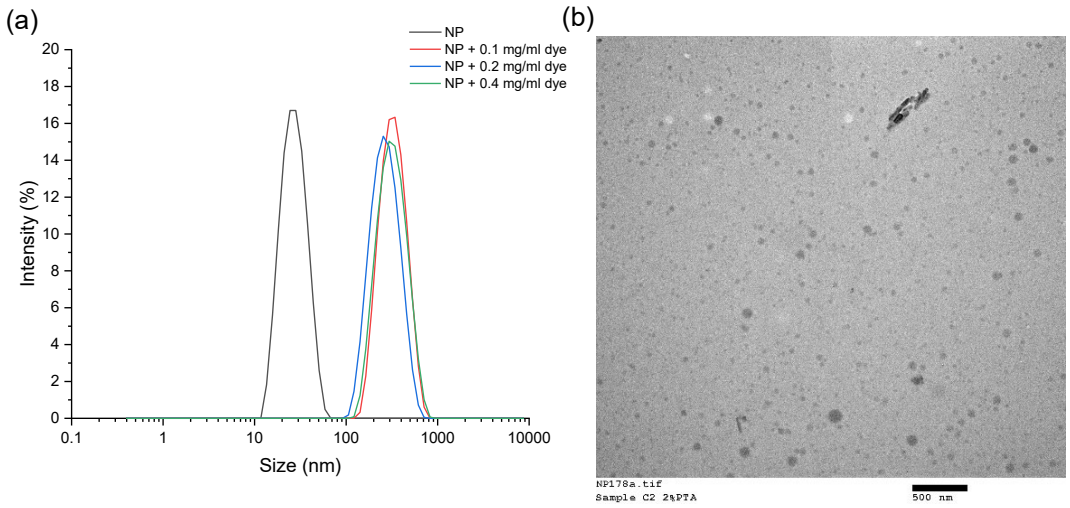

Figure 3.17. *(a) DLS size measurements of the NP2 PECs and the dye-loaded PECs. The mean hydrodynamic diameters of the nanoparticles loaded with 0.1, 0.2, and 0.4 mg/ml of phthalocyanine in water were 243 ± 25 nm, 236 ± 18 nm, and 268 ± 8 nm, respectively. (b) TEM image of NP2 encapsulated with 0.1 mg/ml dye.*

According to the DLS results, phthalocyanine loaded PECs were monodispersed (**Figure 3.17**). The mean diameters of PECs encapsulated with 0.1, 0.2, and 0.4 mg/ml phthalocyanine were 243 ± 25 nm, 236 ± 18 nm, and 268 ± 8 nm, respectively. TEM imaging confirmed the formation of spherical nanoparticles with mean diameters of 75 ± 13 nm when 0.1 mg/ml phthalocyanine was used for the encapsulation process. These results confirmed that the PECs could encapsulate a hydrophobic compound efficiently. Therefore, the next step was to explore the encapsulation of drugs into the PEC nanoparticles. **Table 3.4** shows the list of active agents studied for encapsulation into the PECs.

Table 3.4. *List of active agents used for the encapsulation study.*

Active agent	Molecular formula	Molecular weight (g/mol)	LogP
phthalocyanine	$C_{32}H_{18}N_8$	514.5	6.4
paclitaxel	$C_{47}H_{51}NO_{14}$	853.9	3.0
gemcitabine	$C_9H_{11}F_2N_3O_4$	263.2	-1.4
5-fluorouracil	$C_4H_3FN_2O_2$	130.08	-0.9
carmofur	$C_{11}H_{16}FN_3O_3$	257.26	2.6
dexamethasone	$C_{22}H_{29}FO_5$	392.5	1.8

3.4.8 Drug encapsulation and release of anticancer drugs

In a preliminary study, paclitaxel (a BCS class IV drug) was encapsulated into NP2 PECs. The results are summarised in **Table 3.5**. First, 0.2 mg/ml paclitaxel stock solutions were used to prepare paclitaxel loaded PECs with total polymer concentration of 1 mg/ml. Entrapment efficiency and loading

capacity were found to be 1.5% and 0.3%, respectively. Increasing the concentration of paclitaxel resulted in lower EE% and LC%. Increasing the total polymer concentration in solution from 1 mg/ml to 2 mg/ml, while maintaining the 0.2 mg/ml concentration of paclitaxel, resulted in a slight increase in encapsulation efficiency (to 2.0 %) but a decrease in the loading capacity (to 0.19%). The results clearly indicate the inability of the nanoparticles to encapsulate paclitaxel. Paclitaxel is a hydrophobic drug with a molecular weight of 853.9 g/mol. The nanoparticles were expected to encapsulate paclitaxel efficiently as they showed high encapsulation efficiency of the model hydrophobic dye with molecular weight of 514.5 g/mol. The difference between the encapsulation efficiency of paclitaxel and that of phthalocyanine could be because paclitaxel is a larger molecule. Running methanol through the 0.45 μm filter and analysing the sample showed that paclitaxel was entrapped in the filter. These results oppose the hypothesis that the structure of the PEC nanoparticles should allow them to encapsulate hydrophobic drugs.

Table 3.5. *Encapsulation efficiency and drug loading capacity of paclitaxel and gemcitabine loaded NP2 nanoparticles.*

Drug	Total polymer concentration (mg/ml)	Drug concentration (mg/ml)	EE (%)	LC (%)
Paclitaxel	1	0.2	1.5	0.30
		0.3	0.2	0.04
		0.6	0.1	0.05
	2	0.2	2.0	0.19
	4	0.2	1.5	0.08
Gemcitabine	1	0.1	34.0	2.5
		0.2	36.0	5.4
		0.3	37.0	8.1
		0.4	36.0	10.6
		0.5	33.0	12.0
		0.6	33.0	14.7

Next, NP2 PECs were loaded with different concentrations of gemcitabine (a BCS class III drug). The results are summarised in **Table 3.5**. Starting with 0.1 mg/ml gemcitabine solution, the encapsulation efficiency and loading capacity of the drug were found to be 34% and 2.5% respectively. The encapsulation efficiency and loading capacity increased when the concentration of gemcitabine was elevated to 0.3 mg/ml. A further increase in the concentration of gemcitabine resulted in a decrease in the encapsulation efficiency, while the loading capacity reached its highest value (14.7%) when 0.6 mg/ml gemcitabine was used for the preparation of loaded nanoparticles.

According to DLS, the hydrodynamic diameter and the PDI of the nanoparticles increased when loaded with gemcitabine (**Figure 3.18**). The mean diameter and PDI of nanoparticles prepared by using 0.3 mg/ml gemcitabine were found

to be 111 nm and 0.30. The zeta potential of these nanoparticles also increased to +9 mV. This could be due to the presence of some of the drug on the surface of the nanoparticles as well as the presence of free drug in solution. TEM imaging confirmed presence of two particle populations; nanoparticles with mean diameters of 103 ± 19 nm (**Figure 3.19a**) as well as larger particles with mean diameters of 553 ± 58 nm (**Figure 3.19b**) when 0.3 mg/ml gemcitabine was used for the encapsulation process.

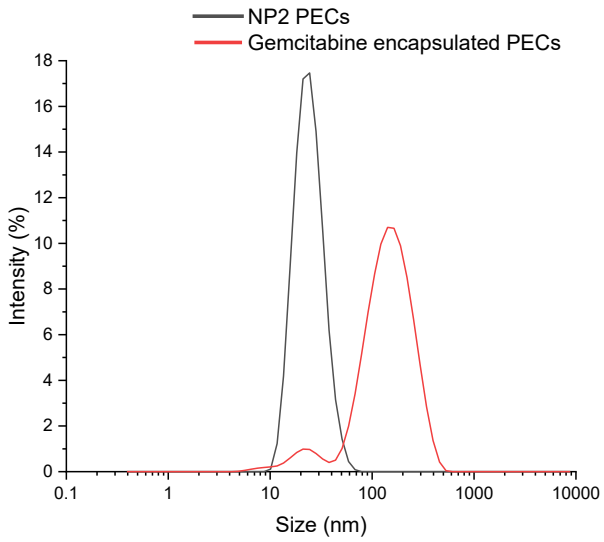

Figure 3.18. *DLS size measurements of the NP2 PECs and the gemcitabine-loaded PECs. An initial concentration of 0.3 mg/ml of gemcitabine was used for the loading of the PECs. The encapsulation efficiency and loading capacity of the drug were 37% and 8.1% respectively.*

Paclitaxel is a hydrophobic drug whereas gemcitabine is hydrophilic. The difference between the encapsulation efficiency of paclitaxel and gemcitabine into the PEC nanoparticles is due to the difference in the water-solubility of the drugs and the inability of the charge neutralised core of the PECs to load large amounts of the hydrophobic drug. Higher quantities of gemcitabine on the other hand could be encapsulated, as the hydrophilic drug is also present at the shell of the PECs.

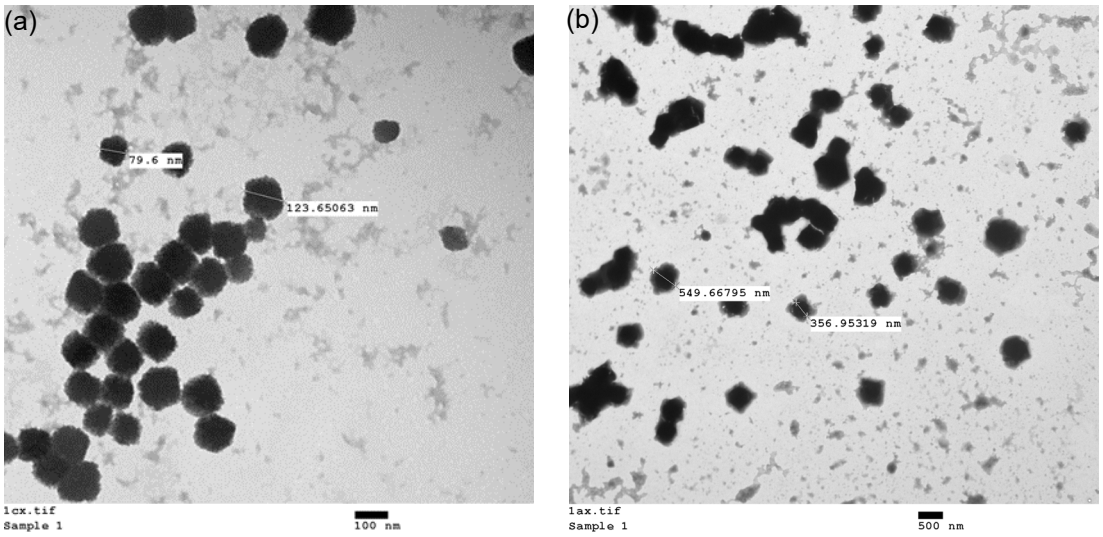

Figure 3.19. *TEM images of gemcitabine loaded NP2 PECs. An initial concentration of 0.3 mg/ml of gemcitabine was used for the encapsulation of the PECs.*

Preliminary screening of the release profile of gemcitabine loaded PECs was conducted using dialysis membranes in PBS at pH 7.4, 6.5, and 5.5 (**Figure 3.20**). A gemcitabine concentration of 0.3 mg/ml was used for the loading. Free gemcitabine was cleared completely from the dialysis membrane after 24 hours. The data showed that 4% of the drug was released after 1 hour at pH 7.4. This increased to 24% after 4 hours. The initial release of drug from the nanoparticles at pH 6.5 and 5.5 was higher than at pH 7.4. This was followed by a decrease in drug concentration in both media after 4 hours. The decrease in the amount of drug in solution was thought to be due to the crystallisation of the drug molecules. The experiments were found not to reach 100% release, thought to be because the drug could not diffuse from the dialysis bag to the outer medium. This was not expected as the MWCO of the dialysis tubes was 3500 which should allow the drug molecules to pass through. These unexpected findings probably arose due to the aggregation of gemcitabine loaded PECs in PBS within the dialysis bag. This hypothesis was supported

by the cloudy appearance of the samples inside the dialysis membranes. Flocs were likely formed because of the low zeta potential of the particles (+9 mV) and the insufficient repulsion between them.

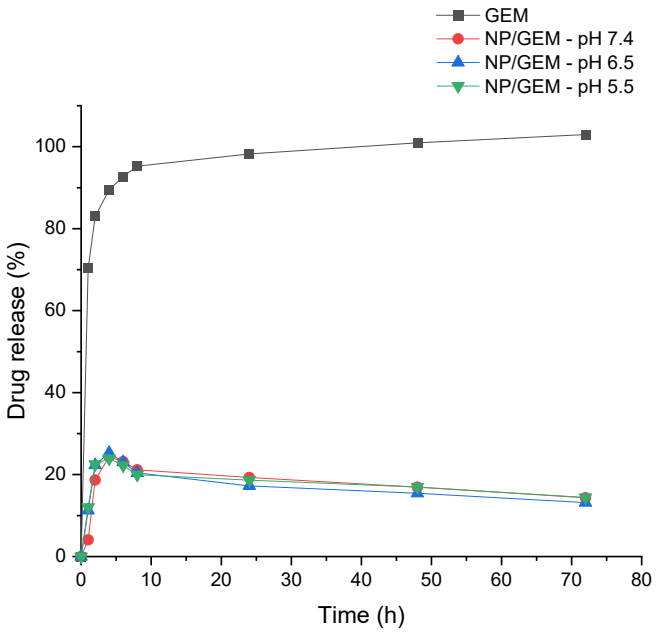

Figure 3.20. *In vitro drug release profiles of gemcitabine and gemcitabine-loaded PECs dispersed in PBS pH 7.4, 6.5, and 5.5 over 72 hours.*

Encapsulation of 5-fluorouracil and its hydrophobic derivative, carmofur, was also investigated, using 0.2 mg/ml solutions of each drug solutions and a 1 mg/ml total polymer concentration at a polycation/polyanion molar ratio of 1:1. The encapsulation efficiency and loading capacity of 5-fluorouracil loaded PECs were 40% and 7.5%, respectively. The hydrodynamic size and PDI were 30 ± 12 nm and 0.32, respectively (**Figure 3.21**). The zeta potential was -14.3 ± 0.6 mV. Encapsulation of carmofur into the nanoparticles resulted in formation of PECs with mean diameter of 31 ± 14 nm and PDI of 0.33 (**Figure 3.21**). The zeta potential was -12.6 ± 0.6 mV, and encapsulation efficiency and loading capacity were 72% and 12.6%, respectively.

The encapsulation of 5-fluorouracil or carmofur into the PECs did not change the overall charge of the nanoparticles drastically. The hydrodynamic diameters of 5-fluorouracil or carmofur-loaded PECs were smaller than that of the gemcitabine-loaded PEC nanoparticles. The smaller particle sizes are likely due to the stronger interactions between the components, leading to the formation of more compact particles. Carmofur is a derivative of 5-fluorouracil. It contains a carbonyl reactive group and a hydrophobic fatty acid tail. The results show that carmofur was encapsulated into the PECs at a higher encapsulation efficiency compared to 5-fluorouracil. This might be due to the ability of carmofur to be loaded into the core of the nanoparticles and also exist in the hydrophilic segment of the PECs.

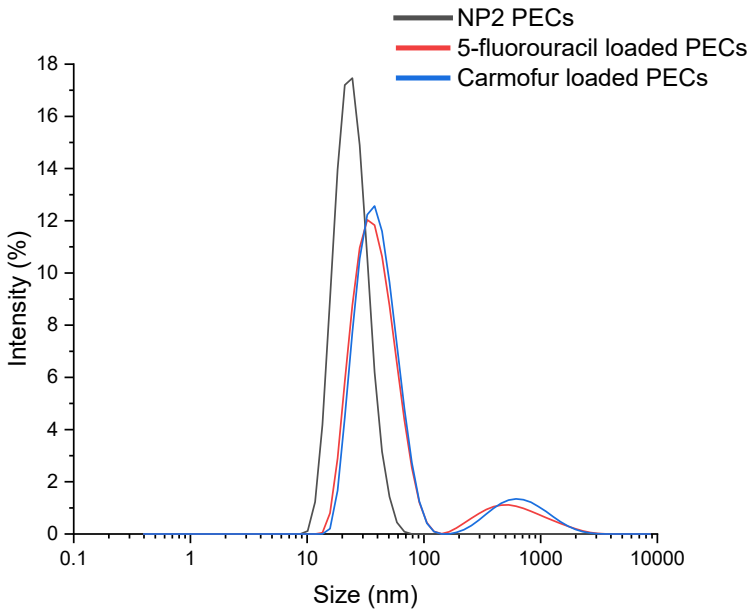

Figure 3.21. *DLS size measurements of NP2 PECs, and 5-fluorouracil and carmofur loaded NP2 PECs.*

The release profiles of 5-fluorouracil and carmofur loaded PECs in PBS at pH 7.4 and 5.5 were investigated using dialysis membranes as described above

(**Figure 3.22**). Free 5-fluorouracil and carmofur were released from the dialysis membranes within the first hour of the experiment in both media. The data also showed a burst release of > 80% of both drugs from the PECs in the first hour. The concentration of 5-fluorouracil in both media reached a maximum after 24 hours while the maximum concentration of carmofur was reached after 6 hours. There were no significant differences in the release profiles of the drugs at pH 7.4 and 5.5, indicating the inability of the nanoparticles to efficiently contain the drugs in the PECs. Thus, although the NPs can entrap 5-FU and carmofur, there are no marked differences in release profile over the pure drug.

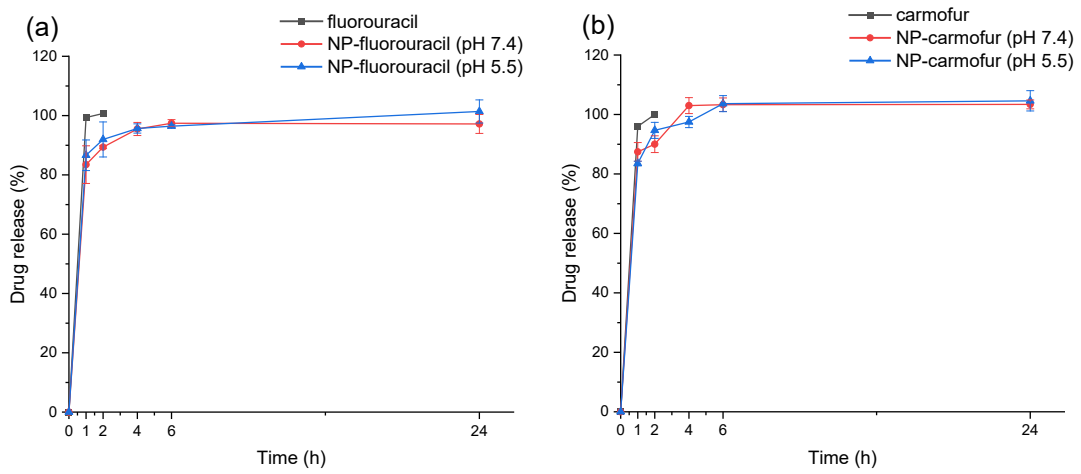

Figure 3.22. *In vitro drug release profiles of (a) fluorouracil load nanoparticles and (b) carmofur loaded nanoparticles dispersed in PBS pH 7.4 and 5.5.*

The results obtained from the dye and drug encapsulation indicate that encapsulation in the PEC nanoparticles is limited to molecules with amine groups capable of interacting with the excess negative charges of the polyanion (PMAA) on the surface of the nanoparticles. As a result, the PECs did not entrap the hydrophobic paclitaxel molecules efficiently. The PECs

showed high encapsulation efficiency of hydrophilic drugs; however, the drugs were released very rapidly.

3.4.9 Dexamethasone-loaded gels

An alternative use of the PECs in drug delivery could be as part of a multi-component solid formulation. One example of this is Ozurdex (an intravitreal implant), which contains 0.7 mg dexamethasone and is available for the treatment of macular oedema and inflammation of the uvea in adults (100). The use of an intravitreal implant for delivery of the drug is favourable compared to the systemic administration of this steroid (90). PECs could potentially be applied to modulate the release properties of such a system.

Hydrogels have been previously reported to prolong the release of therapeutic agents and are promising for implant formulations. However, a burst release of therapeutic agents from hydrogels is often recorded due to the high-water content of the formulations (101). In this study, suspensions of dexamethasone loaded PECs were used to prepare in situ collapsing NIPAAM hydrogels and assess the possibility of using the PECs to develop a formulation that could prolong the release of the drug.

Gels prepared with 20 µl of poly(ethylene glycol) diacrylate (PEGDA) crosslinker appeared slightly cloudy, whereas gels made with a lower amount of PEGDA (10 µl) were clear (**Figure 3.23**). The injectability of the gels was determined qualitatively using 23 G needles. Gels prepared using 10 µl of the crosslinker were easily injectable, while the gels prepared with 20 µl of PEGDA were less easy to inject. Similar results were reported in a previous study (90).

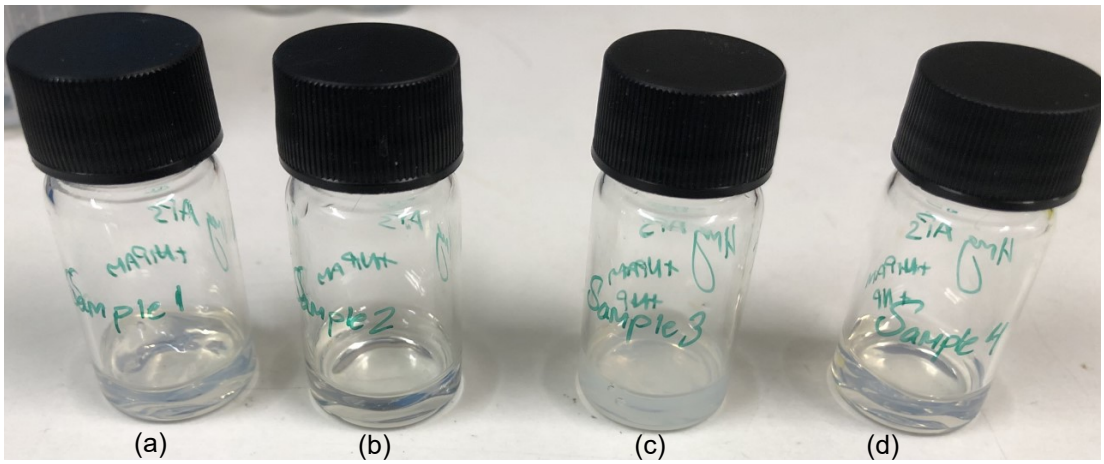

Figure 3.23. *A photograph of (a) NIPAAM hydrogel (20 µl PEGDA), (b) NIPAAM hydrogel (10 µl PEGDA), (c) NP/NIPAAM hydrogel (20 µl PEGDA), and (d) NP/NIPAAM (10 µl PEGDA).*

The volume phase transition temperatures (VPTT) were found to be 35.2 °C and 37.5 °C for the unloaded gels prepared with 10 and 20 µl of PEGDA. These VPTT values were similar to those previously reported for similar gels (90). Addition of PEC nanoparticles to the gels resulted in a slight increase in the VPTT of the gels, to 37.1 °C for the gels with 10 µl of PEGDA and 38.4 °C for the gels with 20 µl of PEGDA (**Figure 3.24**).

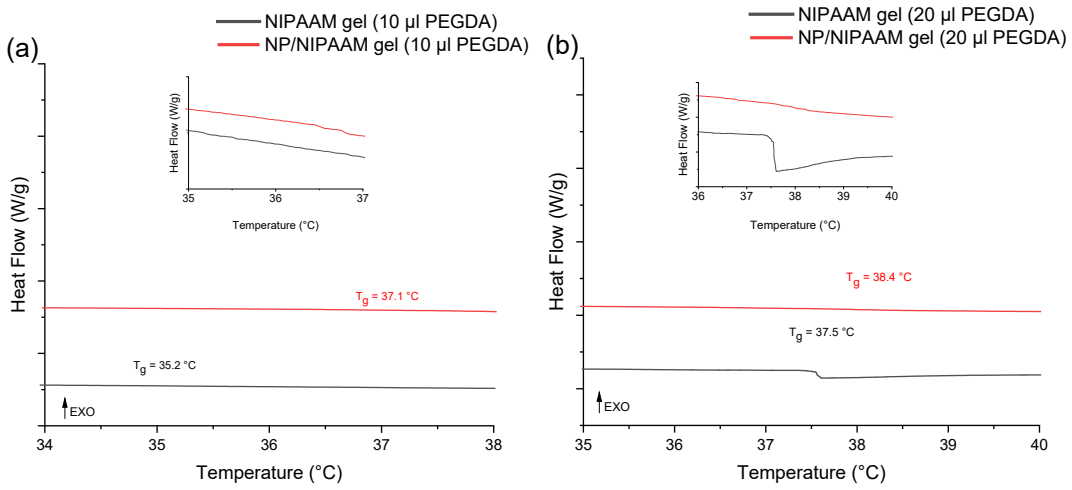

Figure 3.24. *DSC thermograms of (a) NIPAAM and NP/NIPAAM gels containing 10 µl of PEGDA; and (b) NIPAAM and NP/NIPAAM gels containing 20 µl of PEGDA.*

Dexamethasone was encapsulated into NP2 PECs, with a drug concentration of 0.2 mg/ml. The encapsulation efficiency and loading capacity were found to be 8.6% and 1.4% respectively. The low values of encapsulation efficiency and loading capacity are due to the inability of the nanoparticles to encapsulate dexamethasone. A large amount of dexamethasone was found trapped inside the 0.45 µm filters and then removed from the system after the work-up process. This was in agreement with what we learnt from the encapsulation of paclitaxel.

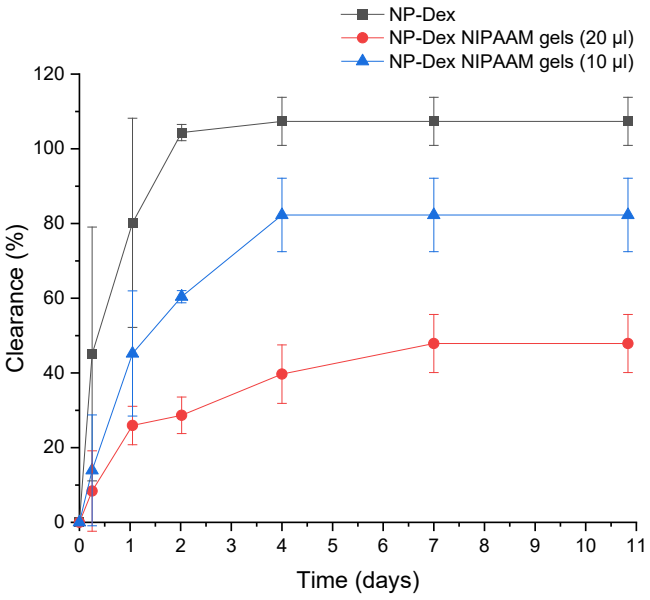

Figure 3.25. *In vitro release profiles of dexamethasone loaded nanoparticles and NIPAAM gels at 37 °C. The error bars represent standard deviation (n=2).*

Dexamethasone-loaded nanoparticles were then used in the preparation of NIPAAM gels and the release of dexamethasone from PECs and NP/NIPAAM gels was studied using the PK-Eye model (**Figure 3.25**). The PK-Eye model mimics the intraocular aqueous outflow and can be used to estimate the clearance times of therapeutics from the back of the eye (102). The release

profile of dexamethasone from the PECs comprised an initial burst phase (45% after 6 hours) followed by complete clearance after 2 days. Loading the PECs in the gel delayed the initial clearance of the drug. The dexamethasone-loaded NP/NIPAAM gels prepared using 10 µl PEGDA released 14% of the encapsulated drug in the first 6 hours. This formulation plateaued at 83% clearance after the 4th day of experiment. Release of dexamethasone was prolonged when 20 µl of the crosslinker was used for the preparation of the gels with 8% of the drug cargo being released in the first 6 hours. By the 7th day, 48% of the drug was cleared from the eye model.

The hydrogels prepared in presence of dexamethasone loaded nanoparticles in solution did not go through complete collapsing at 37 °C as their VPTT values were slightly higher than the temperature set for the experiment. Although formulating the dexamethasone loaded nanoparticles in the form of gels did not display a prolonged release profile which is needed for intravitreal delivery of the drug, they managed to delay the release of the drug which is promising and shows that there is scope to optimise the formulation more to achieve the desirable results.

3.5 Conclusion

Polyelectrolyte complex nanoparticles were prepared by mixing solutions of polyanion and polycation. Upon mixing aqueous solutions of poly(PEGMA-co-DMAMEA) with poly(MAA), PEC nanoparticles were spontaneously formed. Mixing solutions of 1:1 molar ratio polycation to polyanion with polyelectrolytes of similar chain lengths and a low weight fraction of PEGMA in the polymer

mixture led to the formation of stable spherical sub-100 nm nanoparticles with a negative net charge at physiological pH. The optimal formulation was the NP2 PECs prepared by self-assembly of poly($PEGMA_{0.23}$-co-$DMAEMA_{0.77}$)$_{99}$ and poly$(MAA)_{75}$. NP2 PECs had a mean diameter of 25 ± 3 nm, PDI of 0.08, and zeta potential of -23.2 ± 1.4 mV.

The ability of the optimal PEC nanoparticles to incorporate a number of anticancer drugs was assessed. The PEC nanoparticles gave low encapsulation efficiency and drug loading with the hydrophobic drug paclitaxel. Efficient encapsulation of hydrophilic drugs (gemcitabine, 5-fluorouracil, and carmofur) was possible, but the drug release profiles did not meet the desired requirements. Gemcitabine-loaded PECs showed rapid but incomplete release of the drug, while PECs containing 5-fluorouracil or carmofur gave a burst release of approaching 100%.

Finally, dexamethasone-loaded PECs were incorporated into thermoresponsive NIPAAM gels to explore the potential of the PECs in implantable formulations. Incorporating PECs into NIPAAM delayed the release of dexamethasone, resulting in a lower equilibrium release percentage, but sustained release was not achieved. More work is thus required to optimise the formulation further.

Another approach to benefit from the use of the RAFT-synthesised polymers in formulations is to produce amorphous solid dispersions of poorly water-soluble drugs. The next chapter covers the fabrication processes as well as the characterisation of amorphous solid dispersions.

Chapter 4 Amorphous solid dispersions of lidocaine with methacrylic acid polymers

4.1 Introduction

In this project, we focused on polymeric amorphous solid dispersions and their ability to kinetically stabilise a model drug. Lidocaine (2-diethylamino-*N*-(2,6-dimethylphenyl)acetamide) is a commonly used local anaesthetic. Lidocaine (LID) also has antibacterial and antifungal properties and has been widely studied (103). It is considered to be a BCS class II drug as its absorption is limited by dissolution rate. The chemical structure of lidocaine is shown in **Figure 4.1**. Lidocaine is a hydrophobic molecule and a weak base with a pK_a of 7.9. It contains a secondary amide and a tertiary amine group (103). Therefore, at physiological pH, the drug in its free base form is partially ionised and poorly water-soluble. In this project, lidocaine was used as a model drug. The hydrochloride salt of lidocaine is clinically registered. Lidocaine HCl is soluble in water as its amine group is protonated with a positive charge. Solubility of lidocaine HCl in the stomach, however, is reduced due to the common ion effect. Also, depending on the pH, permeation of lidocaine HCl is hindered due to the charge of the salt form (103, 104).

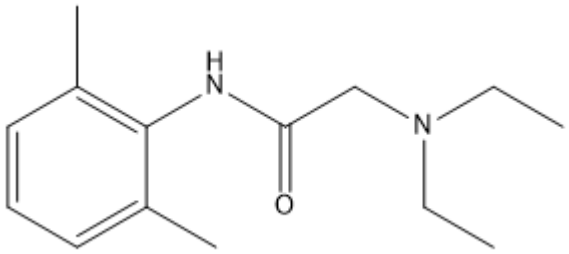

Figure 4.1. *Chemical structure of lidocaine.*

Hydrophilic polymers were chosen for the formation of lidocaine ASDs as they can enhance the wettability of the formulation and drug dissolution (52). One of the polymer carriers selected for this study was the weakly acidic methacrylic acid (MAA) polymers synthesised via RAFT polymerisation. Polymethacrylate derivatives have been widely utilised to produce amorphous solid dispersions. For instance, Eudragit L100-55, an anionic copolymer based on methacrylic acid and ethyl acrylate, was used to prepare complexes with lidocaine and lidocaine hydrochloride using melt extrusion (105). Eudragit E and E PO, cationic copolymers based on dimethylaminoethyl methacrylate, butyl methacrylate, and methyl methacrylate, were used to prepare solid dispersions of itraconazole and indomethacin, respectively (106, 107). In this project, we examine the impact of defined polymers capable of interacting with the model drug and their ability to modify its properties.

4.2 Objectives

The aim of this chapter was to prepare amorphous solid dispersions (ASDs) by ball milling lidocaine, a basic drug, with various polymers including the RAFT-synthesised acidic poly(methacrylic acid) with degree of polymerisation of 80. Different processes such as quench cooling using DSC or liquid nitrogen

as well as ball milling were used to prepare ASDs. Ball milling was chosen as the method for preparing amorphous solid dispersions as it is a simple method and is suitable for small sample quantities. This technique also generates high yields of very fine particles. Lidocaine is a BCS class II drug and was chosen as the model drug along with its hydrochloride salt form. Amorphous solid dispersions of lidocaine hydrochloride were also prepared for the purpose of comparing the interactions between the acidic MAA polymers and the basic drug lidocaine in its free base or hydrochloride salt form. The miscibility and the interaction between the polymers and lidocaine in amorphous solid dispersions were investigated using X-ray diffraction, differential scanning calorimetry, and Fourier-transform infrared spectroscopy. Solid state characteristics of the amorphous solid dispersions of lidocaine hydrochloride salt were also examined.

Lidocaine free base was hypothesised to form stable amorphous solid dispersions with PMAA owing to charge transfer and electrostatic interactions between the drug molecules and the polymers. Positively charged lidocaine molecules in the hydrochloride salt form of the drug however were hypothesised to have weaker interactions with the acidic polymers and the unionised polymers in the formulation were expected to cause lower drug solubility. Amorphous materials are thermodynamically unstable and may crystallise over time therefore the stability of the lidocaine ASD and lidocaine HCl ASD formulations were tested following 9 and 8 months of storage at high temperature (40 °C) and humidity conditions (75% RH), respectively. Lastly, dissolution testing of the formulations was carried out in water, phosphate buffered saline and two acidic media. The ASDs of the salt form of lidocaine

were also subjected to dissolution tests and the results were compared with the results obtained from dissolution tests of lidocaine free base and its amorphous dispersions.

4.3 Experimental

4.3.1 Materials

Methacrylic acid polymers with 20 and 80 repeat units synthesised via RAFT polymerisation as detailed in Section 2.3.4 of Chapter 2 were used. Polyvinylpyrrolidone (PVP, M_w = 10000 Da), poly(acrylic acid) (PAA, M_w = 1800 Da), lidocaine, lidocaine hydrochloride, and hydrochloric acid (HCl) were purchased from Sigma-Aldrich. Fasted state simulated intestinal fluid (FaSSIF) pH 6.5 was purchased from Fisher Scientific.

4.3.2 Preparation of ASDs

Two different ratios of $PMAA_{80}$ to lidocaine were used (30 and 70% w/w) in attempts to prepare samples using a DSC. Samples were heated to 100 °C (above the melting point of lidocaine) at a rate of 10 °C/min and cooled to -80 °C followed by a second cycle of heating to 100 °C at a rate of 10 °C/min.

In the second method of preparation, two different ratios of $PMAA_{80}$ and lidocaine (30, and 70% w/w) were mixed and crushed together in a mortar using a pestle. Samples were then placed in an aluminium bowl which was placed on a hot plate. The temperature was set to 100 °C. Samples in the bowl melted after a few seconds. After 2 minutes, liquid nitrogen was poured onto the samples to quench cool them.

Thereafter, lidocaine in its free base form was milled with each polymer ($PMAA_{80}$, $PMAA_{20}$, PVP, and PAA) at polymer/drug weight ratios of 30, 50, and 70%. Milling was performed at room temperature using a Form-Tech Scientific FTS1000. 1 g of the drug/polymer mixture was added to 15 ml stainless steel grinding jars. Two stainless steel milling balls with 7 mm diameters were used. Ball milling was operated at a frequency of 30 Hz (1800 rpm). In order to find the optimal milling time, a sample with 70% (w/w) $PMAA_{80}$ and 30% lidocaine was milled for 4 hours. At 1, 2, 3, and 4 h, small samples were taken for analysis by X-ray diffraction (XRD). The rest of the samples were milled for one hour (two 25-minute milling intervals with a 10-minute break in between). The same procedure was carried out using lidocaine hydrochloride in combination with two polymers ($PMAA_{80}$ and PVP).

4.3.3 X-ray diffraction

XRD was performed using a MiniFlex 600 diffractometer (Rigaku). Samples on glass sample holders were scanned from 3 to 50º 2θ in steps of 0.02º. The scan rate was 5 degrees/minute. The instrument produces Cu Kα radiation (1.5418 Å). The output voltage and current were 40 kV and 15 mA, respectively.

4.3.4 Fourier transform infrared spectroscopy (FTIR)

A Perkin-Elmer Spectrum 100 attenuated total reflection-FTIR (ATR-FTIR) was used to analyse the drugs, polymers, their physical mixtures (before milling), and the milled ASD samples. A spectral range of 650-4000 cm^{-1}, resolution of 4 cm^{-1}, and scan number of 8 were used.

4.3.5 Thermogravimetric analysis

TGA was carried out using a Discovery instrument (TA Instruments, Waters LLC). Nitrogen was used as the purge gas with a flow rate of 25 ml/min. 5-8 mg polymer or ASD samples were analysed in aluminium pans. Samples were heated from 40 to 300 °C at a rate of 10 °C/min.

4.3.6 Differential scanning calorimetry

DSC was carried out using a Q2000 calorimeter (TA Instruments, Waters LLC). Nitrogen was used as the purge gas with a flow rate of 50 ml/min. 3-7 mg were analysed in aluminium pans sealed with non-hermetic lids. Polymer samples and ASDs were first heated up to 100 °C to remove any water present. Samples were then equilibrated at -80 °C and reheated to 100 °C at a rate of 10 °C/min.

The theoretical glass transition (T_g) values of the ASDs were calculated using Gordon-Taylor equation:

$$T_g = \frac{w_1 T_{g1} + k w_2 T_{g2}}{w_1 + k w_2} \qquad (4.1)$$

K is calculated as follows:

$$k = \frac{T_{g1}\rho_1}{T_{g2}\rho_2} \qquad (4.2)$$

where w_1 and w_2 refer to weight fractions of the components 1 and 2, T_g is the glass transition temperature of the mixture, T_{g1} and T_{g2} correspond to the glass

transition temperature of each component. In Equation 4.2, ρ_1 and ρ_2 refer to the densities of the components.

4.3.7 Dynamic vapor sorption

DVS was carried out using Q5000 SA (TA instruments). Approximately 10-15 mg of samples were placed in the instrument. The temperature was maintained at 25 °C. Relative humidity (RH) was equilibrated at 0% until percentage weight change was lower than 0.01 % for 5 minutes. Relative humidity was then raised to 90% at a rate of 0.5% per minute. The relative humidity was next reduced to 0% at a rate of 0.5% per minute. Samples were analysed by XRD to detect any crystallisation following the DVS analysis.

4.3.8 Molecular modelling

HyperChem 8.0.10, a molecular modelling software package, was used to calculate the molecular mechanics in vacuo. The structures of each polymer and drug were first sketched using ChemDraw 20.1. PMAA and PVP oligomers with 10 repeat units were chosen as representative of the polymers. Each chemical structure was then imported to HyperChem. Hydrogen atoms were explicitly included, and a 3-D structure was generated. The structures underwent geometric minimisation using the MM+ force field, for which nonbonded electrostatic interactions were calculated using bond dipole interactions. Next, energetic minimisation was carried out using AMBER 3 (Assisted Model Building and Energy Refinement) force fields, where distance-dependent dielectric (scale factor of 1) interactions were calculated for atoms separated by three or more bonds (electrostatic and van der Waals 1-4 scale

factors were set to 0.5). The force fields were computed using the Polak-Ribiere conjugate gradient as the minimisation algorithm. The root-mean-square (RMS) gradient termination condition was set to 0.01 kcal/(Å mol). Force field components such as bond stretching, bond angle, dihedral, van der Waals, electrostatic, and hydrogen bonding were included in the calculations. The energetically minimised structures of a polymer and a drug were then merged. The polymer-drug complexes underwent the same minimisation measures.

4.3.9 Stability study

Stability studies were carried out at room temperature (ranging between 20 and 25 °C) and under accelerated storage conditions of 40 °C and 75% RH. Samples were analysed by XRD every week in the first month and then once every 4 weeks.

4.3.10 Dissolution study

An excess amount of the drug (with respect to the expected saturated solubility of lidocaine and lidocaine HCl) in its pure form or in ASD (80-270 mg) was added to a vial filled with 8 ml water. The vials were placed in an incubator at 37 °C under stirring using a hot plate stirrer. At different time points, 0.5 ml aliquots were taken from each sample and filtered with 0.45 µm filters. The filtered samples were then diluted and the concentration of the drugs in each sample was determined on an Agilent Cary 60 UV-Vis spectrophotometer. The same procedure was carried out to investigate the solubility of the drugs in phosphate buffered saline (PBS) with pH of 7.45. Solubility of lidocaine and

lidocaine HCl was also tested in two acidic media; fasted state simulated intestinal fluid (pH 5) and fasted state simulated gastric fluid (pH 2). UV absorbances were measured at 226 nm. The pH of each sample was recorded before and after the 2 h timepoint using a HI 2210 pH meter (Hanna instruments).

Solubility of ASD samples stored under accelerated storage conditions was also tested after 8 weeks. To compare the dissolution profiles of freshly prepared and aged samples, two fit factors F_1 (the difference factor) and F_2 (the similarity factor) were used (108).

$$F_1 = \left(\frac{\sum|R_t - T_t|}{\sum R_t}\right) \times 100 \qquad (4.3)$$

$$F_2 = 50 \times \left\{100 \times \left[1 + \frac{\sum(R_t - T_t)^2}{n}\right]^{-0.5}\right\} \qquad (4.4)$$

R_t and T_t represent the concentration of lidocaine in freshly prepared ASD sample (reference) and the aged sample (test) that was solubilised in water at time point *t*, respectively. *n* is the number of time points.

4.4 Results and discussion

4.4.1 Preparation of polymeric amorphous solid dispersions of lidocaine

Initial samples were first prepared by mixing $PMAA_{80}$ with lidocaine followed by vortexing the mixtures for 1 minute. Two different ratios of polymers to lidocaine, 30:70 and 70:30 w/w (expressed as 30% and 70% w/w $PMAA_{80}$/LID) were used. DSC was used to examine the ability of $PMAA_{80}$ (M_w = 7200 Da) to form amorphous solid dispersions with lidocaine. DSC confirmed that lidocaine

free base is crystalline with a clear melting endotherm peak at 68.5 °C (**Figure 4.2**). This is in accordance with the data in the literature with other studies reporting a melting transition of the pure drug in the range of 68 to 69 °C (103, 105). The polymer used in this study ($PMAA_{80}$) is amorphous. This was confirmed by the absence of a melting endotherm (**Figure 4.2**). Depression of the melting point was observed in the samples as the ratio of polymer to drug in the formulation was increased. This was expected as adding impurities (polymer in this case) lowers the melting point. There are clear melting endotherms in the second heating cycles with the polymer-drug mixtures, showing the inability of the polymers to form ASDs with lidocaine via this route even at the higher polymer to drug weight ratio (70% w/w $PMAA_{80}$/LID) (**Figure 4.2**). This was also proved by the absence of T_g in the thermograms of these samples. Lidocaine present in the formulations was recrystallised during the cooling step. This was confirmed by the presence of an exothermic peak around 23 °C.

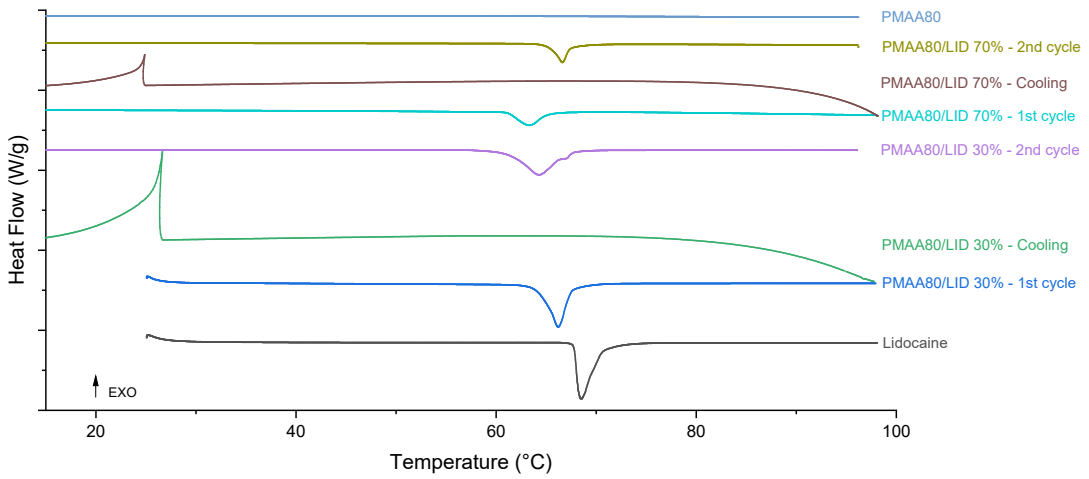

Figure 4.2. *DSC thermograms of the first heating cycle of lidocaine and $PMAA_{80}$, and the thermograms of $PMAA_{80}$/LID mixtures (30% and 70% w/w $PMAA_{80}$/LID) obtained from the first and second heating cycles.*

Cooling the molten drug slowly allows drug molecules time to nucleate and to produce an ordered crystal lattice and thus a crystalline form. If, however, the molten drug is cooled rapidly, the drug molecules may not have time to reorganise in an orderly manner lacking a crystal lattice. Also, homogenous mixtures of drug and polymer cannot be prepared using DSC. Therefore, to ensure rapid cooling and prevent drug molecules to reorganise in an orderly manner as well as mixing of the components, physical mixture samples of $PMAA_{80}$ and lidocaine (30, and 70% w/w $PMAA_{80}$/LID) were crushed and grinded in a mortar and quench cooled using liquid nitrogen. The samples turned from a mixture of pink and white solids into a pale pink powder immediately after the liquid nitrogen had evaporated. Samples were taken for analysis using DSC. The presence of melting endotherms and absence of T_g in the first heating cycle of the samples indicate that amorphous solid dispersions were not formed using this method (**Figure 4.3**). This is due to the rapid recrystallisation of lidocaine as well as the inability of this method to mix and blend the polymer and the drug (44).

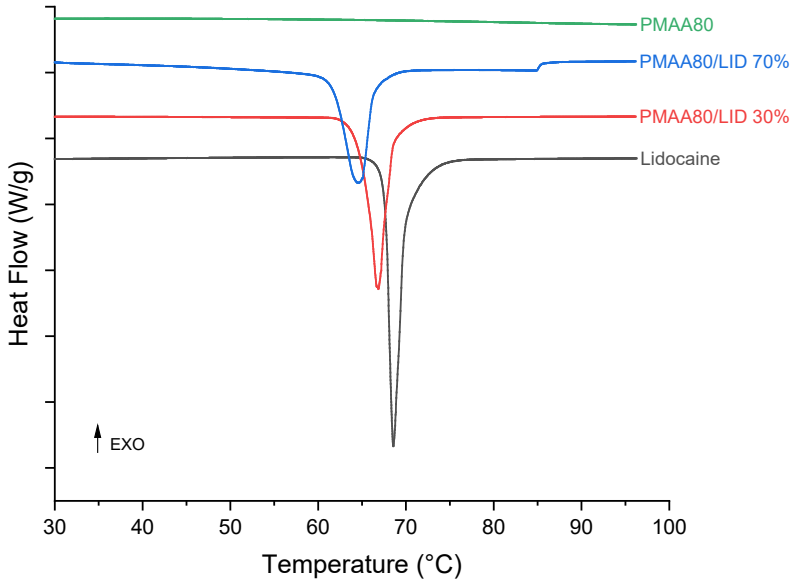

Figure 4.3. *DSC thermograms of lidocaine, $PMAA_{80}$ and $PMAA_{80}$/LID mixtures (30% and 70% w/w $PMAA_{80}$/LID) obtained from the first heating cycle following rapid cooling using liquid nitrogen.*

Ball milling was the next method used to form amorphous solid dispersions of lidocaine. First, $PMAA_{80}$ was milled with lidocaine at 70% w/w $PMAA_{80}$/LID over a 4-hour period. According to XRD, ASDs were formed after 1 hour of milling (**Figure 4.4a**). Upon further milling, three peaks at 18, 38, and 44° 2θ were detected. Crystallisation of the ASDs could occur during the ball milling process because of the increased temperature and molecular mobility. In a study done by Mesallati et al., milling of ciprofloxacin with HPMCAS was carried out at 2-5 °C to avoid increased temperature during the milling process and the recrystallisation of the amorphous material (44). However, the DSC thermograms of the samples collected at different timepoints did not show any sign of melting event which suggests that the XRD peaks were from the sample holders (**Figure 4.4b**). Nevertheless, milling time was kept at 1 hour as ASDs were clearly formed following one hour of milling.

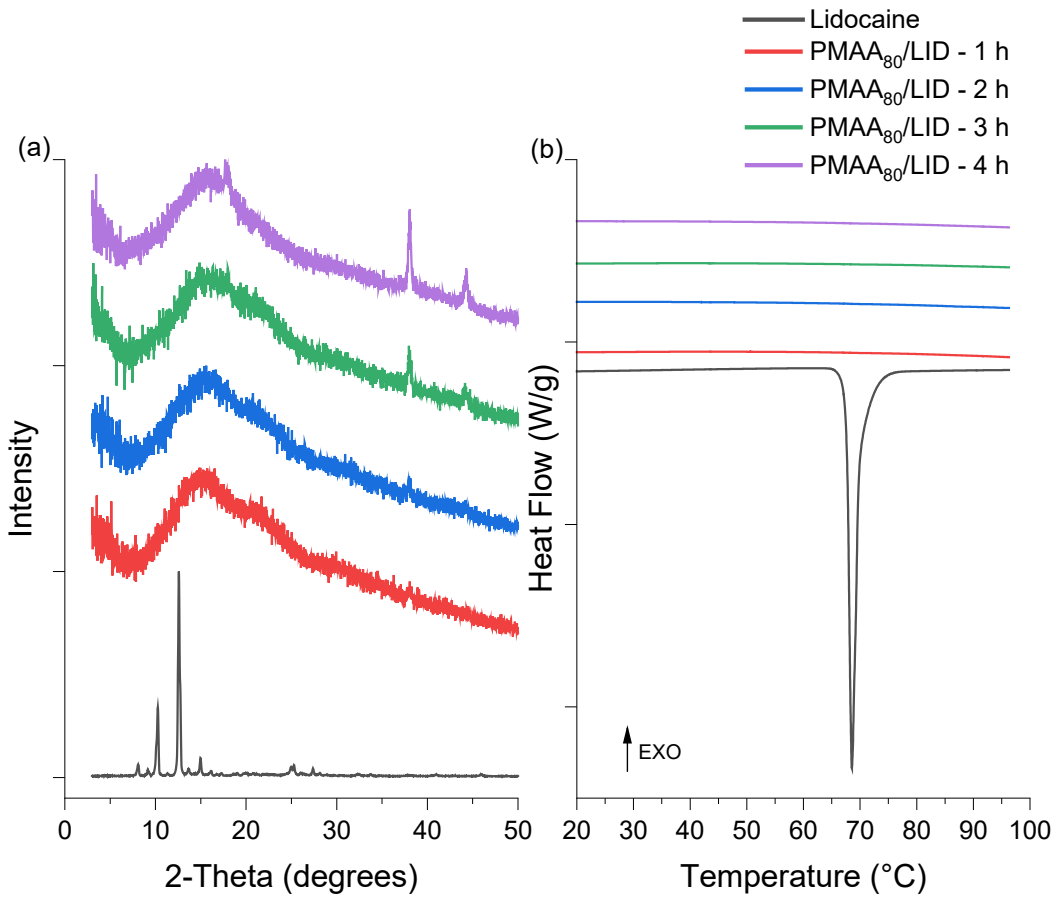

Figure 4.4. *(a) XRD analysis following milling of lidocaine with $PMAA_{80}$ at 70% w/w $PMAA_{80}$/LID for 1, 2, 3, and 4 hours; (b) DSC thermograms of lidocaine and the 70% w/w $PMAA_{80}$/LID samples at different timepoints. Ball milling for 1 hour appeared to be sufficient to yield amorphous solid dispersions.*

4.4.2 Characterisation of polymeric amorphous solid dispersions of lidocaine free base

4.4.2.1 Poly(methacrylic acid)$_{80}$

Three different ratios of $PMAA_{80}$ to lidocaine (30, 50, and 70% w/w polymer/drug) were used to prepare ASDs. As shown in **Figure 4.5**, the XRD pattern of the 70% w/w $PMAA_{80}$/LID mixture before milling (BM) displayed a pattern similar to that of the pure drug in its crystalline form which suggests there is insufficient mixing of the $PMAA_{80}$ and lidocaine. The intensity of the Bragg reflections in the XRD were reduced as the formulation contained only

30% of lidocaine. After milling (AM), the patterns in **Figure 4.5** contained only broad haloes, confirming an amorphous material had been formed. This is in agreement with the literature, where commercial methacrylic acid polymers with high molecular weights and molecular weight distributions including Eudragit L100 and L100-55 have been used to produce amorphous solid dispersions of Ciprofloxacin with a polymer concentration of 40% w/w using ball milling (44).

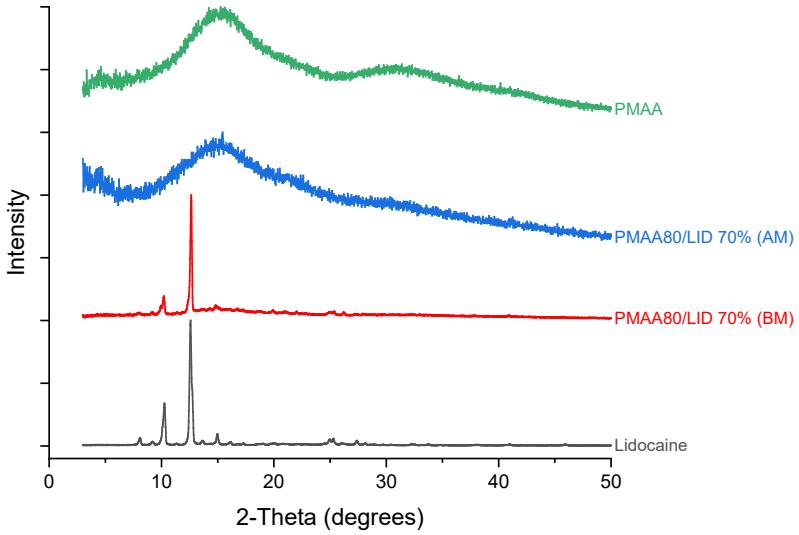

Figure 4.5. *XRD analysis of 70% w/w PMAA$_{80}$/LID before and after milling for 1 hour.*

Two other polymer-to-drug ratios (50% and 30% w/w PMAA$_{80}$/LID) were used to examine the ability of PMAA$_{80}$ to form ASDs with a higher loading of lidocaine (**Figure 4.6a**). Reducing the polymer ratio in the mixtures from 70% to 50% and 30% w/w PMAA$_{80}$/LID increased the intensity of the lidocaine Bragg reflections before milling (due to dilution). These formulations did not produce fully amorphous material and characteristic peaks of crystalline lidocaine could still be detected at 10 and 12.5° 2θ (**Figure 4.6a**).

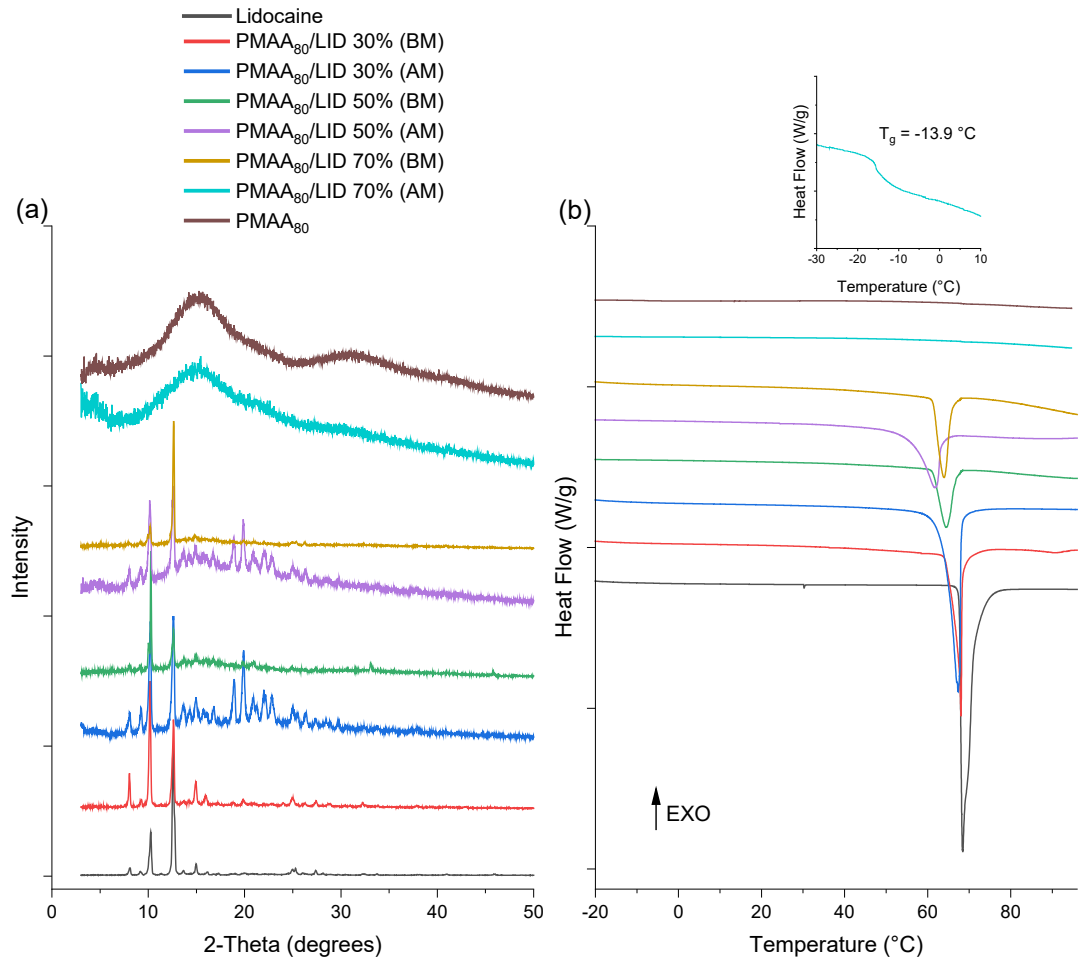

Figure 4.6. *(a) XRD analysis of lidocaine, PMAA$_{80}$, and their mixtures with 30, 50, and 70% w/w PMAA$_{80}$/LID before milling (BM) and after milling (AM) for 1 hour; and (b) DSC thermograms of PMAA$_{80}$ and lidocaine physical mixtures and ASDs obtained from the first heating cycle. The thermogram of the 70% w/w PMAA$_{80}$/LID sample did not display melting endotherms which indicates absence of crystalline material in the formulation.*

As shown in **Figure 4.6b**, the milled 70% w/w PMAA$_{80}$/LID did not display a melting endotherm in the first heating cycle. This suggests that the physical form of this sample is amorphous. The onset of melting endotherms in the physical mixture samples before milling decreased as the amount of PMAA$_{80}$ increased relative to lidocaine. Also, the melting endotherms of the 30 and 50% w/w PMAA$_{80}$/LID formulations decreased after milling compared to their physical mixtures. For example, the onset of the melting endotherm of 30% w/w PMAA$_{80}$/LID in the first heating cycle was lower and broader after milling,

decreasing by 2.21 °C from 67.69 °C before milling to 65.48 °C after milling. The melting point of 50% w/w $PMAA_{80}$/LID decreased by 2.71 °C from 65.66 °C before milling to 62.95 °C after milling. Melting endotherms were also present in the second heating cycle followed by milling and an initial heating to 100 °C which indicates ASDs were not formed when higher drug to polymer ratios were used.

DSC was also used to determine the experimental glass transition temperature (T_g) of the ASD samples. A single T_g was observed in the thermograms of the milled 70% w/w $PMAA_{80}$/LID ASD formulation indicating that the drug is miscible with $PMAA_{80}$. The theoretical glass transition was calculated using Gordon-Taylor equation (4.1). The density and T_g values of 1.138 g/cm^3 and -60 °C were used for lidocaine (105). Polymer's density and T_g values of 1.29 and -6 °C were also used for calculating the K value. The experimental T_g of the 70% w/w $PMAA_{80}$/LID formulation (-13.9 °C) was higher than the predicted theoretical T_g (-26.4 °C) indicating the existence of a drug-polymer interaction (35). Similar positive T_g deviations of lidocaine-Eudragit L100-55 ASDs was reported by Liu et al. (105). The T_g of the ASDs prepared in this study are low which could mean that they will need to be stored in ultracold storage conditions (T_g – 50 °C) to avoid crystallisation.

TGA was then used to determine the mass loss profile of the samples with temperature. The thermal degradation of the pure drug and the milled samples are shown in **Figure 4.7**. Degradation of the pure crystalline form of lidocaine starts at approximately 150 °C. Significant weight loss and degradation of lidocaine was reported to occur above 130 °C (109).

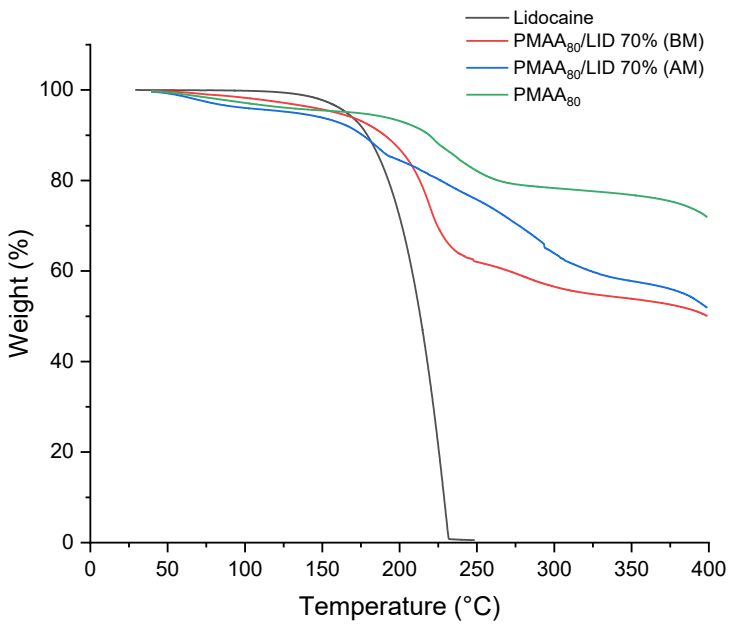

***Figure 4.7**. TGA curves of lidocaine, $PMAA_{80}$, and $PMAA_{80}$/LID samples with 70% w/w $PMAA_{80}$/LID before and after milling.*

The TGA profile for $PMAA_{80}$ displays multistage decomposition. A 5% weight loss attributed to water loss occurs at around 100 °C. A subsequent 15% weight loss between 180-275 °C can be attributed to formation of anhydride and decarboxylation reactions occurring through pendent carboxylates on the polymer chain (**Scheme 4.1**) (110). Complete decomposition of the polymer occurs above 350 °C.

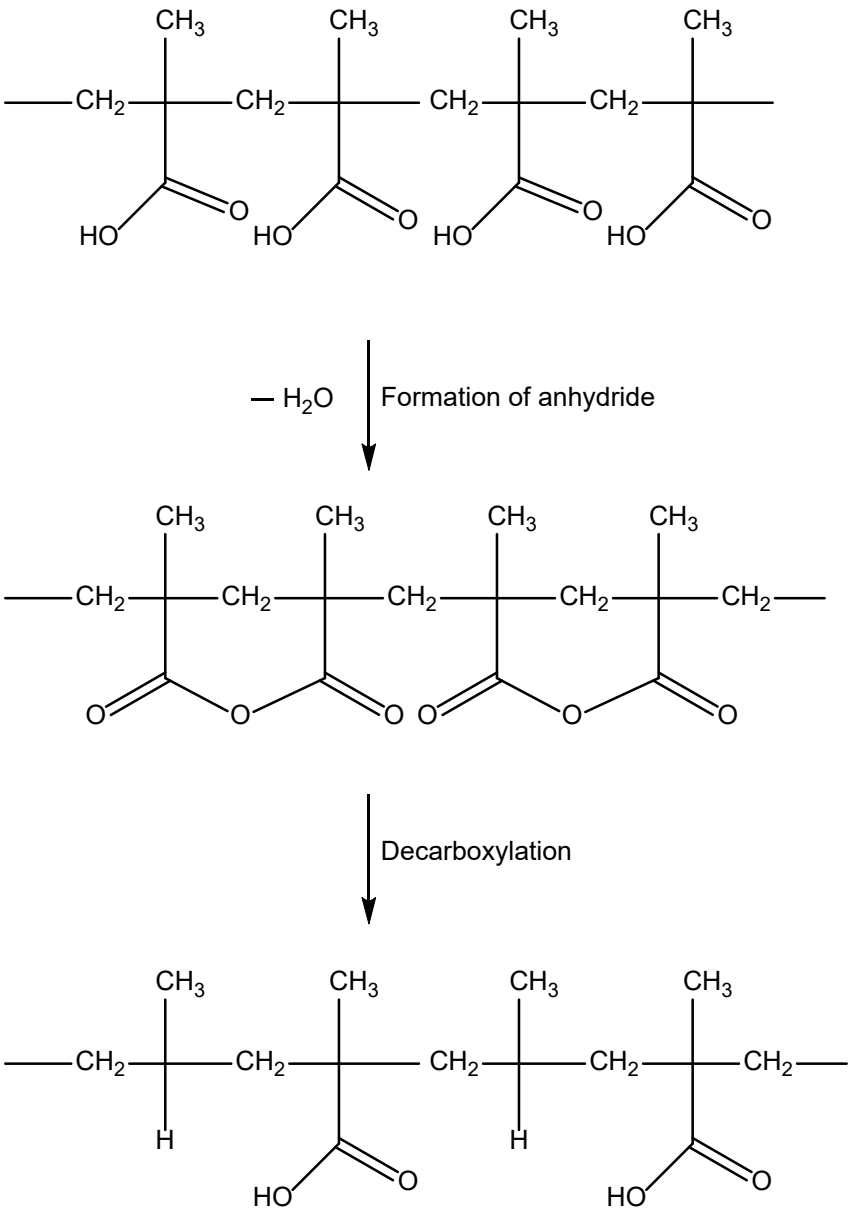

Scheme 4.1. *A schematic representation of formation of anhydride between the adjacent carboxylic groups during decomposition of PMAA.*

Below 150 °C, the 70% w/w $PMAA_{80}$/LID ASDs lost 4-5% of their mass presumably as a result of water evaporation. Initial water loss at around 100 °C is usually observed in the TGA of amorphous solid dispersions (44). The ASD formulation undergoes two subsequent decompositions. The first decomposition between 160-190 °C is attributed to the degradation of lidocaine followed by a second degradation above 210 °C which is caused by

degradation of the polymer. The non-milled sample however undergoes a more substantial degradation above 160 °C. At 231 °C, where lidocaine is completely degraded, the residual mass of this sample is equal to the initial mass of PMAA used in the mixture. This is not the case in the milled samples however where the complete degradation of lidocaine in formulation is delayed.

The interactions between lidocaine and $PMAA_{80}$ were further analysed using FTIR. The FTIR spectra of lidocaine, $PMAA_{80}$, and the three milled formulations at different weight ratios were obtained (**Figure 4.8a**). The bands at 3250 cm^{-1} and 2800 cm^{-1} in the FTIR spectrum of the drug were attributed to the N-H stretching of the amide group and the C-H stretching of the drug, respectively. The lidocaine tertiary amine produced signals in the 1000-1360 cm^{-1} region. The band at 1661 cm^{-1} and 1488 cm^{-1} in the FTIR spectrum of lidocaine were assigned to C=O stretching of the amide group and the secondary amide N-H bending, respectively. In the FTIR spectrum of the polymer, the band at 1700 cm^{-1} was attributed to C=O stretching of the acid group.

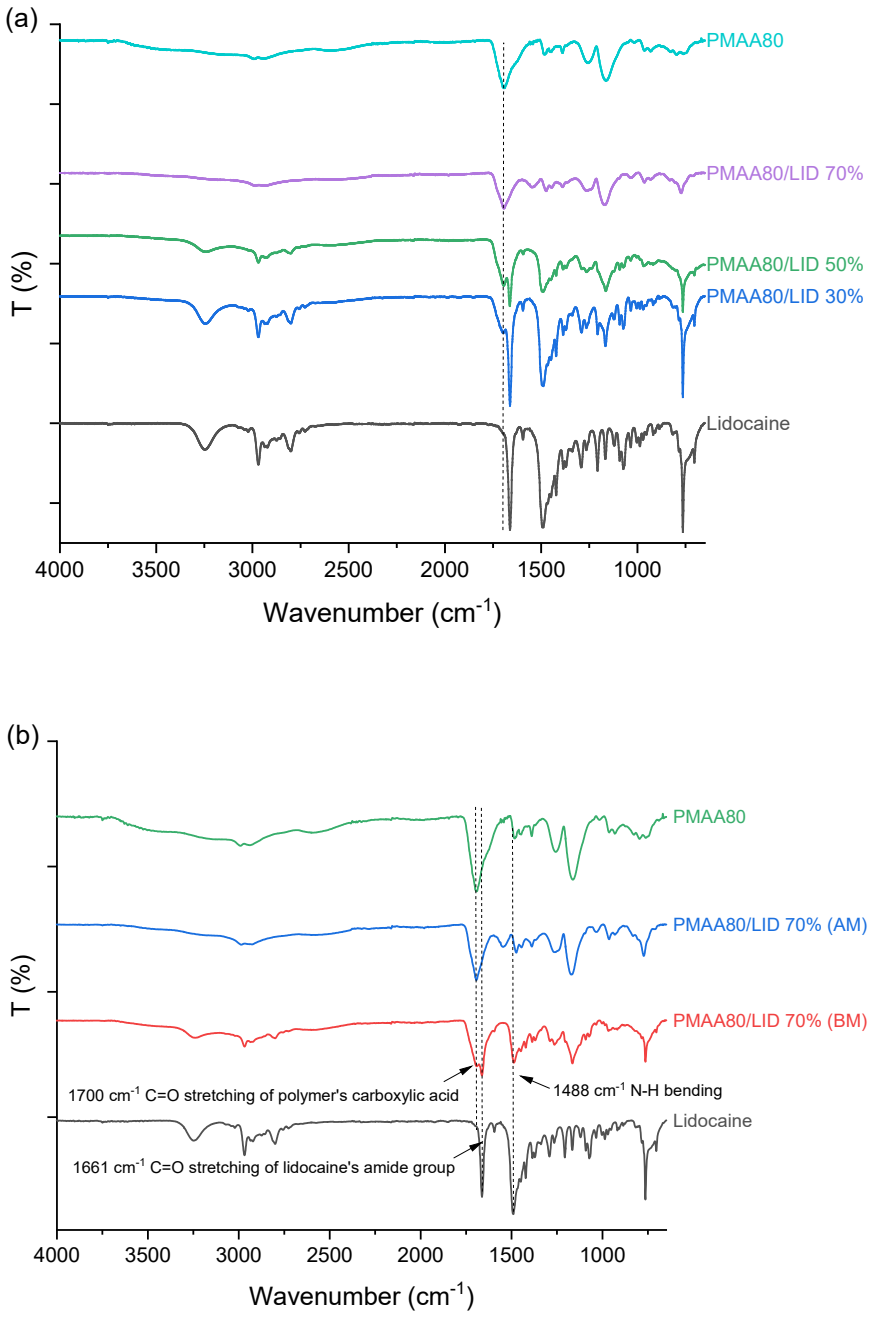

Figure 4.8. *FTIR spectra of (a) $PMAA_{80}$, lidocaine, $PMAA_{80}$/LID milled formulations with 30, 50, 70% w/w $PMAA_{80}$/LID; and (b) 70% w/w $PMAA_{80}$/LID before and after ball milling.*

The 30% w/w polymer/drug formulation and crystalline lidocaine have very similar spectra with sharp peaks corresponding to the drug. The band for the C=O group of the polymer appears as a small shoulder on the left (higher wavenumber) of the lidocaine signal. In the 50% w/w $PMAA_{80}$/LID formulation

this polymer peak is more visible. The 70% w/w polymer/drug formulation after milling displayed a similar spectrum to that of the pure polymer. There is only one clear signal in the 1612-1761 cm^{-1} region, and an absence of the lidocaine amide group band at 3250 cm^{-1}. However, the signal at 764 cm^{-1} confirms the presence of lidocaine in the 70% w/w $PMAA_{80}$/LID formulation.

The spectra of the 70% w/w $PMAA_{80}$/LID formulation before and after milling are shown in **Figure 4.8b**. The peaks in the spectrum of the milled sample are broader than those in the sample before milling. In the spectra of the physical mixture of the polymer and the drug (before milling), the bands attributing to lidocaine (e.g., at 3250 cm^{-1} and 1661 cm^{-1}) can be seen though with lower intensity than in the crystalline pure drug. These peaks are not visible in the spectrum of the milled ASD. Another difference between the before and after milling samples is the presence of a distinct peak at 1544 cm^{-1} in the FTIR spectrum of the milled ASD which is attributed to the drug molecule's tertiary amine N^{+}-H (105). This indicates that the drug is in its free base form in the samples before milling, whereas after milling, the drug exists in its ionised form in the polymer matrix (**Figure 4.9**). The acid-base interactions between the drug and the polymer must have occurred during ball milling. In addition, this high intensity peak can only be seen when a polymer to drug ratio of 70 to 30 is used which indicates excess amount of methacrylic acid was needed to produce the interaction with the drug.

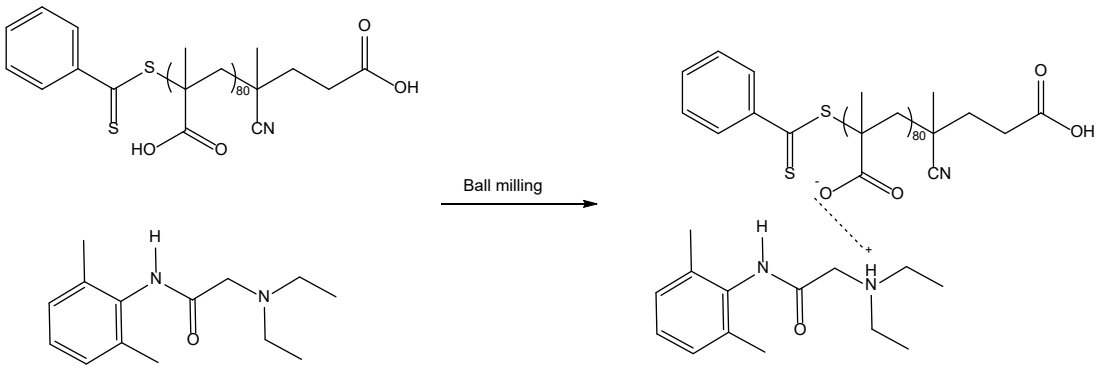

Figure 4.9. *An illustration of the interaction between the carboxylic acid group of $PMAA_{80}$ and the ionised tertiary amine group of the drug following ball milling.*

The FTIR results agree with XRD and DSC results of the $PMAA_{80}$/LID ASDs. Polymer/drug interactions play a key role in developing ASDs as well as improving their physical stability (55). The significant changes in the spectra of the milled 70% w/w $PMAA_{80}$/LID compared to their physical mixture sample as well as the formulations with higher drug loading indicate greater polymer/drug interactions. The strong polymer/drug interactions present in the 70% w/w $PMAA_{80}$/LID ASDs may be due to the higher proportion of carboxylic acid groups in the formulation compared to the formulations with higher drug loading. In addition, as the drug loading in the formulations decreased, the carbonyl group band at 1700 cm^{-1} became broader and incorporated the stretches of lidocaine at 1661 cm^{-1} indicating the presence of counterionic interactions between the weakly acidic polymers and the basic drug. This peak is more intense in the spectrum of the milled samples indicating increased polymer/drug interactions after milling.

4.4.2.2 Poly(methacrylic acid)$_{20}$

To examine whether the degree of polymerisation of poly(methacrylic acid) impacts the formation of amorphous solid dispersions of lidocaine, PMAA with a DP of 20 ($PMMA_{20}$) was milled with lidocaine. XRD indicated that $PMMA_{20}$, like $PMAA_{80}$, also formed amorphous material with lidocaine following milling at a 70% w/w $PMMA_{20}$/LID (**Figure 4.10a**). A T_g at -13 °C was visible in the thermogram of the milled 70% w/w $PMAA_{20}$/LID sample. In the other formulations, although depression of the melting endotherms after milling can be seen in **Figure 4.10b**, the presence of melting endotherms in their thermograms indicates that ASDs were not formed following milling of the components.

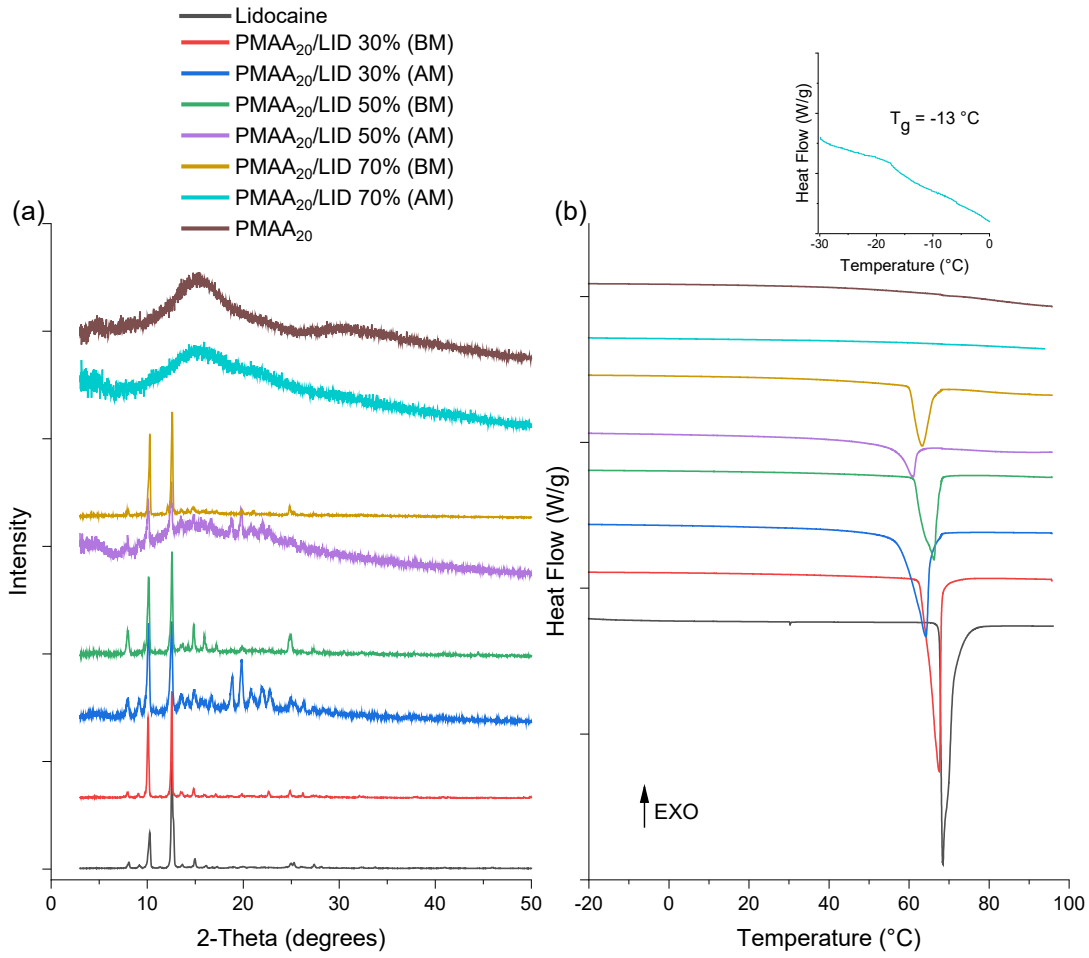

Figure 4.10. *(a) XRD analysis of lidocaine, PMAA$_{20}$, and their mixtures at different polymer/drug ratios before (BM) and after milling (AM); and (b) DSC thermograms of PMAA$_{20}$ and lidocaine physical mixtures and ASDs obtained from the first heating cycle. The thermogram of the milled 70% w/w PMAA$_{20}$/LID sample did not display melting endotherms which indicates absence of crystalline material in the formulation.*

The thermal degradation of 70% w/w PMAA$_{20}$/LID samples before and after milling are similar to those of the PMAA$_{80}$/LID with the milled samples delaying the complete degradation of the drug (**Figure 4.11**). Similar to the PMAA$_{80}$/LID ASDs, the PMAA$_{20}$/LID ASDs undergo two subsequent decompositions. The first degradation occurs between 160 and 190 °C due to the degradation of the drug. The second decomposition above 210 °C is caused by degradation of the polymer.

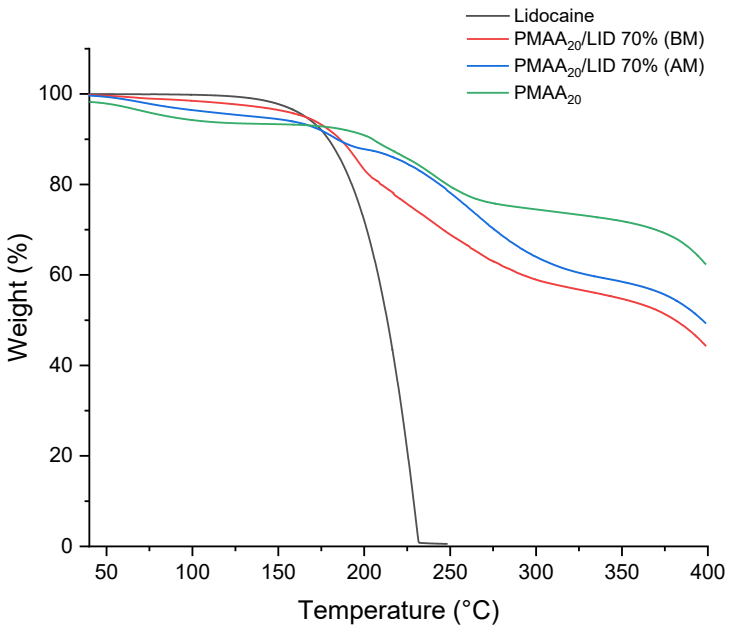

Figure 4.11. *TGA curves of lidocaine, $PMAA_{20}$, and $PMAA_{20}$/LID samples with 70% w/w $PMAA_{20}$/LID before and after milling.*

FTIR spectra of milled lidocaine and $PMAA_{20}$ ASDs and the raw materials are shown in **Figure 4.12**. The spectra of $PMAA_{20}$/LID samples are similar to those of $PMAA_{80}$/LID samples. The spectrum of the 70% w/w $PMMA_{20}$/LID formulation displays broad bands and a single signal between 1620-1766 cm^{-1} incorporating the C=O stretching of both the drug and polymer. In the 30% and 50% w/w $PMAA_{20}$/LID formulations, this band appears as a small signal next to a sharp peak arising from the characteristic lidocaine stretch at 1661 cm^{-1}. Similar to the 70% w/w $PMAA_{80}$/LID ASDs, the only milled sample that displayed a distinct peak at 1544 cm^{-1} representing the drug molecule's tertiary amine N^{+}-H in their FTIR spectrum was the milled 70% w/w $PMAA_{20}$/LID ASDs. The changes in the peak positions and the emergence of new peaks in the 70% w/w $PMAA_{20}$/LID formulation were a result of the amorphous nature of this formulation and interactions between the acidic polymers and the basic drug.

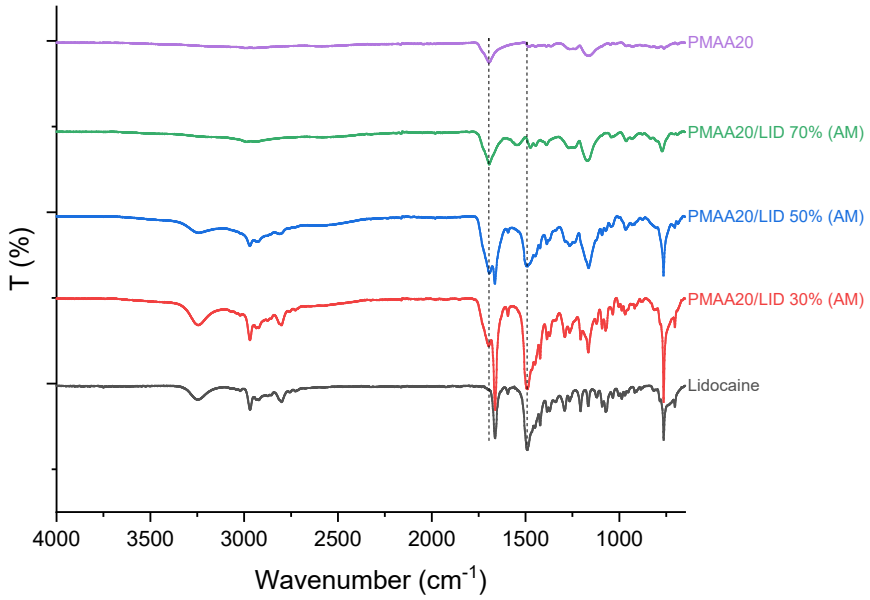

Figure 4.12. *FTIR spectra of $PMAA_{20}$, lidocaine, $PMAA_{20}$/LID milled formulations with 30, 50 and 70% w/w $PMAA_{20}$/LID.*

4.4.2.3 Polyvinylpyrrolidone

Next, PVP of comparable molecular weight (10000 Da) to the methacrylic acid polymer with DP of 80 was used to investigate whether formulating lidocaine with a commercially available polymer could form ASDs. PVP is a non-charged amorphous polymer with a high T_g (128 °C) that is commonly used to enhance the physical properties of poorly water-soluble drugs (111, 112). PVP has previously been used to prepare amorphous formulations of indomethacin and griseofulvin by electrospinning (113). Olaparib ASDs were also formed using a copolymer consisting of PVP following hot-melt extrusion and ball milling (54).

Following ball milling, homogenous samples were obtained. As the drug loading in the formulations decreased, the intensity of the Bragg reflections in the XRD of the formulations after milling decreased and broad haloes

appeared (**Figure 4.13a**). This is due to the presence of larger amount of polymer in the formulation. However, despite the use of a polymer with a high T_g, ASDs were not formed following milling of lidocaine with different amounts of PVP. PVP was also reported to be unable to yield amorphous solid dispersions following milling with different concentrations of ciprofloxacin (44). Similarly in this study, the interactions between PVP and lidocaine were not sufficiently strong to yield fully amorphous material. **Figure 4.13b** shows the DSC thermograms of PVP/LID samples before and after milling. Depression of the melting point was observed in the milled samples. PVP/LID samples at all three concentrations displayed broader melting endotherms after milling compared to before milling. However, the presence of melting endotherms in their thermograms, in both first and second heating cycles, indicates that ASDs were not formed following milling of the components. Glass transition temperature was not observed in the DSC thermograms of any of the formulations.

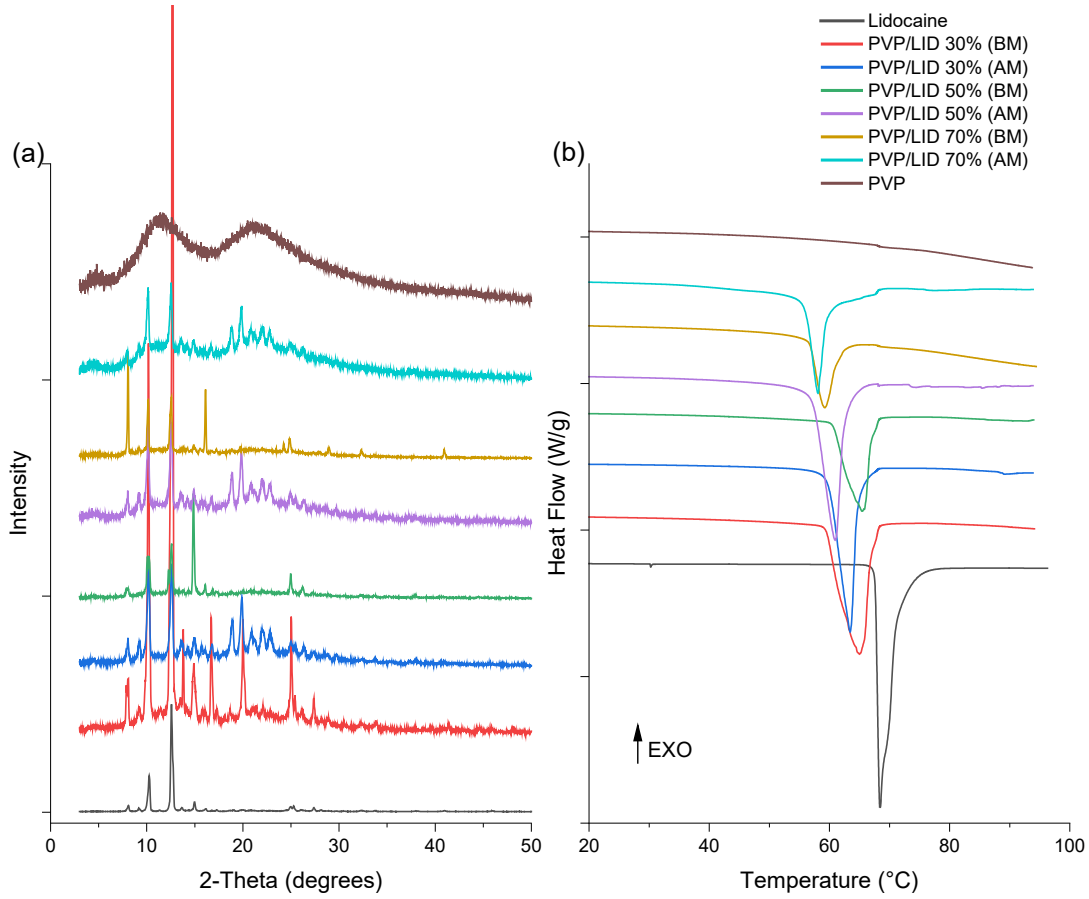

Figure 4.13. *(a) XRD analysis of milled samples of PVP and lidocaine at three different polymer/drug ratios; and (b) DSC thermograms of lidocaine, PVP, and their mixtures with 30, 50, and 70% w/w PVP/LID before and after milling obtained from the first heating cycle.*

The degradation behaviour of PVP and 70% w/w PVP/LID formulation before and after milling is shown in **Figure 4.14**. Prior to reaching 100 °C, PVP lost 5% of its mass as a result of water evaporation. PVP did not undergo any degradation below 340 °C. This was expected as the degradation temperature of PVP was previously reported to lie above 300 °C (114). When PVP was combined with lidocaine, it increased the degradation temperature of the drug from 150 °C to around 280 °C.

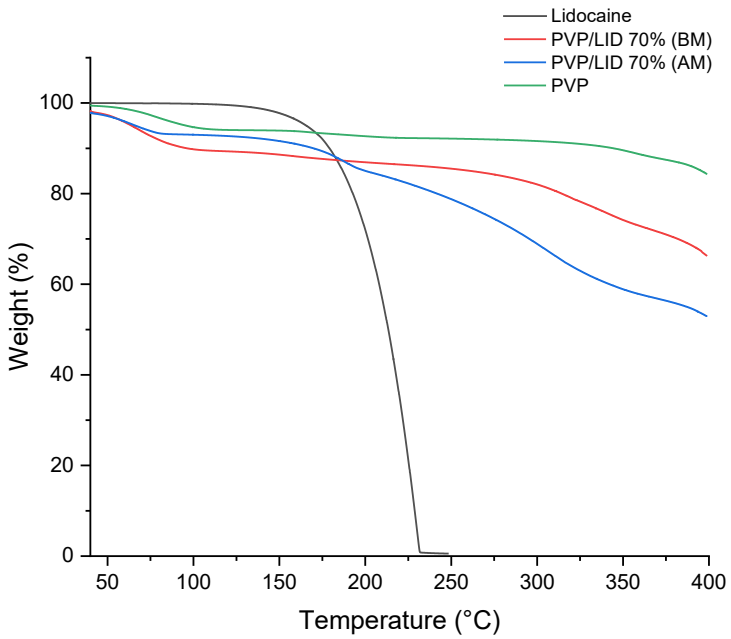

Figure 4.14. *TGA curves of lidocaine, PVP, and PVP/LID samples with 70% w/w PVP/LID before and after milling.*

The FTIR spectra of PVP and PVP/LID formulations after milling are shown in **Figure 4.15**. As expected, the spectra of the milled PVP/LID samples largely resemble the spectrum of crystalline lidocaine. In the carboxylate region of the spectrum of PVP, a band at 1647 cm^{-1} can be seen. In all three PVP formulations, this peak is merged with the C=O stretching in the secondary amide group of lidocaine at 1661 cm^{-1} and only one band is visible. This band is sharper in the formulations with higher drug loading. In the spectra of the 30% and 50% w/w PVP/LID formulations, this peak appears at 1661 cm^{-1} and in the spectrum of the 70% w/w PVP/LID formulation, the peak appears at 1659 cm^{-1}. The small shift in the peak position in the spectrum of the 70% w/w PVP/LID formulation and its broader nature may be a result of the presence of interactions between the drug and PVP. However, these interactions were not strong enough to yield fully amorphous material.

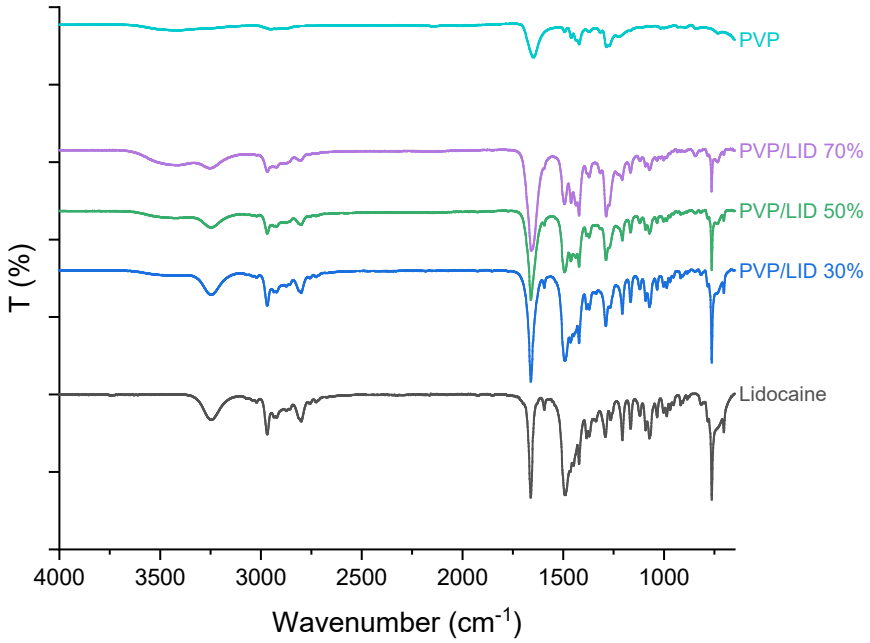

Figure 4.15. *FTIR spectra of PVP, lidocaine, PVP/LID milled formulations with 30, 50 and 70% w/w PVP/LID.*

4.4.2.4 Poly(acrylic acid)

The next polymer used in combination with lidocaine was poly(acrylic acid) (PAA). PAA is amorphous and has been used to produce ASDs of poorly soluble drugs (115). PAA used in this study had molecular weight of 1800 which is comparable with the molecular weight of $PMAA_{20}$. Similar to PVP, poly(acrylic acid) was not able to form amorphous solid dispersions with lidocaine when three different polymer to drug ratios (30, 50, and 70% w/w PAA/LID) were used to prepare the samples (**Figure 4.16a**). Decreasing the drug loading of the formulations resulted in XRD patterns with broad haloes. However, sharp characteristic peaks of lidocaine at 10 and 12.50 2θ degrees could still be seen.

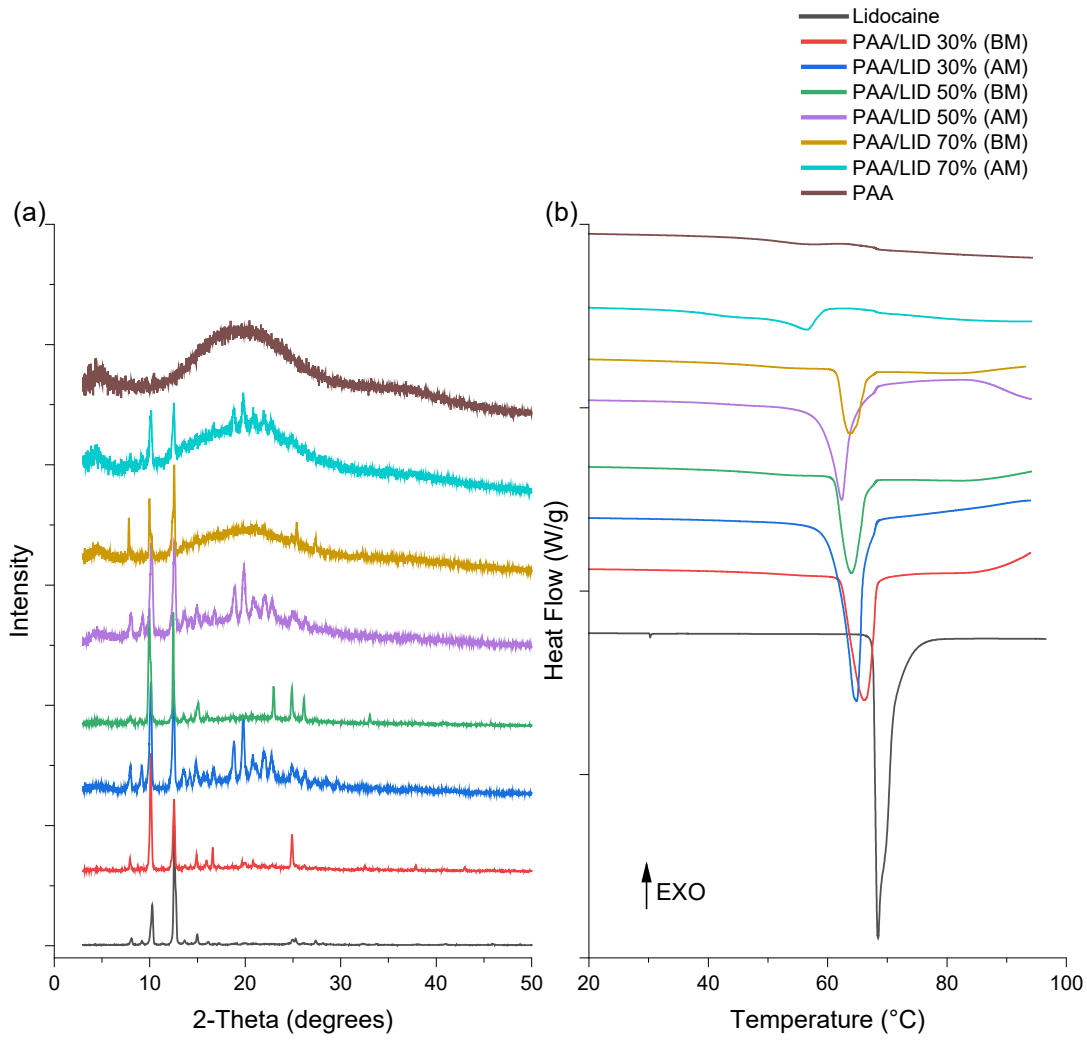

Figure 4.16. *(a) XRD analysis of milled samples of lidocaine and PAA at different weight ratios before and after milling; and (b) DSC thermograms of the first heating cycles of lidocaine, PAA, and PAA/LID (30, 50, and 70% w/w PAA/LID) before and after milling.*

Similar to PVP, the PAA/LID formulations displayed melting endotherms in the first heating cycle after milling (**Figure 4.16b**). However, unlike PVP, milled samples of 50 and 70% w/w PAA/LID formulations did not display melting endotherms in the second heating cycle followed by an initial heating to 100 °C (**Figure 4.17**).

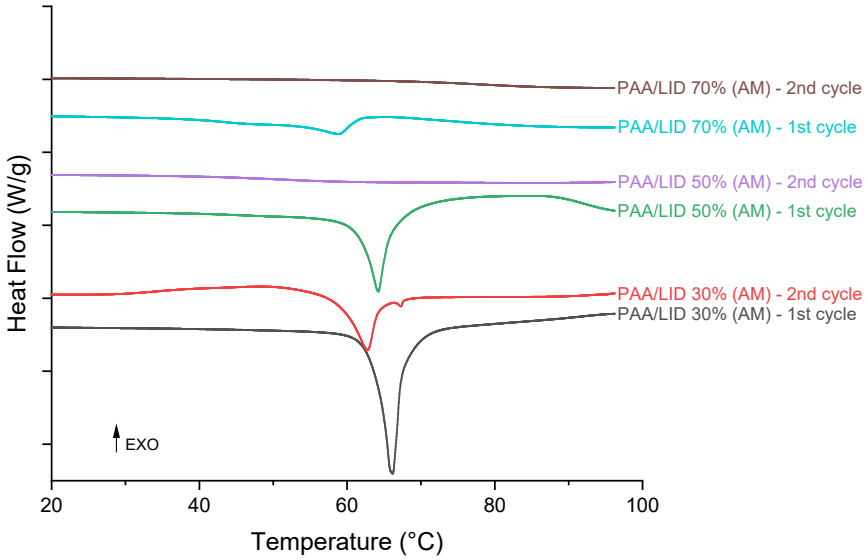

Figure 4.17. *DSC thermograms of PAA/LID ASD formulations after milling, showing data obtained from the first and second heating cycles.*

As shown in **Figure 4.18**, PAA/LID samples lose 5% of its weight at around 100 °C due to water evaporation and degrades above 210 °C. This polymer, when combined with lidocaine, delays the complete degradation of the drug. Milled PAA/LID samples undergo thermal degradation above 190 °C compared to thermal degradation of around 175 °C before milling.

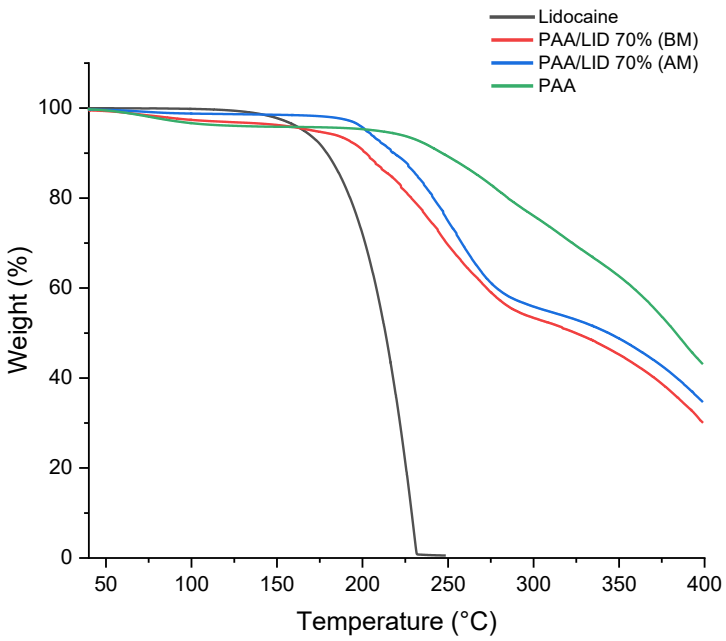

Figure 4.18. *TGA curves of lidocaine, PAA, and PAA/LID samples with 70% w/w PAA/LID before and after milling.*

The interactions between poly(acrylic acid) (PAA) and lidocaine were also investigated. The IR absorption bands became broader as the proportion of lidocaine was reduced in the formulations (**Figure 4.19**). The peak at 1697 cm^{-1} was attributed to the C=O of carboxylic acid group of the polymer. This peak appears as a small shoulder on the left (higher wavenumber) of the stretching band of lidocaine's secondary amide group and becomes more visible with increasing amounts of polymer relative to lidocaine. Although ball milling the samples caused visible changes to the spectra of PAA/LID formulations, acrylic acid polymers were unable to interact with drug molecules and generate fully amorphous material with lidocaine.

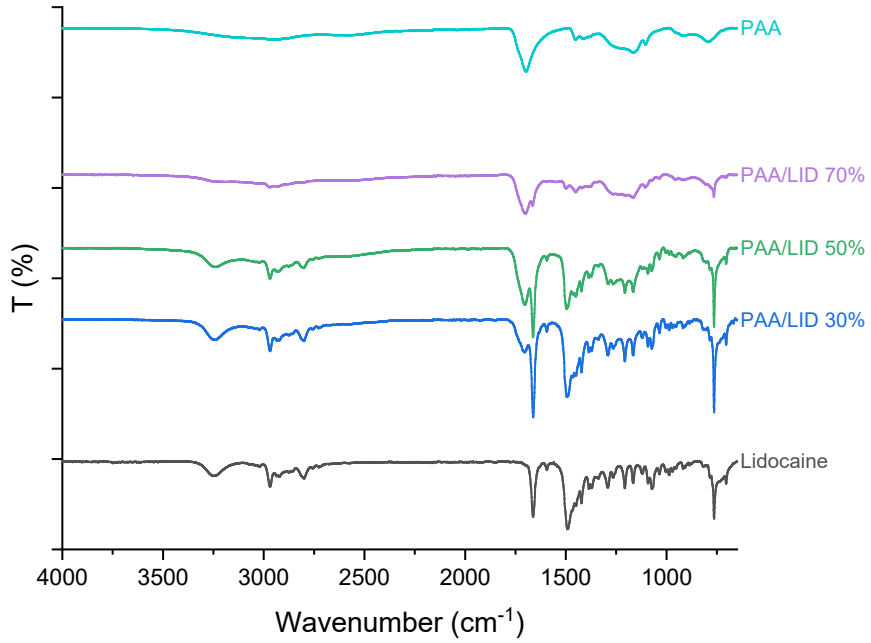

Figure 4.19. *FTIR spectra of PAA, lidocaine, and PAA/LID milled formulations with 30, 50 and 70% w/w PAA/LID.*

4.4.3 Molecular modelling of lidocaine ASDs

The interactions between the polymers and lidocaine were investigated in more detail using a molecular modelling software. The molecular modelling procedure is similar to that reported by Lopez et al. (113). Molecular models of PMAA, PVP, PAA, lidocaine, PMAA/LID, PVP/LID, and PAA/LID were constructed using the HyperChem software. The structure of the polymer decamers and the drugs in their neutral form were individually optimised. The optimised structures of a polymer and a drug were then merged and optimised again. **Figure 4.20** shows the geometric arrangements of the energy-minimised polymer-drug complexes. The PMAA chain shows a flexible conformation probably due to the repulsive forces between the carboxylic acid groups as well as presence of methyl groups on the backbone of the polymer.

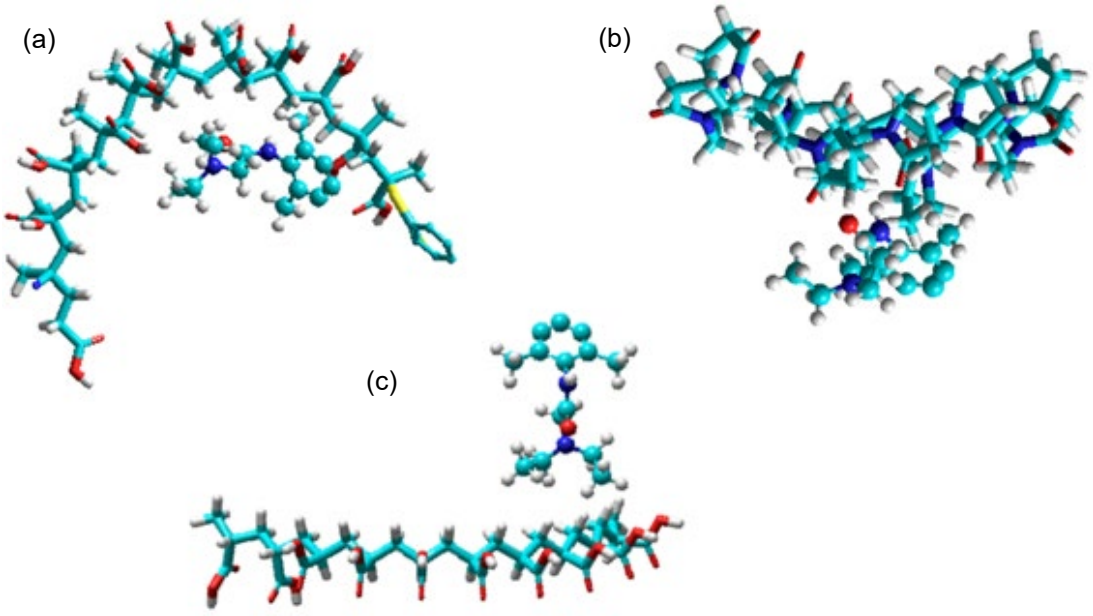

Figure 4.20. *Optimised geometric arrangements of (a) $PMAA_{10}$/LID, (b) PVP_{10}/LID, and (c) PAA_{10}/LID. The decameric polymers can be seen in tubes and lidocaine in balls.*

The energetic contributions to the overall energy for the polymers and drugs alone as well as the polymer-drug complexes are presented in **Table 4.1**. A negative difference (∆E) between the total energy of the polymer-drug complex and the sum of the energies of the polymer and drug molecules indicates stabilisation of the complexes. The combined energy of $PMAA_{10}$ and lidocaine is 507.77 kcal mol^{-1}, whereas the total energy of the optimised complex is 490.79 kcal mol^{-1} giving a ∆E of -16.98 kcal mol^{-1}, which indicates the existence of interactions between the polymer and drug. ∆E values of -14.01 kcal mol^{-1} and -3.02 kcal mol^{-1} were calculated for the optimised complexes of PVP_{10}/LID and PAA_{10}/LID, respectively.

Table 4.1. *Details of the optimised geometry energetics of PMAA/LID, PVP/LID, and PAA/LID molecular models. The calculations were done inputting the unionised polymer and drug molecules for analysis.*

	Minimised energy contributions (kcal mol $^{-1}$)					
Species	**bond stretching**	**bond angle**	**Dihedral**	**van der Waals**	**hydrogen bonding**	**total**
$PMAA_{10}$	11.84	290.36	10.38	36.58	-0.29	348.87
PVP_{10}	4.18	88.61	39.89	-11.37	0	121.3
PAA_{10}	1.56	7.64	2.76	-3.55	-0.13	8.28
Lidocaine	3.0	140.58	8.36	6.96	0	158.9
$PMAA_{10}$/LID	14.23	430.87	17.01	28.98	-0.3	490.79
PVP_{10}/LID	7.36	229.29	45.89	-16.36	-0.0049	266.18
PAA_{10}/LID	4.55	148.3	11.15	0.29	-0.13	164.16

Lidocaine possesses a secondary amide group that can act as hydrogen bond acceptor and donor. PMAA and PAA are weakly acidic polymers that possess hydrogen bond donor carboxylic acid whereas PVP possesses hydrogen bond acceptors. The negative ΔE values recorded for all the optimised complexes suggest presence of interaction between the polymers and the drug within the mixtures. The hydrogen bonding within $PMAA_{10}$/LID is greater than that in the PVP_{10}/LID or PAA_{10}/LID complexes which could support formation of ASDs following milling of PMAA and lidocaine. The preliminary modelling is consistent with there being increased polymer/drug interactions between PMAA and lidocaine compared to PVP/LID and PAA/LID.

4.4.4 Stability of the lidocaine ASD formulation

After ball milling, $PMAA_{80}$/LID and $PMAA_{20}$/LID formulations exist as amorphous solid dispersions. However, it is vital to investigate the ability of these formulations to maintain the amorphous form over time, especially in the presence of humidity since water is a plasticiser. In addition, high temperatures could result in an increase in molecular mobility in ASDs and cause phase separation and recrystallisation of the drug (47).

According to DVS results, following raising the RH to 90%, the milled 70% w/w $PMAA_{80}$/LID ASDs sorbed the largest amount of water (11% weight change) compared to the samples before milling and the raw materials (**Figure 4.21**). The polymer alone and the physical mixture formulation also sorbed water and a change of mass of 6.9% and 6.7% was recorded for these samples, respectively. In contrast, at 90% relative humidity, lidocaine in its free base form experienced only 0.5% weight change. These results were expected as amorphous materials are hygroscopic and water is adsorbed and absorbed into their structure whereas crystalline material can only adsorb water by surface adsorption (49). In addition, the polymer used in the formulation, $PMAA_{80}$, is a hydrophilic polymer. In the DVS plot of the amorphous solid dispersion, there was no sign of mass loss at elevated relative humidity. This indicates that crystallisation did not occur during the process of increasing the relative humidity in the DVS (116).

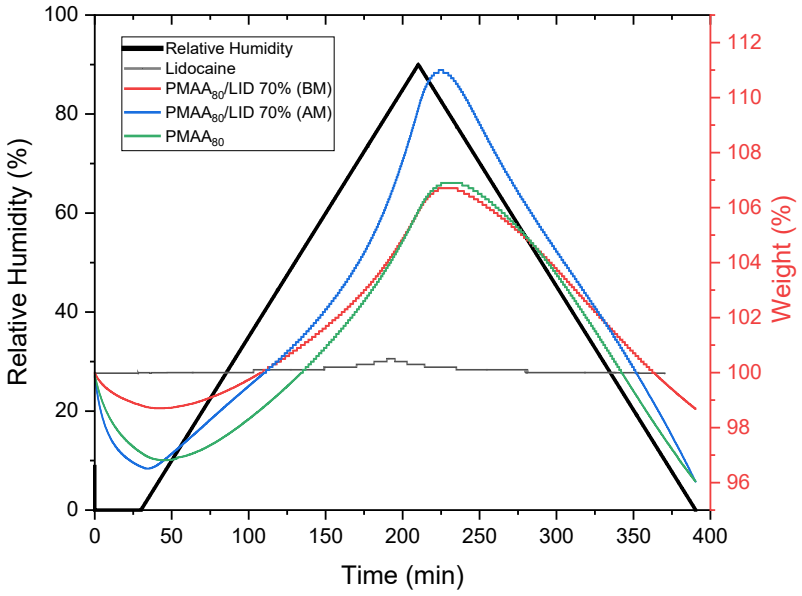

Figure 4.21. *DVS analysis of lidocaine, $PMAA_{80}$, and 70% w/w $PMAA_{80}$/LID samples before and after milling.*

In a similar study, the DVS plot of amorphous solid dispersions of PVP and griseofulvin showed no sign of mass loss after reaching 75% RH (116). However, the XRD of the sample displayed sharp Bragg reflections comparable to the characteristic peaks of the crystalline griseofulvin, indicating a physical form change following an increase in the relative humidity during the DVS experiment. This is because water sorption can cause crystallisation of amorphous material by lowering T_g and increasing the molecular mobility. In this project, however, the 70% w/w $PMAA_{80}$/LID ASDs remained amorphous, according to the XRD analysis (**Figure 4.22**). This could be due to the interaction between the drug and $PMAA_{80}$.

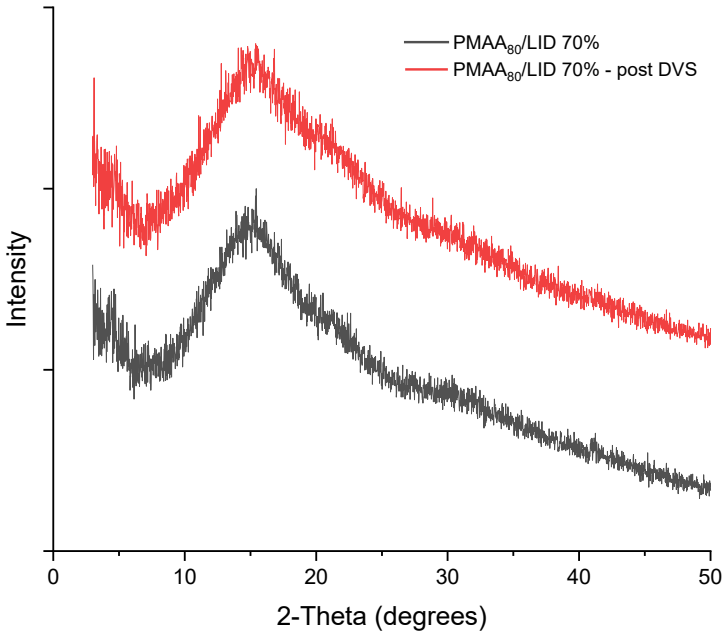

Figure 4.22. *XRD analysis of milled 70% w/w $PMAA_{80}$/LID ASDs before and after DVS analysis. The temperature was maintained at 25 °C. Relative humidity (RH) was equilibrated at 0% and was raised to 90% at a rate of 0.5% per minute.*

In this study, the lidocaine ASDs formed have low T_g (below zero), therefore the stability of the 70% w/w $PMAA_{20}$/LID and $PMAA_{80}$/LID ASD samples were assessed by XRD and DSC after storing the samples in the lab at room temperature as well as under accelerated aging conditions (40 °C and 75% RH). The XRD and DSC of the aged samples were the same as the freshly milled samples. According to the XRD patterns (**Figure 4.23a**), the samples remained amorphous after 9 months of storage in both conditions. DSC thermograms of the aged samples also showed no visible melting endotherm (**Figure 4.23b**).

A drug in its amorphous form has higher free energy compared to its crystalline form and therefore recrystallisation is thermodynamically favoured (52). During storage, the energy of the amorphous material is reduced to a more

stable/lower energy state without recrystallisation (117). This is called relaxation. Recrystallisation could occur over time and cause further reduction of excess energy present in amorphous material and result in a decline in the stability and solubility of the drug. However, in this study, the stability of the aged ASD samples was found to be unaffected. There was no sign of relaxation (usually appearing as an endothermic event near the glass transition) in the DSC thermograms of the ASDs. This suggests that the low T_g of the samples did not cause acceleration of the molecular mobility and did not impact their physical stability.

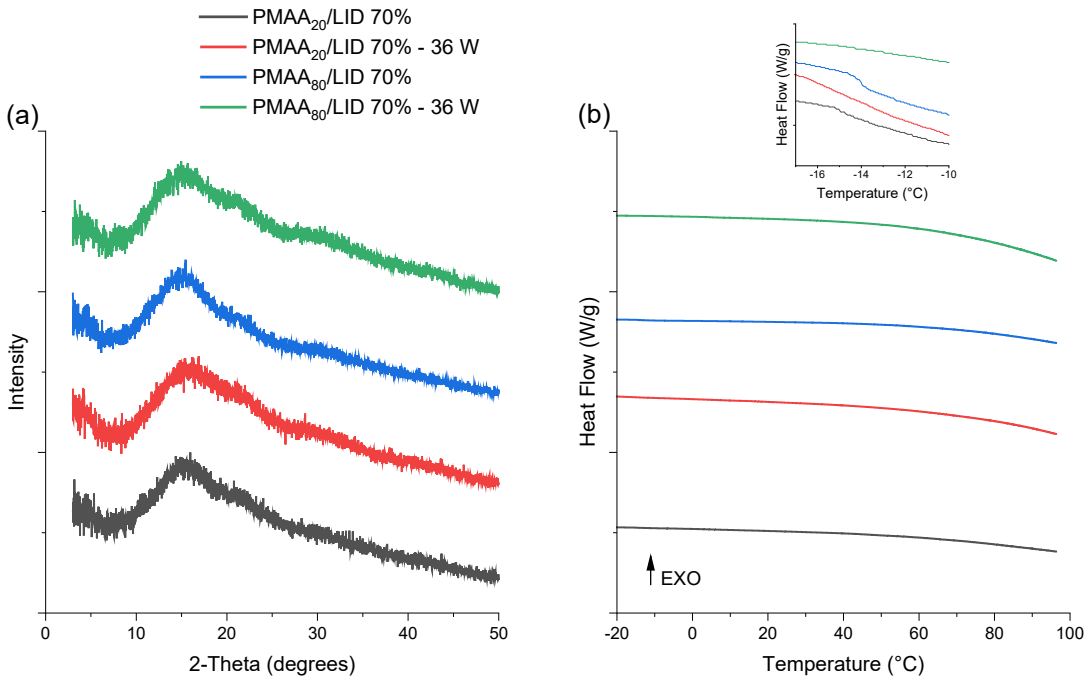

Figure 4.23. *(a) XRD analysis and (b) DSC thermograms of the milled 70% w/w $PMAA_{20}$/LID and $PMAA_{80}$/LID amorphous solid dispersions on day 0 and after 36 weeks of storage in accelerated storage conditions (40°C, 75% RH).*

It is well known that the addition of polymers with high T_g increases the T_g of the ASD formulation also known as the antiplasticisation effect. However, antiplasticisation is not the only factor responsible for reducing mobility and

preventing crystallisation. The interactions between drug molecules and polymer molecules may also play a major role to stabilise ASD formulations. The presence of interactions between the components of a formulation can reduce the molecular mobility of the drug, thus acting to increase the energy needed for recrystallisation. Similar conclusions were made by Khougaz et al. (114). They reported formation of ASDs of a model drug, MK-0591, with a lower final T_g than the T_g of the drug. The presence of a drug-polymer interaction was reported to be the key factor for stabilising the formulation and the FTIR analysis validated the existence of ion-dipole interactions between the drug's carboxylate group and PVP carbonyl group. Similarly, in this study, the interaction between PMAAs and the basic drug is the main reason methacrylic acid polymers were able to inhibit crystallisation over 9 months of storage in a high temperature and humidity condition.

4.4.5 Dissolution of the lidocaine ASD formulation

In vitro dissolution of the 70% w/w polymer/drug ASDs ($PMAA_{80}$/LID and PVP/LID) in water under non-sink conditions (relative to the solubility of the crystalline drug) were determined to assess the ability of the ASDs to generate and maintain supersaturation of the drug. The supersaturated state has a high energy. Consequently, drugs in supersaturated solutions usually precipitate since it is thermodynamically favoured. This eventually results in less absorption *in vivo* (58). Polymers in this study were used to inhibit crystallisation and precipitation of lidocaine by maintaining the supersaturated state.

Each experiment used 10 mg/ml of lidocaine in the solvents in the form of the pure drug or the equivalent mass of ASD formulations. Lidocaine free base displays a solubility of approximately 2.2 mg/ml in water after 2 hours. The 70% w/w $PMAA_{80}$/LID ASDs showed higher solubility in water compared to the pure drug and also rapid dissolution (**Figure 4.24a**). The concentration of lidocaine from $PMAA_{80}$/LID ASDs in water reaches 9 mg/ml after 10 minutes.

The PVP/LID formulation was also found to improve the solubility of lidocaine in water in spite of its partially crystalline physical form. The lidocaine concentration in water from this formulation reaches 7 mg/ml. Similarly, in a study, partially amorphous formulations of PVP and dipyridamole as well as PVP and cinnarizine prepared by spray drying were found to enhance the solubility of the drugs (118).

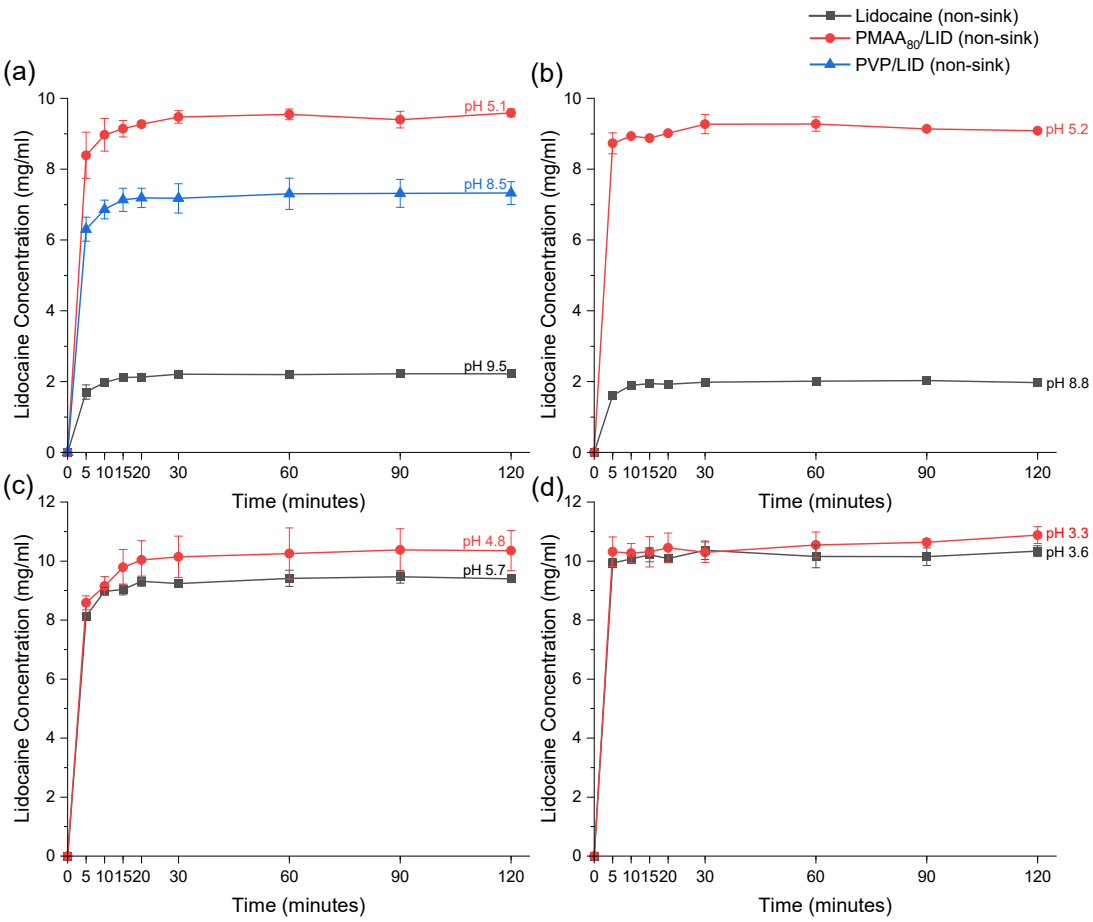

Figure 4.24. *Solubility studies of lidocaine and ASDs in (a) water, (b) PBS pH 7.4, (c) fasted state simulated intestinal fluid (FaSSIF), and (d) fasted state simulated gastric fluid (FaSSGF) at 37 °C under non-sink conditions. The ASDs had a polymer to drug ratio of 70 to 30 w/w. The average pH of the solutions at the end of the experiments were recorded. The error bars represent the standard deviations.*

The same procedure was carried out to study the dissolution profiles of lidocaine and the 70% w/w $PMAA_{80}$/LID ASDs in PBS (pH 7.4) (**Figure 4.24b**). Addition of lidocaine increased the pH of the media to 8.8. The concentration of lidocaine reached around 2 mg/ml after 15 minutes and remained constant. Using the Henderson-Hasselbalch equation, the solubility of lidocaine free base at pH 8.8 was determined to be 2.9 mg/ml. Under non-sink conditions, the ASD samples reached a concentration of lidocaine 5.4 times more than that reached by the crystalline drug. The higher solubility of the ASDs in water and PBS compared to that of the pure drug using non-sink conditions could be

due to the presence of acidic polymers (PMAA) which decrease the pH of the media to 5.1 and 5.2, respectively. Bergstrom et al. compared experimentally determined solubilities of 25 basic drugs in phosphate buffer with theoretically calculated solubility values calculated using the Henderson-Hasselbalch equation (119). The pH-dependent solubility profile of lidocaine was also investigated. It was shown that, theoretically, the addition of acid results in an increase in the solubility of lidocaine. In an experiment, however, the solubility of the drug reached a plateau, and a maximum concentration was achieved at a certain pH. Similarly, in our study, lidocaine shows pH-dependent solubility.

According to a study on ciprofloxacin solid dispersions, the solubility of ASD formulations in FaSSGF were lower than that of the pure crystalline drug as the polymers used were not soluble in acidic solutions and hindered the solubilisation of the drug (44). Therefore, the solubility of pure lidocaine and $PMAA_{80}$/LID ASDs were tested in FaSSIF and FaSSGF to assess the dissolution behaviour of the drug in different parts of the GI tract. The experiment was carried out under non-sink conditions with starting media pH values of 5.5 and 2, respectively. As expected, the solubility of the drug increased drastically and reached 8.1 mg/ml in FaSSIF (**Figure 4.24c**). In FaSSGF, the more acidic media, the concentration of the basic drug increased reaching 9.9 mg/ml in 5 minutes (**Figure 4.24d**). The concentration of lidocaine in all solutions remained constant over 24 hours. The increased solubility of basic drug in this medium could be due to the acidity of the medium and presence of surfactants. The ASDs behaved the same achieving the maximum possible concentration in both media. The pH of the media (FaSSGF) containing lidocaine and ASDs measured at the end of the experiment differed

only by 0.3. The ASDs were able to increase the solubility of lidocaine in different media by reducing the pH of the microenvironment.

Sink conditions were next used to investigate the dissolution profiles of these two samples in PBS (**Figure 4.25**). After 5 minutes, the ASDs achieved maximum lidocaine concentration of 0.4 mg/ml in PBS (pH 6.8), whereas crystalline lidocaine reached a concentration of 0.14 mg/ml. The concentration of lidocaine from the latter sample reached 0.3 mg/ml after one hour. The difference in dissolution rate of lidocaine in PBS under sink conditions cannot only be attributed to changes in pH. The amorphous physical form of the drug as well as the presence of $PMAA_{80}$ are also the reason for the rapid dissolution of the drug. Amorphous solid dispersions can enable more rapid dissolution of a drug substance owing to their disordered structure compared to the crystalline form of the drug and form supersaturated solution. This behaviour was described by Guzman et al as the “spring” and “parachute” model (57). In this study, a decrease in the concentration of lidocaine formulated as ASD in different media was not observed as the experiments were carried out using the excess amount of the drug in its crystalline form.

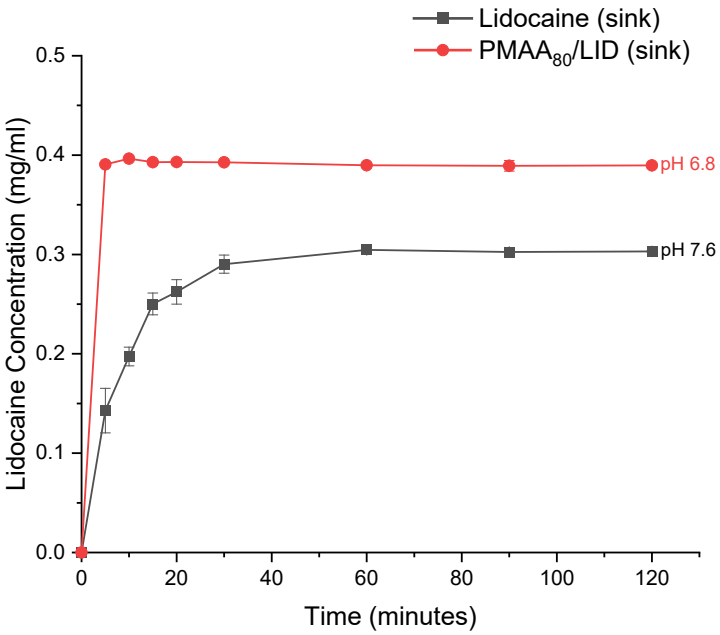

Figure 4.25. *Solubility studies of lidocaine and 70% w/w $PMAA_{80}$/LID ASDs in PBS pH 7.4 under sink conditions. The average pH of the solutions at the end of the experiments were recorded. The error bars represent the standard deviations.*

Solubility of aged samples (stored under accelerated storage conditions for 8 weeks) was also studied. As shown in **Figure 4.26**, the solubility of the samples remained unaffected. Two fit factors F_1 and F_2 were applied to compare the solubility of drug from aged ASDs and those of the fresh samples using Equations 4.3 and 4.4. F_1 values lower than 15 indicate the difference between the solubility profiles of the samples. F_2, on the other hand, measures the similarity of the solubility profiles of the samples at each time point. Strong similarity is indicated when an F_2 value is between 50 and 100 (120). F_1 and F_2 values of 5.13 and 97.74 were calculated, showing strong similarity between the solubility of lidocaine from aged and fresh ASDs.

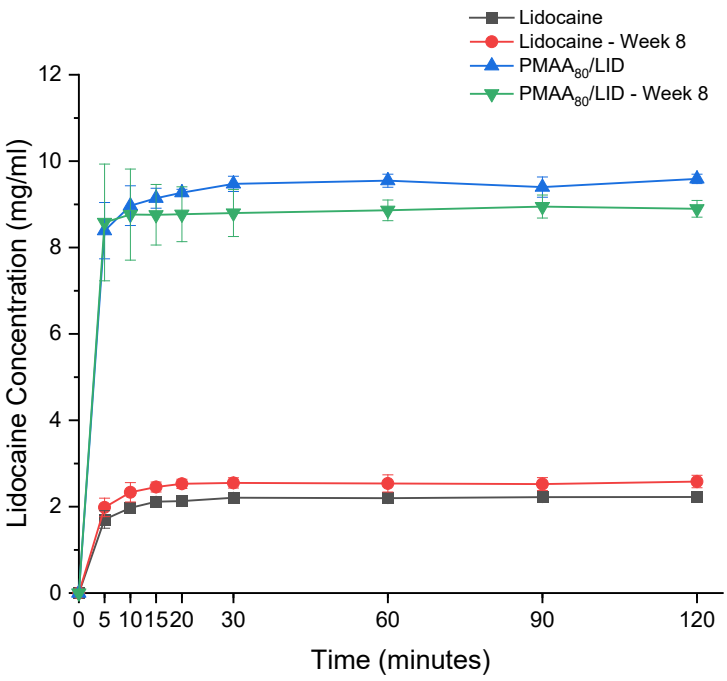

***Figure 4.26**. Solubility studies of lidocaine and milled 70% w/w $PMAA_{80}$/LID in water on day 0 and week 8 at 37 °C. The error bars represent the standard deviations.*

4.4.6 Characterisation of polymeric amorphous solid dispersions of lidocaine HCl

4.4.6.1 Poly(methacrylic acid)$_{80}$

The ability of the hydrochloride salt form of lidocaine to form amorphous solid dispersions was also investigated to assess the influence of different drug forms of lidocaine on the physical stability of the ASDs as well as their dissolution properties. Lidocaine HCl was milled with $PMAA_{80}$. Similar to $PMAA_{80}$/LID samples, the XRD analysis showed that formation of amorphous material was only possible by milling PMAA polymers with lidocaine HCl at a polymer/drug mass ratio of 70% w/w for 1 hour (**Figure 4.27a**). The other formulations displayed low intensity Bragg reflections after milling, which suggests that their physical form is not fully amorphous.

Lidocaine hydrochloride has a melting point of approximately 79 °C (105). The DSC thermogram of lidocaine HCl used in this study displayed a sharp endothermic peak at 80.5 °C. The melting point and the T_g of LID HCl is higher than the melting point of lidocaine in its free base form due to the existence of electrostatic interactions. As shown in **Figure 4.27b**, the 70% w/w $PMAA_{80}$/LID HCl sample did not display a melting event in the first heating cycle after milling which indicates that ASDs were successfully produced following ball milling $PMAA_{80}$ and lidocaine HCl. This is in agreement with the XRD analysis of the sample.

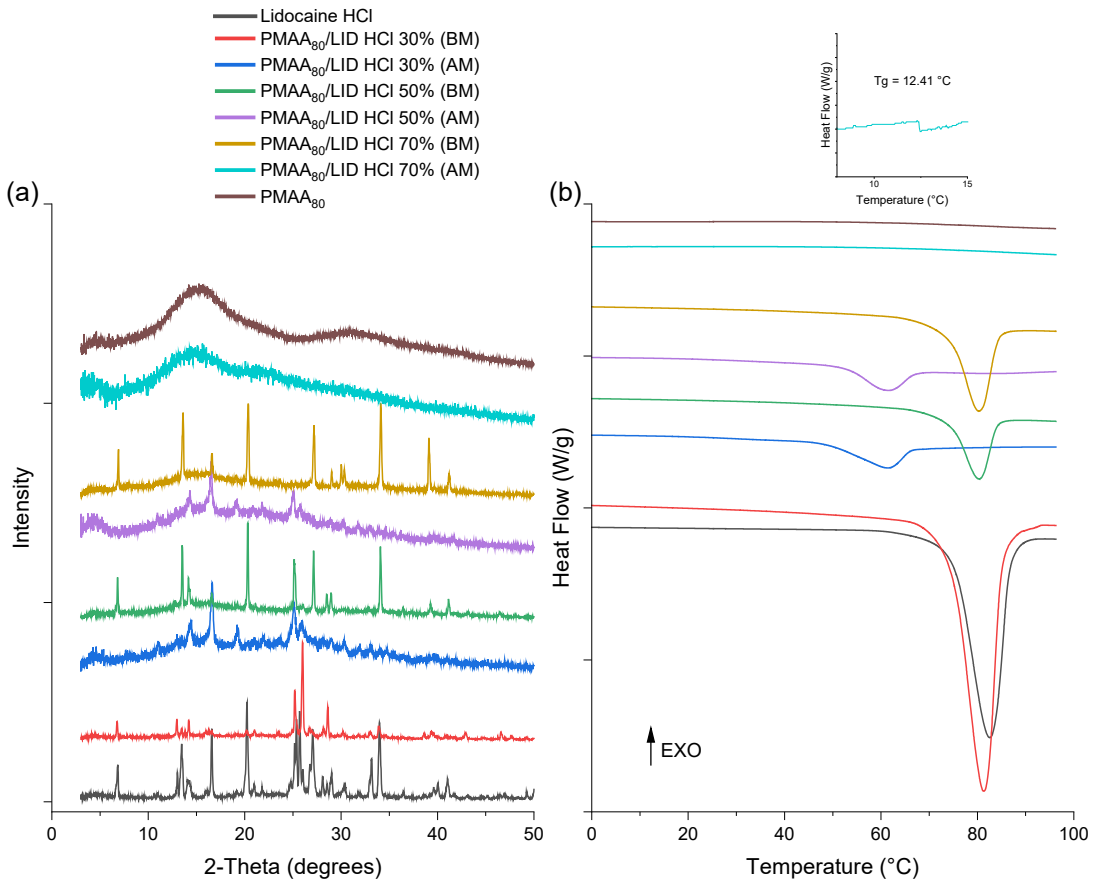

Figure 4.27. *(a) XRD analysis of 30, 50, and 70% w/w $PMAA_{80}$/LID HCl before and after milling for 1 hour; and (b) DSC thermograms of lidocaine HCl and $PMAA_{80}$/LID HCl samples before and after milling obtained from the first heating cycle.*

The miscibility of the components was confirmed by the presence of a single T_g. The 70% w/w $PMAA_{80}$/LID HCl milled ASD displayed an experimental T_g value of 12.4 °C which was higher than the theoretical T_g (5.3 °C). A positive deviation of 7.1 °C indicates strong drug-polymer interaction (35). The positive deviation between $PMAA_{80}$ and the free base form of the lidocaine (12.5 °C) was greater which suggests existence of a stronger polymer-drug interaction compared to the formulation with the salt form of the drug. This is due to the presence of HCl in the salt form of the drug and the interaction between HCl and lidocaine.

Thermal degradation of lidocaine HCl and the 70% w/w $PMAA_{80}$/LID HCl formulation before and after milling were investigated using TGA (**Figure 4.28**). Prior to reaching 200 °C at around 100 °C, water evaporation from the lidocaine hydrochloride sample causes 6% weight loss. The degradation of the drug starts above this temperature. A complete loss of mas is seen at around 300 °C. Similar thermal degradation of lidocaine hydrochloride was reported previously (121). Below 100 °C, $PMAA_{80}$/LID HCl ASDs lost 3% of their mass through water evaporation. $PMAA_{80}$/LID HCl ASDs undergo two subsequent decompositions; the first decomposition around 210 °C is due to the degradation of lidocaine HCl and is followed by mass loss above 270 °C caused by degradation of the polymer. The milled formulation delays the complete degradation of the drug with 30% weight loss in the formulation occurring around 300 °C.

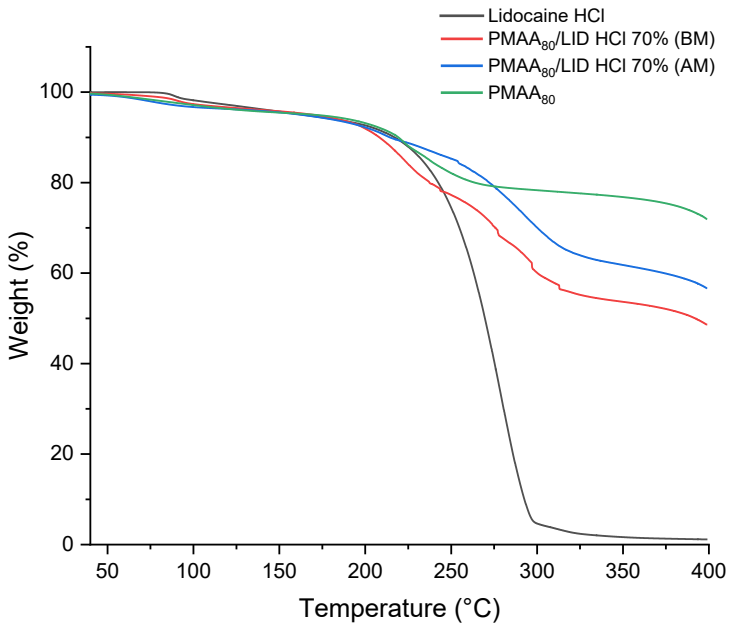

Figure 4.28. *TGA curves of lidocaine HCl, $PMAA_{80}$, and $PMAA_{80}$/LID HCl samples (70% w/w $PMAA_{80}$/LID HCl) before and after milling.*

The interactions between lidocaine HCl and $PMAA_{80}$ at different polymer/drug weight ratios were analysed using FTIR (**Figure 4.29a**). In the spectrum of lidocaine HCl, N-H stretching can be seen at 3390 and 3450 cm^{-1}. The band at 1655 cm^{-1} is assigned to C=O stretching. The two sharp peaks at 1473 cm^{-1} and 1543 cm^{-1} can be attributed to the N-H bending of the drug molecule's secondary amide and the tertiary amine N^{+}-H. In comparison with lidocaine free base, the spectrum of lidocaine HCl displayed an additional peak in this region as it possesses the N^{+}-H group. These peaks could also be observed in the spectra of all three of the $PMAA_{80}$/LID HCl formulations. In contrast, the only $PMAA_{80}$/LID sample that exhibited the N^{+}-H bending peak distinctly was the milled 70% w/w $PMAA_{80}$/LID sample. Similar FTIR results of lidocaine and lidocaine HCl were reported by X. Liu et al. where the interaction between Eudragit L100-55 and lidocaine in its free base and hydrochloride salt form were investigated (105).

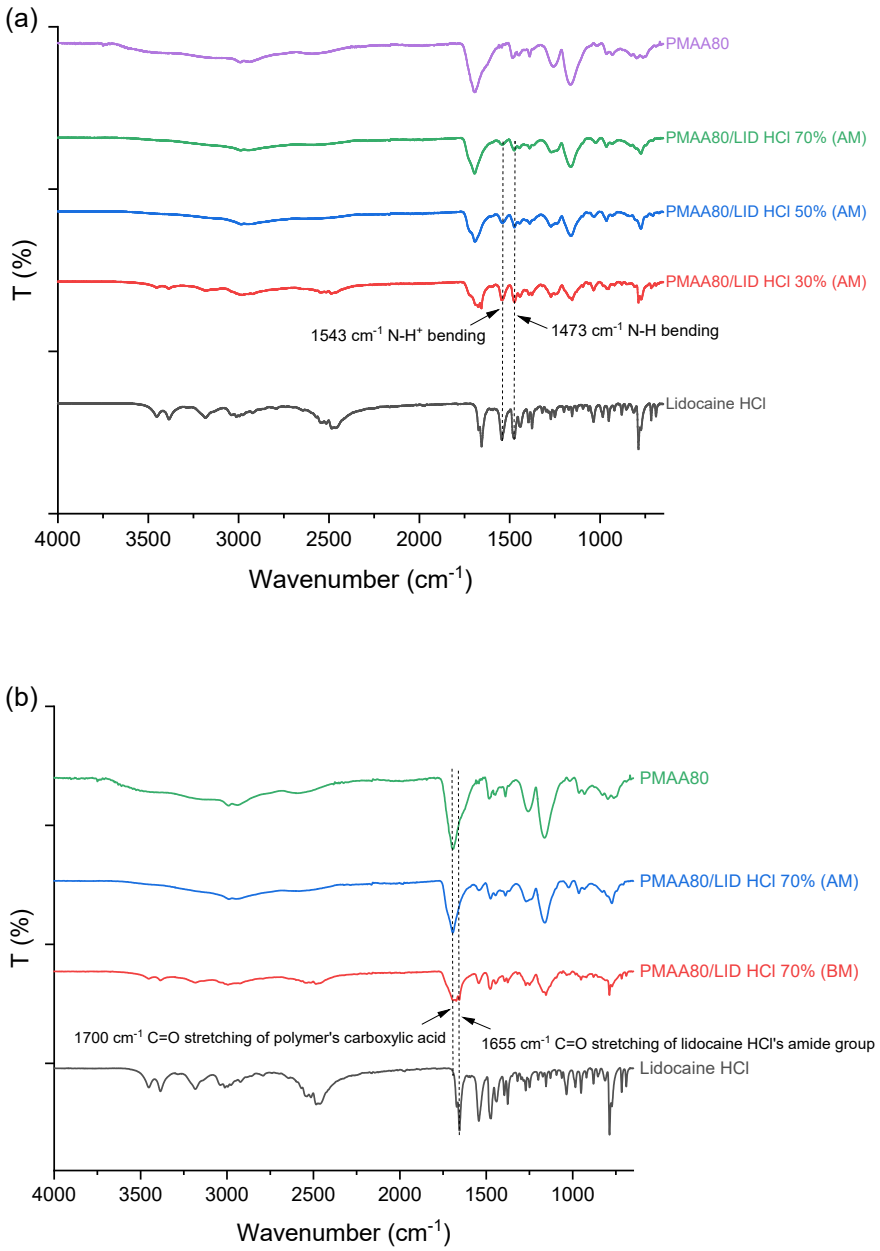

Figure 4.29. *FTIR spectra of (a) $PMAA_{80}$, lidocaine HCl, and $PMAA_{80}$/LID HCl milled formulations (30, 50, 70% w/w $PMAA_{80}$/LID HCl); and (b) 70% w/w $PMAA_{80}$/LID HCl before and after ball milling.*

The milled 70% w/w $PMAA_{80}$/LID HCl formulation has a similar spectrum to that of the pure polymer. Unlike the physical mixture sample (before milling), the spectrum of the milled sample displays a broad band in the 1580-1766 cm^{-1} region as a result of the merging of the C=O stretching bands of the drug and the polymer (**Figure 4.29b**). The bands at 3390 cm^{-1} and 3450 cm^{-1} in the

spectrum of the milled sample are not visible which signals strong polymer/drug interactions and that the drug is well dispersed in the polymer. Therefore, it was concluded that the formulations with 30% drug loading of lidocaine HCl possessed a sufficient amount of methacrylic acid to produce acid-base interactions and form ASDs. The differences in the FTIR spectrum of the samples before milling and the milled samples indicate that the interactions between the amine group of the drug and the carboxylic acid group of $PMAA_{80}$ occurred during the ball milling process.

4.4.6.2 Polyvinylpyrrolidone

Lidocaine HCl was next milled with PVP of similar molecular weight to $PMAA_{80}$. As shown in **Figure 4.30a**, the milled 70% w/w PVP/LID HCl has a pattern similar to that of the polymer: except for a small peak at 16.6°, broad haloes are seen. The samples with lowest drug loading are thus partially amorphous. The PVP/LID HCl samples became sticky after milling, and it was difficult to remove them from the milling jar. Milled samples of 70% w/w PVP/LID HCl showed a small melting endotherm at 66 °C which indicates the samples are not fully amorphous and agrees with the small amount of crystalline material present (**Figure 4.30b**). In their first heating cycle, the DSC thermograms of milled PVP/LID HCl samples displayed broader melting endotherms at a lower temperature.

In the second heating cycle, all of the physical mixture samples (before milling) including the 30 and 50% w/w $PMAA_{80}$/LID HCl and all the PVP/LID HCl samples did not display melting endotherms. Therefore, amorphous solid

dispersions of lidocaine hydrochloride may possibly be prepared through hot-melt extrusion or combining milling and melt/quench cool methods.

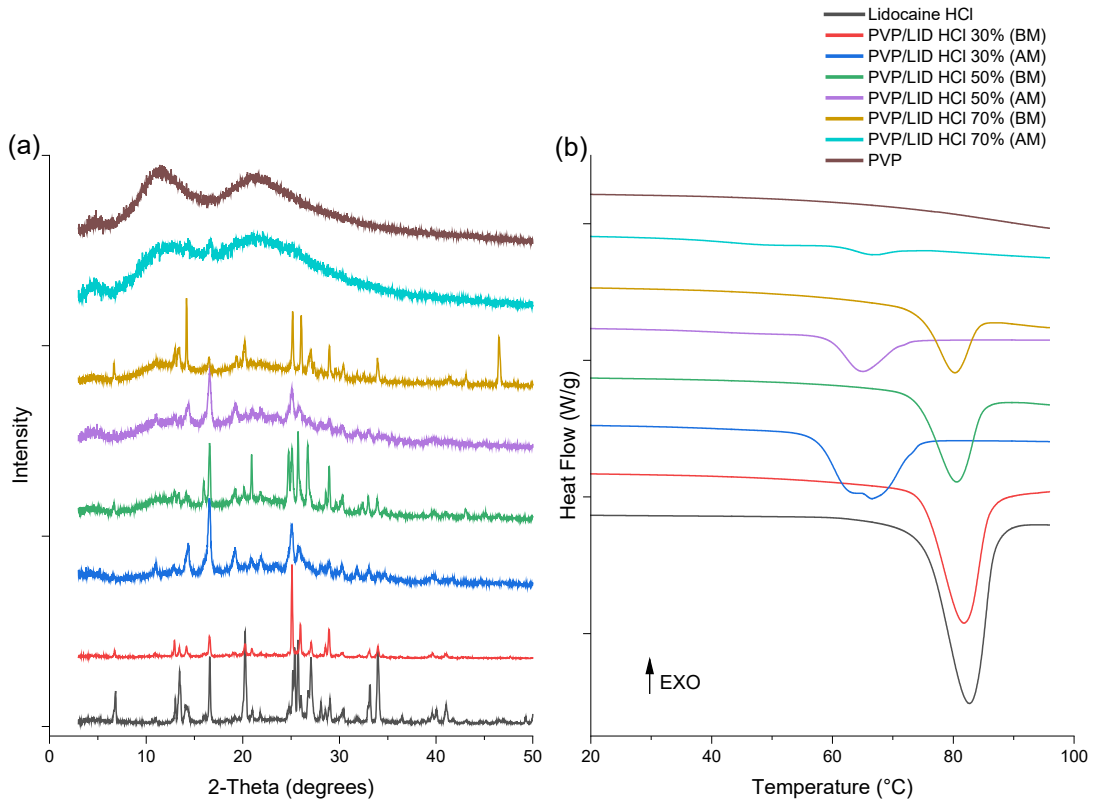

Figure 4.30. *(a) XRD analysis of 30, 50, and 70% w/w PVP/LID HCl before and after milling for 1 hour; and (b) DSC thermograms of lidocaine HCl and PVP/LID HCl samples before and after milling obtained from the first heating cycle.*

Thermal degradation of the 70% w/w PVP/LID HCl samples before and after milling were investigated using TGA. Below 100 °C, milled PVP/LID HCl samples lost 7% of their mass through water evaporation (**Figure 4.31**). The thermal decomposition of lidocaine HCl in the PVP/LID HCl samples starts at 230 °C. The decomposition of the drug is clearly delayed when formulated with PVP.

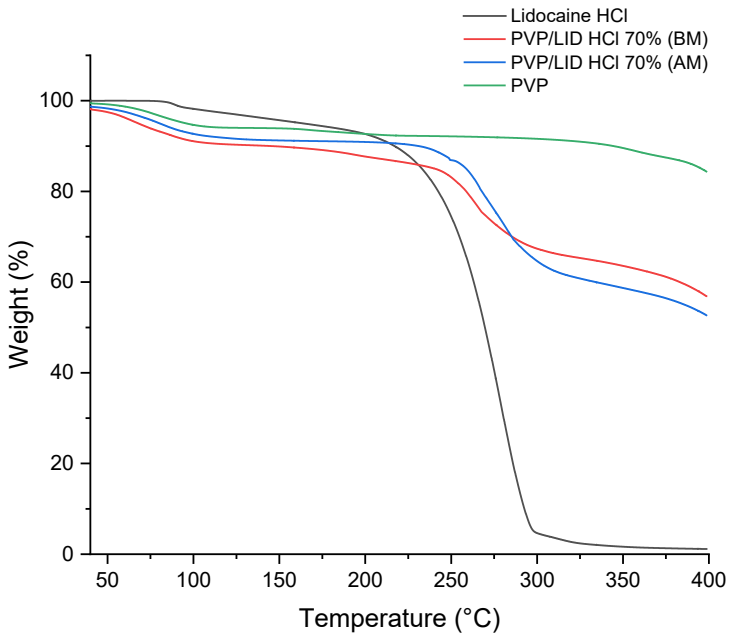

Figure 4.31. *TGA curves of lidocaine HCl, PVP, and 70% w/w PVP/LID HCl samples before and after milling.*

The spectra of all three PVP/LID HCl milled samples resemble the spectrum of lidocaine HCl (**Figure 4.32**). In all three formulations, PVP's band at 1647 cm^{-1} is merged with the C=O stretching in the secondary amide group of lidocaine HCl at 1655 cm^{-1} and only one band is visible. No shifting of the peak assigned to the carbonyl group of the drug was detected in the FTIR spectra of the milled samples. The presence of sharp characteristic bands of lidocaine HCl in the milled samples of PVP/LID HCl is an indication of the presence of uncomplexed crystalline lidocaine HCl in the formulation.

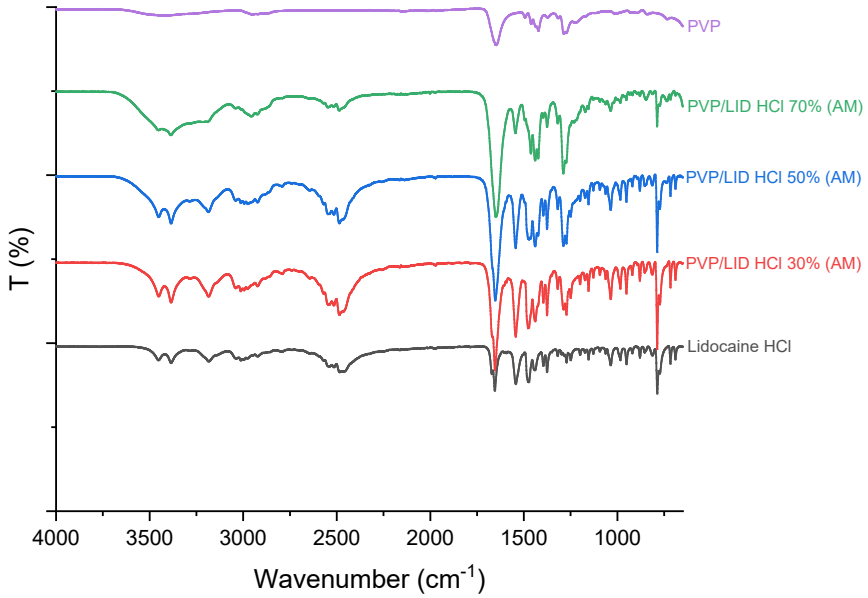

Figure 4.32. *FTIR spectra of lidocaine HCl, PVP, and milled PVP/LID HCl formulations (30, 50 and 70% w/w PVP/LID HCl).*

4.4.7 Molecular modelling of lidocaine HCl ASDs

The interaction between the polymers and lidocaine HCl was examined using HyperChem. Each component was minimised energetically individually and then again in combination. The details are given in **Table 4.2**. The geometric arrangements of the energy-minimised polymer-drug complexes are shown in **Figure 4.33**.

Table 4.2. *Details of the optimised geometry energetics of PMAA/LID HCl and PVP/LID HCl molecular models. The calculations were done inputting the unionised polymer and drug molecules for analysis.*

	Minimised energy contributions (kcal mol $^{-1}$)					
Species	**bond stretching**	**bond angle**	**dihedral**	**van der Waals**	**hydrogen bonding**	**total**
$PMAA_{10}$	11.84	290.36	10.38	36.58	-0.29	348.87
PVP_{10}	4.18	88.6	39.89	-11.37	0	121.3
Lidocaine HCl	3.0	140.58	8.36	5.16	-0.00002	157.1
$PMAA_{10}$/LID HCl	14.13	430.97	18.2	28.83	-0.92	491.21
PVP_{10}/LID HCl	7.21	229.36	48.25	-15.46	-0.17	269.18

The combined energy of $PMAA_{10}$ and lidocaine HCl is 505.98 kcal mol^{-1}, whereas the total energy of the optimised complex is 491.21 kcal mol^{-1} giving a ΔE of -14.77 kcal mol^{-1}. The combined steric energy of PVP_{10} and lidocaine HCl is 278.4 kcal mol^{-1}, whereas the energy of their optimised complex is 269.18 kcal mol^{-1} which gives a ΔE of -9.21 kcal mol^{-1}. The negative ΔE of both formulations indicate stabilisation of the complexes. The data suggest there is a stronger polymer/drug interaction in the PMAA/LID HCl complex compared to the PVP/LID HCl complex. The ΔE values of PMAA/LID HCl and PVP/LID HCl complexes were lower than those calculated when each of the polymers was complexed with lidocaine free base (-16.98 kcal mol^{-1} for PMAA/LID and -14.01 kcal mol^{-1} for PVP/LID) which indicates a more favourable interaction between lidocaine and the polymers. The preliminary results obtained from the molecular modelling revealed that the interactions are stronger in the PMAA/LID complex.

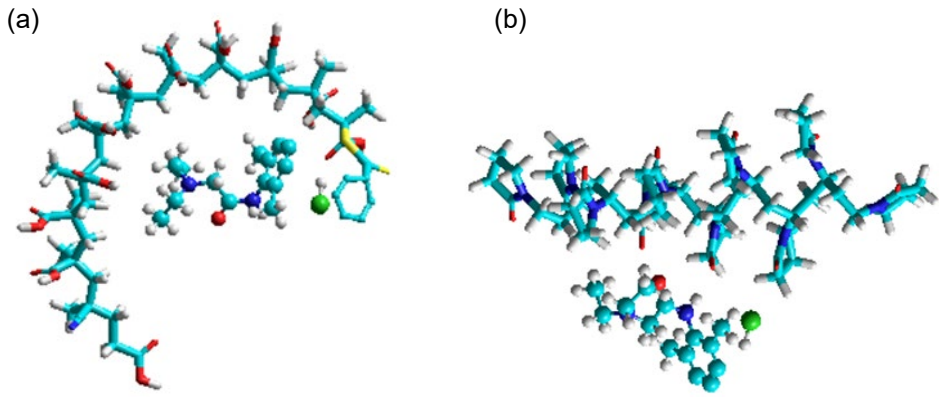

Figure 4.33. *Optimised geometric arrangements of (a) $PMAA_{10}$/LID HCl and (b) PVP_{10}/LID HCl. The decameric polymers can be seen in tubes at the top and lidocaine HCl in balls at the bottom.*

4.4.8 Stability of the lidocaine HCl ASD formulation

The milled 70% w/w $PMAA_{80}$/LID HCl ASDs were stored at room temperature and under accelerated storage conditions (40 °C and 75% RH) and their stability was assessed by XRD and DSC. XRD analysis in **Figure 4.34a** shows that the amorphous state of the drug was preserved over 8 months of storage in a high temperature (40 °C) and high humidity condition (75% RH). There was also no visible melting endotherm in the DSC thermograms of the aged ASD samples (**Figure 4.34b**).

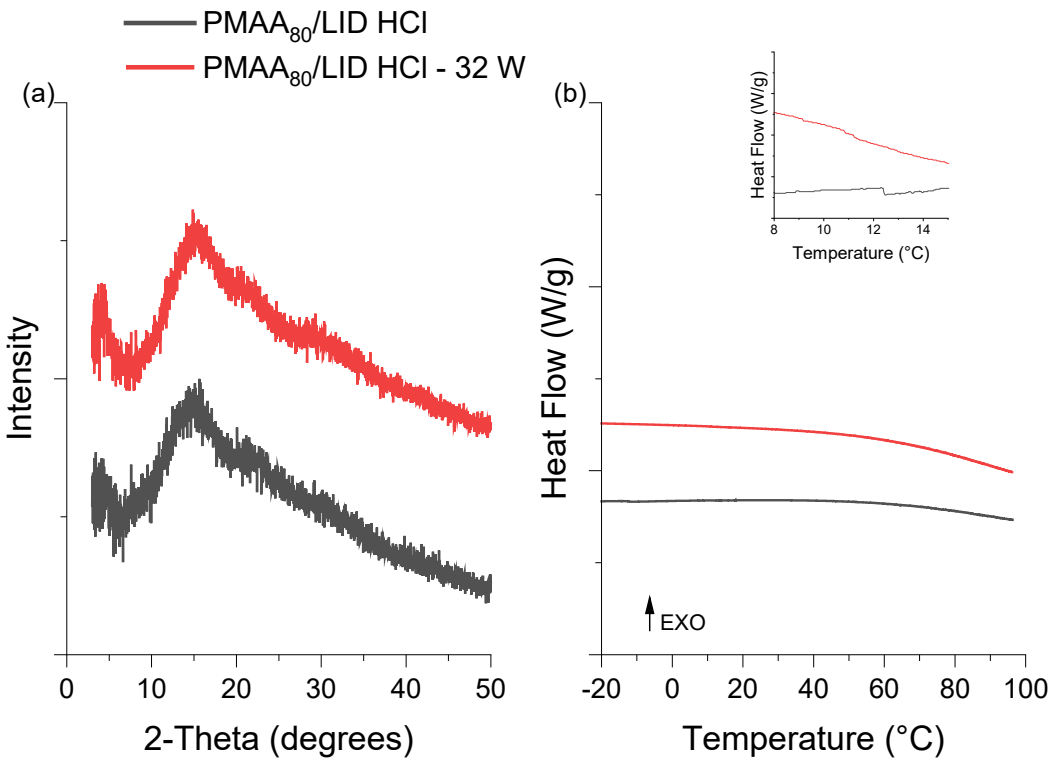

Figure 4.34. *(a) XRD analysis and (b) DSC thermograms of the milled 70% w/w PMAA$_{80}$/LID HCl ASDs on day 0 and week 32 of storage in accelerated storage conditions (40 °C, 75% RH).*

In a similar study, Eudragit L100-55 was used to form polymer/drug complexes with lidocaine and lidocaine HCl by melt extrusion (105). Both formulations consisted of 30% w/w drug and 70% polymer and were amorphous in nature. A positive deviation (experimental T_g > theoretical T_g) for lidocaine/Eudragit L100-55 formulation and a negative deviation for lidocaine HCl/Eudragit L100-55 were recorded. Following 4 months of storage at 40 °C and 70% RH, the lidocaine HCl/Eudragit L100-55 extrudate crystallised. Therefore, it was concluded that lidocaine free base had much stronger acid-base interaction with Eudragit L100-55 than lidocaine HCl. It was hypothesised that the carboxylic acid group of methacrylic acid in Eudragit L100-55 could not interact with the drug's tertiary amine and replace the hydrochloric acid in lidocaine HCl because the tertiary amine group of lidocaine HCl was protonated with

HCl. In this project, however, even though the interaction between the hydrochloride form of the drug and $PMAA_{80}$ was estimated to be less than the interaction between lidocaine free base and $PMAA_{80}$ and smaller positive deviation was observed for $PMAA_{80}$/LID HCl, both ASDs maintained their amorphous physical form over a prolonged period of time.

4.4.9 Dissolution of the lidocaine HCl ASD formulation

Three samples of lidocaine HCl in the form of pure drug and the 70% w/w $PMAA_{80}$/LID with a lidocaine HCl concentration of 10 mg/ml in water were prepared. Lidocaine in its hydrochloride form is soluble in water. Average lidocaine HCl concentration in water reached after 5 minutes was 9.2 and 9.8 mg/ml from the pure drug and the ASD samples, respectively (**Figure 4.35a**). The concentration of the drug in solution remained constant for 24 hours. In PBS, the crystalline drug reached a concentration of 7 mg/ml after 5 minutes and plateaued while the lidocaine concentration from the ASDs after 5 minutes was 8.1 mg/ml and increased to 9 mg/ml at the 30-minute timepoint (**Figure 4.35b**).

Compared to lidocaine in its free base form, lidocaine HCl was found to dissolve faster in water and PBS. This is because the HCl salt dissolves lowering the microenvironment pH and increasing solubility of the drug, whereas lidocaine free base induces an alkaline microenvironment which causes a decrease in drug solubility. The drug release from the ASDs ($PMAA_{80}$/LID and $PMAA_{80}$/LID HCl) also showed pH-dependency. In water, $PMAA_{80}$/LID HCl showed faster dissolution compared to the $PMAA_{80}$/LID ASDs as both the polymer and the hydrochloride salt form of lidocaine lowered

the pH of the solution. In PBS, the dissolution profiles of the drugs from the ASDs were comparable since the pH of the solutions were similar.

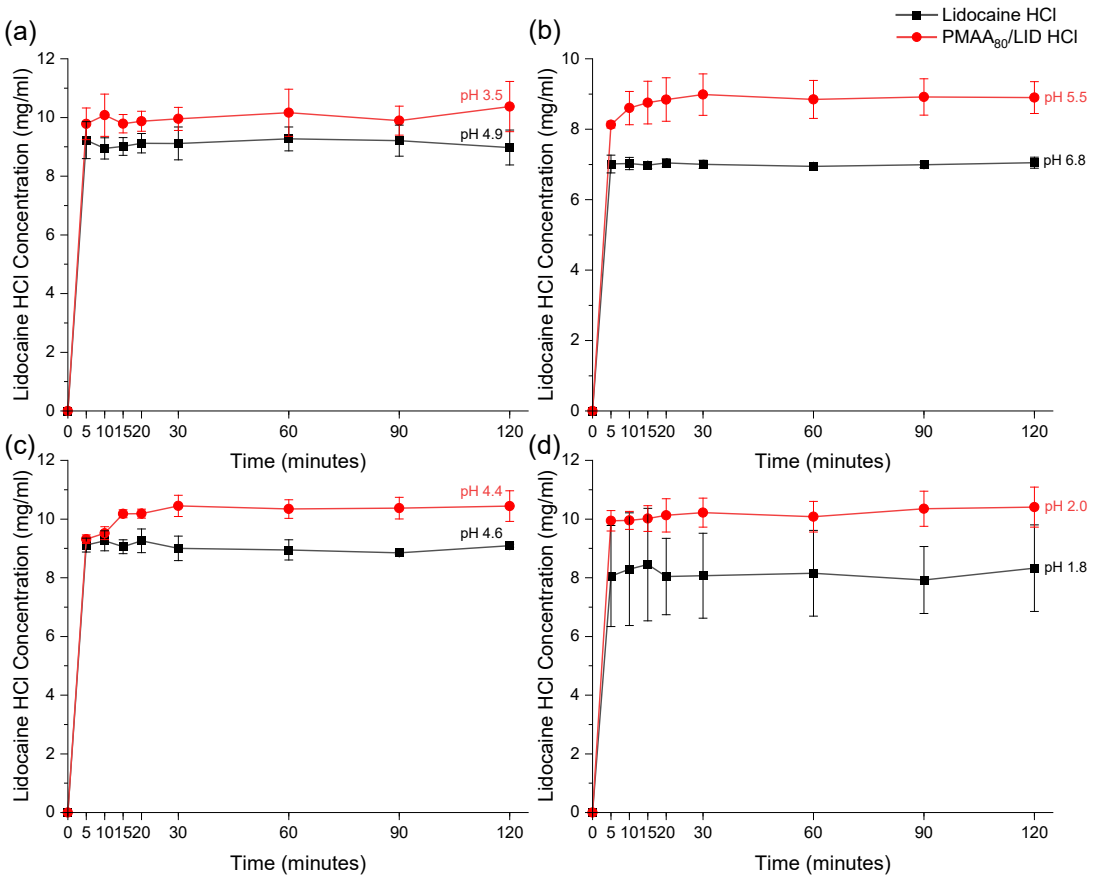

Figure 4.35. *Solubility studies of lidocaine HCl and milled 70% w/w $PMAA_{80}$/LID HCl in (a) water, (b) PBS pH 7.4, (c) fasted state simulated intestinal fluid (FaSSIF), and (d) fasted state simulated gastric fluid (FaSSGF) at 37 °C. The average pH of the solutions at the end of the experiments were recorded. The error bars represent the standard deviations.*

The solubility of pure lidocaine HCl and $PMAA_{80}$/LID HCl ASDs were also tested in FaSSIF and FaSSGF with starting media pH of 5.5 and 2, respectively. On average, the concentration of lidocaine HCl from the ASD samples showed higher solubility in FaSSIF (**Figure 4.35c**) and FaSSGF (**Figure 4.35d**) compared to the pure drug. The pH of the samples containing lidocaine HCl and the ASDs measured at the end of the experiments differed only by 0.2. The concentration of lidocaine in the form of amorphous solid

dispersions reaches the maximum (10 mg/ml) after 5 minutes. The decreased solubility of lidocaine HCl in this media could be due to the media's acidity and the common ion effect. At low pH, presence of excess counterions results is a decrease in the solubility of salt forms of basic drugs (41). Elevated chloride ion concentration was also found to decrease the dissolution of three different salt forms of a basic drug, haloperidol (122). The presence of polymers in the formulation and the physical form of the amorphous solid dispersions is responsible for the slightly higher solubility of lidocaine HCl in different media compared to the pure crystalline drug.

The dissolution profiles of both drugs and their ASDs in FaSSIF were similar. In FaSSGF, however, lidocaine free base showed faster dissolution. As mentioned above, the slower dissolution rate and the lower maximum drug concentration of lidocaine HCl in FaSSGF is due to the lower pH of the media and the common ion effect. The drug release from the ASDs ($PMAA_{80}$/LID and $PMAA_{80}$/LID HCl) were similar and reached the maximum concentration after 5 minutes. This is in contrast to the results reported by X. Liu et al. where at pH 1.2, the drug release from lidocaine-Eudragit L100-55 was significantly lower than the drug release from lidocaine HCl-Eudragit L100-55 complex (105). Unlike the PMAA polymer used in this project, Eudragit L100-55 was reported to have pH-dependent solubility.

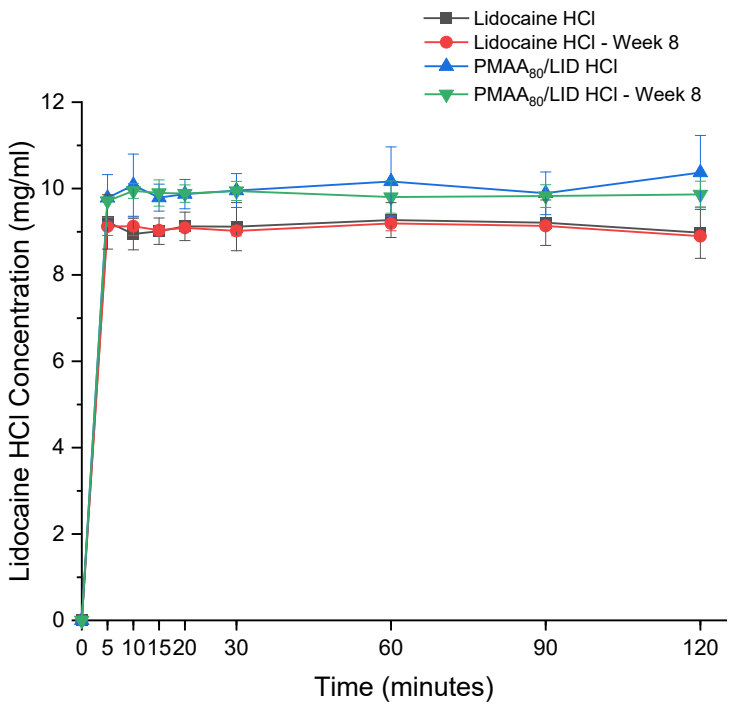

Figure 4.36. *Solubility studies of lidocaine HCl and milled 70% w/w PMAA$_{80}$/LID HCl in water on day 0 and week 8 at 37 °C. The error bars represent the standard deviations.*

Lidocaine HCl and the milled 70% w/w PMAA$_{80}$/LID samples were stored under accelerated storage conditions and their solubility was studied after 8 weeks (**Figure 4.36**). The average solubility of lidocaine HCl and PMAA$_{80}$/LID ASDs remained unchanged and reached 9.1 and 9.7 mg/ml after 5 minutes, respectively. Two fit factors F_1 and F_2 were calculated using equations 4.3 and 4.4 to compare the solubility of drug from fresh and aged ASDs. F_1 and F_2 values of 1.58 and 99.49 were calculated which indicate strong similarity between the solubility of lidocaine HCl from aged and fresh ASDs.

4.5 Conclusion

Preparing amorphous solid dispersions of poorly water-soluble drugs is a formulation strategy to enhance their solubility. The RAFT-synthesised

$PMAA_{80}$ and $PMAA_{20}$ polymers allow ASDs to be made by ball milling at 70% w/w polymer/drug ratio. This work has shown that the chosen acidic polymer, PMAA, was able to produce lidocaine ASDs via formation of stabilising ionic interactions with the basic drug during the milling process.

The presence of N^+-H bending peak and the merging of the C=O stretching bands of the drug and the polymer in the FTIR spectra of the 70% w/w $PMAA_{80}$/LID and $PMAA_{80}$/LID HCl formulations after milling indicated that the interactions between the amine group of the drug and the carboxylic acid group of the polymer occurred during the ball milling process.

Lidocaine free base showed pH-dependent solubility. Addition of lidocaine to media increased the pH, whereas addition of lidocaine HCl decreased the pH. The presence of the polymer in the formulation reduced the microenvironment pH which in turn resulted in an increase in the solubility of the drug. Using the $PMAA_{80}$/LID ASD formulation, maximum lidocaine concentration in different media was achieved.

To conclude, formulating the previously synthesised PMAAs with lidocaine in its free base form and producing amorphous solid dispersions is preferred due to the favourable interaction between the acidic polymer and the basic drug and the increased solubility of the drug. This formulation shows potential for improving aqueous solubility of poorly water-soluble drugs and consequently increasing the absorption and the bioavailability of the drug.

Chapter 5 Conclusion

The use of well-defined methacrylate-based polymers in pharmaceutical formulations was investigated. The first step was to synthesise a small family of polymers and copolymers with different repeat units using RAFT polymerisation. PEGMA polymers with five different chain lengths were synthesised and used as precursors and macro-RAFT agents to synthesise block copolymers with DMAEMA, using sequential RAFT polymerisation. Methacrylic acid polymers with similar chain lengths as the cationic blocks of the copolymers were also synthesised. Synthesis of well-defined polymers and copolymers with targeted DPs and narrow molecular weight distributions, determined by ^{1}H NMR analysis and GPC, respectively, confirmed that under optimal conditions there was a high level of control of the RAFT process over the polymerisation of methacrylate-based polymer.

Mixing solutions of the cationic block copolymers and anionic homopolymers led to the formation of polyelectrolyte complex nanoparticles. The complexation of the polymers was derived by the electrostatic interaction between the oppositely charged polyelectrolytes. Using a 1:1 molar ratio of the cationic copolymer poly(PEGMA$_{0.23}$-co-DMAEMA$_{0.77}$)$_{99}$ and the anionic homopolymer poly(MAA)$_{75}$ led to formation of PECs with a mean diameter of 25 ± 3 nm, PDI of 0.08, and zeta potential of -23.2 ± 1.4 mV. TEM images confirmed the formation of spherical nanoparticles with mean diameter of 20 ± 3 nm. The formation and size distribution of the PECs at a fixed molar ratio was not sensitive to polymer concentration in solution or polymer addition order.

Under physiological conditions, the PDMAEMA block of the copolymer and PMAA are expected to interact and form a charge neutralised core within the PECs. The PEGMA block formed a hydrophilic shell and stabilised the nanoparticles. The PECs were found to be stable at room temperature over 28 days. At a mildly acidic pH of 6.5, the size and size distribution of the PECs increased after 24 hours. At pH 5.5, the increase in the size and size distribution of the PECs started from the first timepoint (0 h). The dissociation of the PECs at acidic pH was due to the reduced negative charge of the anionic homopolymer and the resulting diminished interaction between the oppositely charged polyelectrolytes forming the core of the nanoparticles. Raising the temperature was also found to cause destabilisation of the PECs. This was more evident in slightly acidic solutions.

The ability of the optimal PEC formulation to encapsulate hydrophobic and hydrophilic anticancer drugs, and their potential use as stimuli-responsive drug delivery systems, were investigated. The preliminary results obtained from the encapsulation studies confirmed that encapsulation in the PECs was limited to hydrophilic drugs (gemcitabine, 5-fluorouracil, and carmofur), which can be loaded into the hydrophilic segment of the PECs. The burst release of 5-fluorouracil and carmofur indicated the inability of the PEC nanoparticles to contain these drugs and release the drugs in response to the change in the pH of the media.

In a preliminary study, nanoparticles were encapsulated with dexamethasone. The aim of this study was to assess whether the release of dexamethasone can be prolonged from NIPAAM hydrogels formed in the presence of

dexamethasone loaded PECs compared to the PECs alone. Although the PEC/NIPAAM hydrogels did not prolong the release of dexamethasone sufficiently for use as an intravitreal implant formulation, they did delay the release of the drug compared to the PECs.

The RAFT-synthesised MAA polymers with DPs of 80 and 20, as well as PVP and PAA, were next used to form amorphous solid dispersions of lidocaine free base, a model BCS class II drug. Using the DSC and quench-cooling method did not result in the formation of ASDs, which indicates the inability of these methods to adequately mix the components on a molecular level. ASDs were however produced by ball milling the acidic MAA polymers with the basic drug at a 70/30 w/w polymer/drug ratio. FTIR analysis of the ASDs confirmed the presence of interactions between the polymer and the drug after the 1-hour ball milling process.

Lidocaine free base showed pH-dependent solubility. Under non-sink conditions, *in vitro* dissolution studies confirmed that the $PMAA_{80}$/LID ASDs were able to increase the dissolution rate and solubility of lidocaine in different media by reducing the pH of the microenvironment. Under sink conditions, the dissolution rate of lidocaine was faster when formulated as ASDs compared to the pure crystalline drug.

ASDs of lidocaine hydrochloride were also prepared to compare the interactions between $PMAA_{80}$ and lidocaine in both its free base and hydrochloride salt forms. ASDs were formed by milling $PMAA_{80}$ with lidocaine HCl using a 70/30 w/w polymer/drug mass ratio. The dissolution of lidocaine

HCl showed pH-dependency. The drug dissolved rapidly in water and PBS as it lowered the microenvironment pH. However, in acidic media of FaSSIF and FaSSGF, the maximum lidocaine HCl concentration (100% dissolution) was not achieved by the pure drug. This was thought to be due to the media's acidity and the common ion effect. The dissolution rate of drug from the $PMAA_{80}$/LID HCl ASDs was not affected by pH of the media.

Preliminary results from molecular modelling suggested strong interactions between the polymer and the drug in both the free base and salt forms. The ASD formulations made by milling $PMAA_{80}$ with lidocaine in its free base or hydrochloride salt form had low T_g values (-13.4 °C for $PMAA_{80}$/LID and 12.4 °C for $PMAA_{80}$/LID HCl). However, the low T_g of the $PMAA_{80}$/LID and $PMAA_{80}$/LID HCl ASDs did not lead to molecular mobility under accelerated storage conditions (40 °C and 75% RH) or impact their physical stability over 9 and 8 months, respectively. This is due to the strong interaction between the acidic polymer and the basic drug. The results from this chapter confirm our hypothesis that the RAFT-synthesised MAA polymers are able to produce stable ASDs with a basic model drug. The use of these polymers in fabrication of ASDs can be further investigated.

From our studies, we learnt the potential of monodispersed polymers with well-defined architectures synthesised using RAFT polymerisation in the design of different drug formulations as well as to avoid needlessly overcomplicating a formulation design by choosing the right polymers for instance to achieve the desired effects. Polymers synthesised in this study could be used separately to developed new formulations. These synthetic polymers could be used to

complex with oppositely charged polypeptides and form polyplexes. For instance, complexes of the cationic copolymer and the anionic polypeptide poly-L-glutamic acid could be formed and tested for gene therapy. The MAA polymers could complex with positively charged antimicrobial polypeptides (e.g., arginine and lysine) and the antimicrobial effect of these formulations could be examined.

Moving forward, the ability of PECs other than the optimal formulation to encapsulate the mentioned drugs could be tested to investigate the influence of the different chain lengths of the polyelectrolytes as well as the hydrophilic PEGMA section on the encapsulation and release of the drugs. Future work on the PEC nanoparticles should be mainly focused on the ability of the PECs to encapsulate drugs with higher efficiency and to contain the drugs in media at physiological conditions. For instance, conjugation of the drugs to the anionic homopolymer and its effect on the release of the drugs in media with different pH values should be assessed. Cellular uptake and viability tests can then be performed using a formulation which exhibits a pH-dependent drug release profile.

In chapter 4, lidocaine was used as a model drug. The well-defined methacrylic acid polymers allowed formation of amorphous solid dispersions through charge-to-charge interaction with lidocaine following a simple and short process of ball milling. The use of these acidic polymers to produce ASDs of other similar basic BCS class II or IV drugs could be tested. Ketoconazole, an antifungal drug, is a basic drug with low solubility (BCS class II drug). Formation of ASDs by ball milling ketoconazole and MAA polymers as well as

the effect of the ASD formulation on the pharmaceutical and antifungal properties of the drug should be investigated. Formulating anticancer drugs in the form of amorphous solid dispersions can also be tested. ASD-based oncology products can improve the therapeutic outcome of existing anticancer drugs. Tamoxifen, an anticancer drug used for the treatment of breast cancer, is a BCS class II drug and is a suitable example for such formulation.

In addition, more extensive studies should be carried out to increase the drug loading within the formulations. A different method for preparation of ASDs (e.g., HME) could be used to form the ASDs for comparison. The effect of ball milling at different frequencies and for longer durations on formation of ASDs with higher drug loading should also be tested.

Finally, small quantities of the $PMAA_{80}$/LID and $PMAA_{80}$/LID HCl ASDs were produced in this study using ball milling. The scalability of this preparation method to produce the ASD formulations should be investigated.

References

1. Debotton N, Dahan A. Applications of Polymers as Pharmaceutical Excipients in Solid Oral Dosage Forms. Med Res Rev. 2017;37(1):52-97.

2. Liechty W, Kryscio D, Slaughter B, Peppas N. Polymers for drug delivery systems. Annu Rev Chem Biomol Eng. 2010;1:149-73.

3. Baghel S, Cathcart H, O'Reilly N. Polymeric Amorphous Solid Dispersions: A Review of Amorphization, Crystallization, Stabilization, Solid-State Characterization, and Aqueous Solubilization of Biopharmaceutical Classification System Class II Drugs. J Pharm Sci. 2016;105(9):2527-44.

4. Perrier S. 50th Anniversary Perspective: RAFT Polymerization—A User Guide. Macromolecules. 2017;50(19):7433-47.

5. Mayadunne RTA, Rizzardo E, Chiefari J, Krstina J, Moad G, Postma A, et al. Living Polymers by the Use of Trithiocarbonates as Reversible Addition−Fragmentation Chain Transfer (RAFT) Agents: ABA Triblock Copolymers by Radical Polymerization in Two Steps. Macromolecules. 2000;33(2):243-5.

6. Moad G, Rizzardo E, Thang SH. Radical Addition-Fragmentation Chemistry and RAFT Polymerization. In: Matyjaszewski K, Möller M, editors. Polymer Science: A Comprehensive Reference. 3: Elsevier; 2012. p. 181-226.

7. Chiefari J, Chong YKB, Ercole F, Krstina J, Jeffery J, Le TPT, et al. Living Free-Radical Polymerization by Reversible Addition−Fragmentation Chain Transfer: The RAFT Process. Macromolecules. 1998;31:5559-62.

8. Keddie DJ. A guide to the synthesis of block copolymers using reversible-addition fragmentation chain transfer (RAFT) polymerization. Chem Soc Rev. 2013;43(2):496-505.

9. Moad G, Rizzardo E, Thang SH. Living Radical Polymerization by the RAFT Process. Aust J Chem. 2005;58(6):379-410.

10. Keddie DJ, Moad G, Rizzardo E, Thang SH. RAFT Agent Design and Synthesis. Macromolecules. 2012;45(13):5321-42.

11. Liu J, Huang Y, Kumar A, Tan A, Jin S, Mozhi A, et al. pH-sensitive nano-systems for drug delivery in cancer therapy. Biotechnol Adv. 2014;32(4):693-710.

12. Dai J, Nagai T, Wang X, Zhang T, Meng M, Zhang Q. pH-sensitive nanoparticles for improving the oral bioavailability of cyclosporine A. Int J Pharm. 2004;280(1-2):229-40.

13. Leopold C, Eikeler D. Basic coating polymers for the colon-specific drug delivery in inflammatory bowel disease. Drug Dev Ind Pharm. 2000;26(12):1239-46.

14. Ringsdorf H. Structure and properties of pharmacologically active polymers. J Polym Sci. 1975;51(1):135-53.

15. Rosenblum D, Joshi N, Tao W, Karp JM, Peer D. Progress and challenges towards targeted delivery of cancer therapeutics. Nat Commun. 2018;9(1):1-12.

16. Maeda H, Takeshita J, Kanamaru R. A lipophilic derivative of neocarzinostatin. A polymer conjugation of an antitumor protein antibiotic. Int J Pept Protein Res. 1979;14(2):81-7.

17. Matsumura Y, Maeda H. A new concept for macromolecular therapeutics in cancer chemotherapy: mechanism of tumoritropic accumulation of proteins and the antitumor agent smancs. Cancer Res. 1986;46:6387-92.

18. Noguchi Y, Wu J, Duncan R, Strohalm J, Ulbrich K, Akaike T, et al. Early phase tumor accumulation of macromolecules: a great difference in clearance rate between tumor and normal tissues. Jpn J Cancer Res. 1998;89(3):307-14.

19. Fang J, Nakamura H, H. M. The EPR effect: Unique features of tumor blood vessels for drug delivery, factors involved, and limitations and augmentation of the effect. Adv Drug Deliv Rev. 2011;63(3):136-51.

20. Laouini A, Jaafar-Maalej C, Limayem-Blouza I, Sfar S, Charcosset CF, H. Preparation, Characterization and Applications of Liposomes: State of the Art. J Colloid Sci Biotechnol. 2012;1(2):147-68.

21. Vaupel P. Tumor microenvironmental physiology and its implications for radiation oncology. Semin Radiat Oncol. 2004;14(3):198-206.

22. Tannock IF, Rotin D. Acid pH in tumors and its potential for therapeutic exploitation. Cancer Res. 1989;49(16):4373-84.

23. Joubert F, Martin L, Perrier S, Pasparakis G. Development of a Gemcitabine-Polymer Conjugate with Prolonged Cytotoxicity against a Pancreatic Cancer Cell Line. ACS Macro Lett. 2017;6(5):535–40.

24. Convertine A, Diab C, Prieve M, Paschal A, Hoffman A, Johnson P, et al. pH-responsive polymeric micelle carriers for siRNA drugs. Biomacromolecules. 2010;11(11):2904-11.

25. Ward MA, Georgiou TK. Thermoresponsive Polymers for Biomedical Applications. Polymers. 2011;3(3):1215-42.

26. Emamzadeh M, Desmaële D, Couvreur P, Pasparakis G. Dual controlled delivery of squalenoyl-gemcitabine and paclitaxel using thermo-responsive polymeric micelles for pancreatic cancer. J Mater Chem B. 2018;6:2230-9.

27. Emamzadeh M, Emamzadeh M, Pasparakis G. Dual Controlled Delivery of Gemcitabine and Cisplatin Using Polymer-Modified Thermosensitive Liposomes for Pancreatic Cancer. ACS Appl Bio Mater. 2019;2(1298-1309).

28. Zheng Y, Wang L, Lu L, Wang Q, Benicewicz BC. pH and Thermal Dual-Responsive Nanoparticles for Controlled Drug Delivery with High Loading Content. ACS Omega. 2017;2(7):3399-405.

29. Hoogeveen NG, Cohen Stuart MA, Fleer GJ, Böhmer MR. Formation and Stability of Multilayers of Polyelectrolytes. Langmuir. 1996;12(15):3675-81.

30. Harada A, Kataoka K. Formation of Polyion Complex Micelles in an Aqueous Milieu from a Pair of Oppositely-Charged Block Copolymers with Poly(ethylene glycol) Segments. Macromolecules. 1995;28(15):5294-9.

31. Satoshi KK, K. Water-Soluble Polyion Complex Associates of DNA and Poly(ethylene glycol)−Poly(l-lysine) Block Copolymer. Bioconjugate Chem. 1997;8(5):702-7.

32. Kabanov AV, Bronich TK, Kabanov VA, Yu K, Eisenberg A. Soluble Stoichiometric Complexes from Poly(N-ethyl-4-vinylpyridinium) Cations and Poly(ethylene oxide)-block-polymethacrylate Anions. Macromolecules. 1996;29(21):6797-802.

33. Van der Kooij HM, Spruijt E, Voets IK, Fokkink R, Stuart MAC, Van der Gucht J. On the Stability and Morphology of Complex Coacervate Core Micelles: From Spherical to Wormlike Micelles. Langmuir. 2012;28(40):14180-91.

34. Cohen Stuart MA, Besseling NAM, Fokkink RG. Formation of Micelles with Complex Coacervate Cores. Langmuir. 1998;14(24):6846-9.

35. Baghel S, Cathcart H, O'Reilly NJ. Polymeric Amorphous Solid Dispersions: A Review of Amorphization, Crystallization, Stabilization, Solid-State Characterization, and Aqueous Solubilization of Biopharmaceutical Classification System Class II Drugs. J Pharm Sci. 2016;105(9):2527-44.

36. Amidon G, Lennernäs H, Shah V, Crison J. A theoretical basis for a biopharmaceutic drug classification: the correlation of in vitro drug product dissolution and in vivo bioavailability. Pharm Res. 1995;12(3):413-20.

37. Ku M. Use of the Biopharmaceutical Classification System in early drug development. AAPS J. 2008;10(1):208-12.

38. Butler J, Dressman J. The developability classification system: application of biopharmaceutics concepts to formulation development. J Pharm Sci. 2010;99(12):4940-54.

39. Noyes AA, Whitney WR. The rate of solution of solid substances in their own solutions. J Am Chem Soc. 1897;19(12):930-4.

40. Yu D, Li J, Williams G, Zhao M. Electrospun amorphous solid dispersions of poorly water-soluble drugs: A review. J Control Release. 2018;292:91-110.

41. Serajuddin A. Salt formation to improve drug solubility. Adv Drug Deliv Rev. 2007;59(7):603-16.

42. Miyazaki S, Nakano M, Arita T. A comparison of solubility characteristics of free bases and hydrochloride salts of tetracycline antibiotics in hydrochloric acid solutions. Chem Pharm Bull. 1975;23(6):1197-204.

43. Miyazaki S, Oshiba M, Nadai T. Precaution on use of hydrochloride salts in pharmaceutical formulation. J Pharm Sci. 1981;70(6):594-6.

44. Mesallati H, Umerska A, Paluch KJ, Tajber L. Amorphous Polymeric Drug Salts as Ionic Solid Dispersion Forms of Ciprofloxacin. Mol Pharmaceutics. 2017;14(7):2209-23.

45. Remenar J, MacPhee J, Larson B, Tyagi V, Ho J, McIlroy D, et al. Salt Selection and Simultaneous Polymorphism Assessment via High-Throughput Crystallization: The Case of Sertraline. Org Process Res Dev. 2003;7:990-6.

46. Craig DQ. The mechanisms of drug release from solid dispersions in water-soluble polymers. Int J Pharm. 2002;231(2):131-44.

47. Lin X, Hu Y, Liu L, Su L, Li N, Yu J, et al. Physical Stability of Amorphous Solid Dispersions: a Physicochemical Perspective with Thermodynamic, Kinetic and Environmental Aspects. Pharm Res. 2018;35(6):1-18.

48. Konno H, Handa T, Alonzo DE, Taylor LS. Effect of polymer type on the dissolution profile of amorphous solid dispersions containing felodipine. Eur J Pharm Biopharm. 2008;70(2):493-9.

49. Janssens S, Van den Mooter G. Review: physical chemistry of solid dispersions. J Pharm Pharmacol. 2009;61(12):1571-86.

50. Hancock B, Zografi G. Characteristics and significance of the amorphous state in pharmaceutical systems. J Pharm Sci. 1997;86(1):1-12.

51. Patil HT, RV; Repka, MA. Hot-Melt Extrusion: from Theory to Application in Pharmaceutical Formulation. AAPS PharmSciTech. 2016;17(1):20-42.

52. Bhujbal SV, Mitra B, Jain U, Gong Y, Agrawal A, Karki S, et al. Pharmaceutical amorphous solid dispersion: A review of manufacturing strategies. Acta Pharm Sin B. 2021;11(8):2505-36.

53. Fan W, Zhu W, Zhang X, Xu Y, Di L. Application of the combination of ball-milling and hot-melt extrusion in the development of an amorphous solid dispersion of a poorly water-soluble drug with high melting point. RSC Adv. 2019;9(39):22263–73.

54. Hughes DL. Patent Review of Manufacturing Routes to Recently Approved PARP Inhibitors: Olaparib, Rucaparib, and Niraparib. Org Process Res Dev. 2017;21(9):1227-44.

55. Tran TTD, Tran PHL. Molecular Interactions in Solid Dispersions of Poorly Water-Soluble Drugs. Pharmaceutics. 2020;12(8):745-57.

56. Brough C, Williams R. Amorphous solid dispersions and nano-crystal technologies for poorly water-soluble drug delivery. Int J Pharm. 2013;453(1):157-66.

57. Guzmán HR, Tawa M, Zhang Z, Ratanabanangkoon P, Shaw P, Gardner CR, et al. Combined use of crystalline salt forms and precipitation inhibitors to improve oral absorption of celecoxib from solid oral formulations. J Pharm Sci. 2007;96(10):2686-702.

58. Warren DB, Benameur H, Porter CJ, Pouton CW. Using polymeric precipitation inhibitors to improve the absorption of poorly water-soluble drugs: A mechanistic basis for utility. J Drug Targeting. 2010;18(10):704-31.

59. Gupta P, Kakumanu VK, Bansal AK. Stability and Solubility of Celecoxib-PVP Amorphous Dispersions: A Molecular Perspective. Pharm Res. 2004;21(10):1762-9.

60. Prime KL, Whitesides GM. Adsorption of proteins onto surfaces containing end-attached oligo(ethylene oxide): a model system using self-assembled monolayers. J Am Chem Soc. 1993;115(23):10714-21.

61. Gabizon A, Catane R, Uziely B, Kaufman B, Safra T, Cohen R, et al. Prolonged circulation time and enhanced accumulation in malignant exudates of doxorubicin encapsulated in polyethylene-glycol coated liposomes. Cancer Res. 1994;54(4):987-92.

62. Allen TM, Hansen C, Martin F, Redemann C, Yau-Young A. Liposomes containing synthetic lipid derivatives of poly(ethylene glycol) show prolonged circulation half-lives in vivo. Biochim Biophys Acta. 1991;1066(1):29-36.

63. Owens DE, Peppas NA. Opsonization, biodistribution, and pharmacokinetics of polymeric nanoparticles. Int J Pharm. 2006;307(1):93-102.

64. Suk JS, Xu Q, Kim N, Hanes J, Ensign LM. PEGylation as a strategy for improving nanoparticle-based drug and gene delivery. Adv Drug Deliv Rev. 2016;99(Pt A):28-51.

65. Barenholz Y. Doxil®--the First FDA-approved Nano-Drug: Lessons Learned. J Controlled Release. 2012;160(2):117-34.

66. Müller HJ, Löning L, Horn A, Schwabe D, Gunkel M, Schrappe M, et al. Pegylated Asparaginase (Oncaspar) in Children With ALL: Drug Monitoring in Reinduction According to the ALL/NHL-BFM 95 Protocols. Br J Haematol. 2000;110(2):379-84.

67. Ryan SMM, G.; Wang, X.; Haddleton, D.M.; Brayden, D.J. Advances in PEGylation of Important Biotech Molecules: Delivery Aspects. Expert Opin Drug Deliv. 2008;5(4):371-83.

68. Lutz J-F. Polymerization of oligo(ethylene glycol) (meth)acrylates: Toward new generations of smart biocompatible materials. J Polym Sci Part A: Polym Chem. 2008;46:3459-70.

69. Agut W, Brûlet A, Schatz C, Taton D, Lecommandoux S. pH and Temperature Responsive Polymeric Micelles and Polymersomes by Self-Assembly of Poly[2-(dimethylamino)ethyl methacrylate]-b-Poly(glutamic acid) Double Hydrophilic Block Copolymers. Langmuir. 2010;26(13):10546-54.

70. Bütün V, Armes SP, Billingham NC. Synthesis and aqueous solution properties of near-monodisperse tertiary amine methacrylate homopolymers and diblock copolymers. Polymer. 2001;42(14):5993-6008.

71. Loh XJ. Poly(DMAEMA-co-PPGMA): Dual-responsive “reversible” micelles. J Appl Polym Sci. 2012;127(2):992-1000.

72. Khine YY, Jiang Y, Dag A, Lu H, Stenzel MH. Dual-Responsive pH and Temperature Sensitive Nanoparticles Based on Methacrylic Acid and Di(ethylene glycol) Methyl Ether Methacrylate for the Triggered Release of Drugs. Macromol Biosci. 2015;15(8):1091-104.

73. Okuyama T, Maskill H. Organic Chemistry: A Mechanistic Approach: OUP Oxford; 2013.

74. Izunobi JU, Higginbotham CL. Polymer Molecular Weight Analysis by 1H NMR Spectroscopy. J Chem Educ. 2011;88(8):1098-104.

75. Smith WB, May JA, Kim CW. Polymer studies by gel permeation chromatography. Polym Sci. 1966;4(3):365-74.

76. Shahalom S, Tong T, Emmett S, Saunders BR. Poly(DEAEMa-co-PEGMa): A New pH-Responsive Comb Copolymer Stabilizer for Emulsions and Dispersions. Langmuir. 2006;22(20):8311-7.

77. Mertoglu M, Laschewsky A, Skrabania K, Wieland C. New Water Soluble Agents for Reversible Addition−Fragmentation Chain Transfer Polymerization and Their Application in Aqueous Solutions. Macromolecules. 2005;38(9):3601-14.

78. Fournier D, Hoogenboom R, Thijs HML, Paulus RM, Schubert US. Tunable pH- and Temperature-Sensitive Copolymer Libraries by Reversible Addition−Fragmentation Chain Transfer Copolymerizations of Methacrylates. Macromolecules. 2007;40(4):915-20.

79. Venkataraman S, Ong W, Ong Z, Joachim Loo S, Ee P, Yang Y. The role of PEG architecture and molecular weight in the gene transfection performance of PEGylated poly(dimethylaminoethyl methacrylate) based cationic polymers. Biomaterials. 2011;32(9):3269-78.

80. Samsonova O, Pfeiffer C, Hellmund M, Merkel OM, Kissel T. Low Molecular Weight pDMAEMA-block-pHEMA Block-Copolymers Synthesized via RAFT-Polymerization: Potential Non-Viral Gene Delivery Agents? Polymers. 2011;3(2):693-718.

81. Pelet JM, Putnam D. High Molecular Weight Poly(methacrylic acid) with Narrow Polydispersity by RAFT Polymerization. Macromolecules. 2009;42(5):1494-9.

82. Chaduc I, Lansalot M, D'Agosto F, Charleux B. RAFT Polymerization of Methacrylic Acid in Water. Macromolecules. 2012;45(3):1241-7.

83. Vijayakrishna K, Jewrajka SK, Ruiz A, Marcilla R, Pomposo JA, Mecerreyes D, et al. Synthesis by RAFT and Ionic Responsiveness of Double Hydrophilic Block Copolymers Based on Ionic Liquid Monomer Units. Macromolecules. 2008;41(17):6299-308.

84. Rizzardo E, Chen M, Chong B, Moad G, Skidmore M, Thang SH. RAFT polymerisation: Adding to the picture. Macromol Symp. 2007;248(1):104-16.

85. Harada A, Kataoka K. Polyion complex micelle formation from double-hydrophilic block copolymers composed of charged and non-charged segments in aqueous media. Polym J. 2017;50(1):95-100.

86. Boddohi S, Moore N, Johnson PA, Kipper MJ. Polysaccharide-Based Polyelectrolyte Complex Nanoparticles from Chitosan, Heparin, and Hyaluronan. Biomacromolecules. 2009;10(6):1402-9.

87. JVM W, SP A, S L. A "Holy Trinity" of Micellar Aggregates in Aqueous Solution at Ambient Temperature: Unprecedented Self-Assembly Behavior

from a Binary Mixture of a Neutral−Cationic Diblock Copolymer and an Anionic Polyelectrolyte. Macromolecules. 2003;36(26):9994-8.

88. Sui Z, Jaber JAS, Joseph B. Polyelectrolyte Complexes with pH-Tunable Solubility. Macromolecules. 2006;39(23):8145–52.

89. Xiao L, Huang L, Moingeon F, Gauthier M, Yang G. pH-Responsive Poly(Ethylene Glycol)-block-Polylactide Micelles for Tumor-Targeted Drug Delivery. Biomacromolecules. 2017;18(9):2711-22.

90. Awwad S, Al-Shohani A, Khaw P, Brocchini S. Comparative Study of In Situ Loaded Antibody and PEG-Fab NIPAAM Gels. Macromol Biosci. 2018;18(2):1-12.

91. Koide A, Kishimura A, Osada K, Jang WD, Yamasaki Y, Kataoka K. Semipermeable polymer vesicle (PICsome) self-assembled in aqueous medium from a pair of oppositely charged block copolymers: physiologically stable micro-/nanocontainers of water-soluble macromolecules. J Am Chem Soc. 2006;128(18):5988-9.

92. Harada A, Kataoka K. Chain length recognition: core-shell supramolecular assembly from oppositely charged block copolymers. Science. 1999;283(5398):65-7.

93. Hori M, Cabral H, Toh K, Kishimura A, Kataoka K. Robust Polyion Complex Vesicles (PICsomes) under Physiological Conditions Reinforced by Multiple Hydrogen Bond Formation Derived by Guanidinium Groups. Biomacromolecules. 2018;19(10):4113-21.

94. Schatz C, Domard A, Viton C, Pichot C, Delair T. Versatile and Efficient Formation of Colloids of Biopolymer-Based Polyelectrolyte Complexes. Biomacromolecules. 2004;5(5):1882-92.

95. Birch NP, Schiffman JD. Characterization of Self-Assembled Polyelectrolyte Complex Nanoparticles Formed from Chitosan and Pectin. Langmuir. 2014;30(12):3441-7.

96. Lim C, Youn YS, Lee KS, Hoang NH, Sim T, Lee ES, et al. Development of a robust pH-sensitive polyelectrolyte ionomer complex for anticancer nanocarriers. Int J Nanomed. 2016;11:703-13.

97. Kouchakzadeh H, Shojaosadati SA, Maghsoudi A, Vasheghani Farahani E. Optimization of PEGylation conditions for BSA nanoparticles using response surface methodology. AAPS PharmSciTech. 2010;11(3):1206-11.

98. Gu Z, Yan S, Cheong S, Cao Z, Zuo H, Thomas A, et al. Layered double hydroxide nanoparticles: Impact on vascular cells, blood cells and the complement system. J Colloid Interface Sci. 2018;512:404-10.

99. Martinez de Pinillos Bayona A, Moore CM, Loizidou M, MacRobert AJ, Woodhams JH. Enhancing the efficacy of cytotoxic agents for cancer therapy using photochemical internalisation. Int J Cancer. 2016;138(5):1049-57.

100. Saincher SS, Gottlieb C. Ozurdex (dexamethasone intravitreal implant) for the treatment of intermediate, posterior, and panuveitis: a systematic review of the current evidence. J Ophthalmic Inflammation Infect. 2020;10(1):1-10.

101. Egbu R, Brocchini S, Khaw P, Awwad S. Antibody loaded collapsible hyaluronic acid hydrogels for intraocular delivery. Eur J Pharm Biopharm. 2018;124:95-103.

102. Awwad S, Lockwood A, Brocchini S, Khaw P. The PK-Eye: A Novel In Vitro Ocular Flow Model for Use in Preclinical Drug Development. J Pharm Sci. 2015;104(10):3330-42.

103. Zotova J, Wojnarowska Z, Twamley B, Paluch M, Tajber L. Green Synthesis of Lidocaine Ionic Liquids and Salts: Mechanisms of Formation and Interactions in the Crystalline and Supercooled States. ACS Sustainable Chem Eng. 2020;8:18266−76.

104. Pérez-Isidoro R, Sierra-Valdez FJ, Ruiz-Suárez JC. Anesthetic Diffusion Through Lipid Membranes Depends on the Protonation Rate. Sci Rep. 2014;4(1):1-9.

105. Liu X, Ma X, Kun E, Guo X, Yu Z, Zhang F. Influence of lidocaine forms (salt vs. freebase) on properties of drug-eudragit® L100-55 extrudates prepared by reactive melt extrusion. Int J Pharm. 2018;547(1-2):291-302.

106. Sóti P, Bocz K, Pataki H, Eke Z, Farkas A, Verreck G, et al. Comparison of spray drying, electroblowing and electrospinning for preparation of Eudragit E and itraconazole solid dispersions. Int J Pharm. 2015;494(1):23-30.

107. Liu H, Wang P, Zhang X, Shen F, Gogos C. Effects of extrusion process parameters on the dissolution behavior of indomethacin in Eudragit E PO solid dispersions. Int J Pharm. 2010;383(1-2):161-9.

108. Flanner H, Moore JW. Mathematical Comparison of Curves with an Emphasis on in Vitro Dissolution Profiles. Pharma Tech. 1996;20:64–74.

109. Ma Y, Gill H. Coating solid dispersions on microneedles via a molten dip-coating method: development and in vitro evaluation for transdermal delivery of a water-insoluble drug. J Pharm Sci. 2014;103(11):3621-30.

110. Ho B-C, Lee Y-D, Chin W-K. Thermal degradation of polymethacrylic acid. J Polym Sci Part A: Polym Chem. 1992;30:2389– 97.

111. Huang Y, Dai W-G. Fundamental aspects of solid dispersion technology for poorly soluble drugs. Acta Pharm Sin B. 2014;4(1):18-25.

112. Turner DT, Schwartz A. The glass transition temperature of poly(N-vinyl pyrrolidone) by differential scanning calorimetry. Polymer. 2022;26(5):757-62.

113. Lopez FL, Shearman GC, Gaisford S, Williams GR. Amorphous Formulations of Indomethacin and Griseofulvin Prepared by Electrospinning. Mol Pharmaceutics. 2014;11(12):4327−38.

114. Khougaz K, Clas SD. Crystallization Inhibition in Solid Dispersions of MK-0591 and Poly(vinylpyrrolidone) Polymers. J Pharm Sci. 2000;89(10):1325-34.

115. Xie T, Taylor LS. Improved Release of Celecoxib from High Drug Loading Amorphous Solid Dispersions Formulated with Polyacrylic Acid and Cellulose Derivatives. Mol Pharmaceutics. 2016;13:873−84.

116. Li W, Buckton G. Using DVS-NIR to assess the water sorption behaviour and stability of a griseofulvin/PVP K30 solid dispersion. Int J Pharm. 2015;495(2):999-1004.

117. Graeser KA, Patterson JE, Zeitler JA, Rades T. The Role of Configurational Entropy in Amorphous Systems. Pharmaceutics. 2010;2(2):224-44.

118. Baghel S, Cathcart H, O'Reilly N. Understanding the generation and maintenance of supersaturation during the dissolution of amorphous solid dispersions using modulated DSC and 1 H NMR. Int J Pharm. 2018;536(1):414-25.

119. Bergström C, Luthman K, P. A. Accuracy of calculated pH-dependent aqueous drug solubility. Eur J Pharm Sci. 2004;22(5):387-98.

120. Dissolution Testing of Immediate Release Solid Oral Dosage Forms | FDA, (1997).

121. Li X, Wang C, Yang S, Liu P, B. Z. Electrospun PCL/mupirocin and chitosan/lidocaine hydrochloride multifunctional double layer nanofibrous scaffolds for wound dressing applications. Int J Nanomedicine. 2018;13:5287-99.

122. Li S, Doyle P, Metz S, Royce A, Serajuddin A. Effect of chloride ion on dissolution of different salt forms of haloperidol, a model basic drug. J Pharm Sci. 2005;94(10):2224-31.